Low Cycle Corrosion Fatigue in the North Sea Environment

by

Marc Anthony Anijs

A thesis submitted in partial fulfillment for the
Master of Science Degree

in

Civil Engineering
Structural Engineering

October 2013

"Anfangen ist leicht, beharren eine Kunst."

Hans-Jürgen

DELFT UNIVERSITY OF TECHNOLOGY

Abstract

Civil Engineering
Structural Engineering

Master of Science

by Marc Anthony Anijs

Low cycle corrosion fatigue is an interesting issue in civil Engineering because it may affect the lifetime of structures in negative and unexpected ways. However, analysis of design codes has revealed that low cycle corrosion fatigue is not a major issue in the design of offshore structures because these structures are designed with a global elastic philosophy. This means that the number of cycles that a structure can withstand usually stays well within the high cycle range. The joints (welded or otherwise) revealed to be the less resistant elements to low cycle corrosion fatigue. Furthermore, it was revealed that in the ultra low cycle region the effect of the environment is heavily reduced. It was also revealed that the effect of cathodic protection is strongest in the upper spectrum of the high cycle range and deteriorates in the lower spectrum of the high cycle range. It was also revealed that a structure in air and a structure in seawater with cathodic protection have essentially the same fatigue resistance when in the ultra low cycle range. In the ultra low cycle range, the problem appears to turns into mostly a low cycle fatigue problem. In the ultra high cycle region the problem appears to turns into mostly a corrosion problem. S-N curves that can predict the low cycle fatigue life of structures in a deleterious environment are very rare. The only S-N curve available that can be used for structural steel subjected to low cycle corrosion fatigue is one for tubular sections. However, Mathematical modeling based on regression and a principle of constant slopes in a fatigue cycle region (low cycle, high cycle, ultra high cycle) has made it possible to not only calculate the low cycle corrosion fatigue life of tubular joints but the low cycle corrosion fatigue life of other types of joints as well.

Acknowledgements

This thesis was written under supervision of Prof.ir. F.S.K. Bijlaard & Dr. M.H. Kolstein at the Faculty of Civil Engineering & Geosciences at the TU Delft University of Technology. The author would like to thank especially Prof.ir F.S.K. Bijlaard for his guidance during the writing of this thesis. His ideas and recommendations were invaluable. The author would also like to thank Dr. M.H. Kolstein for his guidance and comments. The author would also like to thank Dr.ir. J.M.C. Mol at the Faculty of 3ME at the TU Delft University of Technology for taking part in the graduation committee.

Contents

List of Figures

List of Tables

Abbreviations

DNV	Det Norske Veritas
API	American Petroleum Institute
ABS	American Bureau of Shipping
EC3	Eurocode 3
HCF	High Cycle Fatigue
LCF	Low Cycle Fatigue
LCCF	Low Cycle Corrosion Fatigue
HCCF	High Cycle Corrosion Fatigue
S-N	Stress Number
ISO	International Organization for Standardization
SCF	Stress Concentration Factor
HSE	Health and Safety Executive
LCHS	Low Cycle High Strain
HCLS	High Cycle Low Stress

Symbols

N	fatigue life	(-)
$\bar{a}$	intercept of the design S-N curve with the logarithm N axis	(-)
m	negative inverse slope of the S-N curve	(-)
$\Delta\sigma$	applied engineering true stress in a fatigue load cycle	MPa (Nmm^{-2})
$\Delta\varepsilon$	applied engineering strain in a fatigue load cycle	(-)
t_{ref}	reference thickness for welded connections	mm
k	thickness exponent on fatigue strength	(-)
t	thickness through which a crack will most likely grow	mm
D	accumulated fatigue damage	(-)
η	usage factor in the Miner Sum	(-)
σ_n	nominally applied stress	MPa (Nmm^{-2})
E	Young's modulus	MPa (Nmm^{-2})
$\sigma_{actualHSS}$	hot spot stress	MPa (Nmm^{-2})
K'	material constant	(-)
n	material constant	(-)
ε_{nl}	non-linear strain	(-)
σ_{pseudo}	pseudo elastic stress	MPa (Nmm^{-2})
ε_f'	fatigue ductility coefficient	(-)
c	fatigue ductility exponent	(-)
$\frac{\Delta\varepsilon_p}{2}$	plastic strain amplitude	(-)
$2N$	number of reversals to failure	(-)

For/Dedicated to/To my Degree for Master of Science

Chapter 1

Introduction

Low cycle corrosion fatigue is an interesting issue in civil engineering because it may affect the lifetime of structures in negative and unexpected ways. Corrosion fatigue is a mode of failure that affects metals in deleterious electrochemical environments. Civil engineering structures, which are subject to aging and are in general exposed to deleterious environments, are for example offshore structures. The stress cycle in structural elements of these structures is likely to be subject to changes. Low cycle corrosion fatigue is defined as sequential stages of damage that progress with every load cycle to a steel element in an electrochemically hazardous environment. The stages are cyclic plastic deformation, micro-crack initiation, small crack growth to linkup and finally coalescence growth of the coalesced crack [1]. In general this crack growth or these crack growths may lead to ultimate failure of a structural element. Low cycle failure is typically less than 10.000 cycles but this number is arbitrary. Low cycle fatigue is usually associated with widespread plasticity in metals, thus, a strain based parameter may be used for fatigue life prediction in metals, contrary to high cycle fatigue, which is usually described by stress-based parameters. The stress range is simply the algebraic difference between the minimum and maximum stress range, at a given location. Fatigue calculations should only be done for locations with a net applied tensile stress. Analysis of low cycle corrosion fatigue problems for offshore structures in the North Sea has revealed that there is very little literature on low cycle corrosion fatigue. The common design codes do not cover this subject as elaborately as they cover high cycle corrosion fatigue. In this thesis the author will investigate the problem of low cycle corrosion fatigue. The author will analyze the standing codes for fatigue in the industry. General searches have not delivered clear design codes

for offshore structures subject to low cycle fatigue in deleterious environments despite the fact that many metal structures are built in seawater. The first research question is, "what do the design codes say about low cycle corrosion fatigue." The second research question is, "how influential is the electrochemical environment for structures subject to low cycle fatigue." The third research question is, "is it possible to find a method for the analysis of low cycle corrosion fatigue in case methods are not available in the literature." The fourth research question is, "what is the weakest part of a structure subjected to low cycle corrosion fatigue." The research questions will be answered by first analyzing the available literature and then some mathematical modeling for low cycle corrosion fatigue will follow in the later sections.

Chapter 2

Literature Review

The relationship between fatigue life N and stress was first proposed by O.H. Basquin in his publication in 1910. Basquin proposed a log-linear relationship between fatigue life N and stress range $\Delta\sigma$. This relationship can be seen in equation 2.1 where A is the stress range that will only experience 1 load cycle and B is the slope of the logarithmic S-N curve.

$$\Delta\sigma = A(N)^B \tag{2.1}$$

S-N curves in design codes for high cycle fatigue are based on the Basquin equation. The design codes available generally cover HCF (and HCCF). The meaning of these abbreviations can be seen in figure 2.1. In [2] the authors investigated low cycle high-strength steel butt welds. The authors of [2] performed their study because the demand for high load capacity in steel construction combined with low construction weight is growing. Furthermore, the carbon footprint of structures can be reduced if less material is used. In [2] the authors placed the boundary between low cycle fatigue and high cycle fatigue at 40.000 cycles, however, this number is arbitrary.

The author of this thesis shares the sentiment that low cycle fatigue, more specifically, low cycle corrosion fatigue is an issue that is worth investigating. The author will investigate the design codes, scientific papers from material science and research available from narrowly related fields to civil engineering pending applicability in a civil engineering environment.
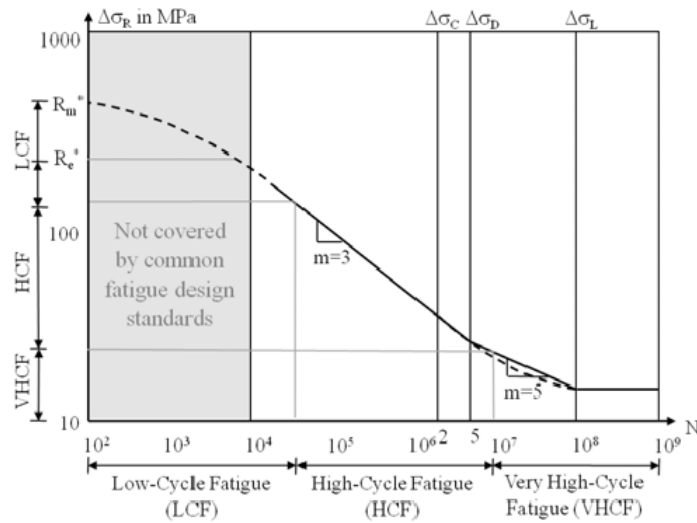
FIGURE 2.1: The different type of fatigue regions with the most common slopes *m* [2]

2.1 Design Codes

In this section the author will cover the design codes which are frequently used. The codes that shall pass the review are the EC3, DNV, API, HSE and ABS.

According to [3] the EC3 and the Canadian code, for both high and low cycle fatigue, are largely similar. In [3] it was stated that stress ranges that are completely in compression do not need to be investigated for fatigue. The EC3 aims to design structures against the limit state of fatigue with an acceptable level of probability that the structure does not fail during its design life. In the EC3 it is stated that no fatigue assessment is normally required for building structures except members supporting appliances or rolling loads, members subject to vibrations from machinery, members subject to wind induced oscillations and members subject to crowd-induced oscillation. Problems such as low cycle fatigue are treated marginally in the EC3. In the EC3 a method is presented for fatigue which puts the emphasis primarily on high cycle fatigue but may also be used for low cycle fatigue according to the EC3. A type of design curve that you may find in the EC3 is given in figure 2.2. The cut-off point for the graph presented in the EC3 is 10.000 cycles which also the case in the API and DNV.

The EC3 is elaborate but makes no effort to address fatigue in deleterious environments. ISO/TR 14345.2012 gives guidance on the best practice of fatigue testing, under constant or variable amplitude, of welded components in the medium and
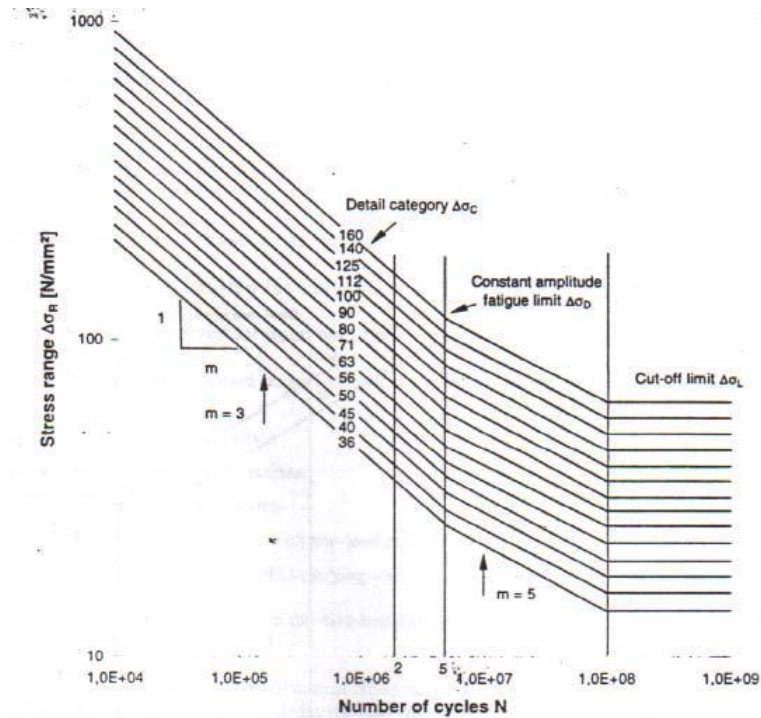
FIGURE 2.2: Characteristic S-N curves in EC3. The curve has been created for high cycle fatigue because this is the common problem. The curve may be extrapolated for low cycle fatigue according to the EC3. This curve does not take into account environmental effects. The tests results have not been acquired for low cycle fatigue. [4]

high cycle range. Low cycle fatigue is not specifically covered just like the EC3. ISO/TR 14345:2012 does not cover corrosion or high-temperature fatigue testing.

In the DNV [5] the authors designed codes for the analysis of fatigue for offshore structures with the North Sea as the environment of reference. The authors stated that the Recommended Practice is valid for steels in air with yield strength up to 960 MPa (which is representative of construction steel for civil engineering purposes). For steel in seawater with cathodic protection or steel with free corrosion the Recommended Practice is valid up till 550 MPa. The Recommended Practice can easily be applied for temperatures up to 100 degrees Celsius. The authors also stated that offshore structures which are subjected to typical wave and wind loading, fatigue damage occurs in the range of larger than 10.000.000 cycles, which is well beyond the range of low cycle fatigue. Low cycle fatigue is typically less than 10.000 cycles. An image of one of the S-N curves in [5] is given in figure 2.3. The expression for prediction of fatigue life in [5] is given in equation 2.2
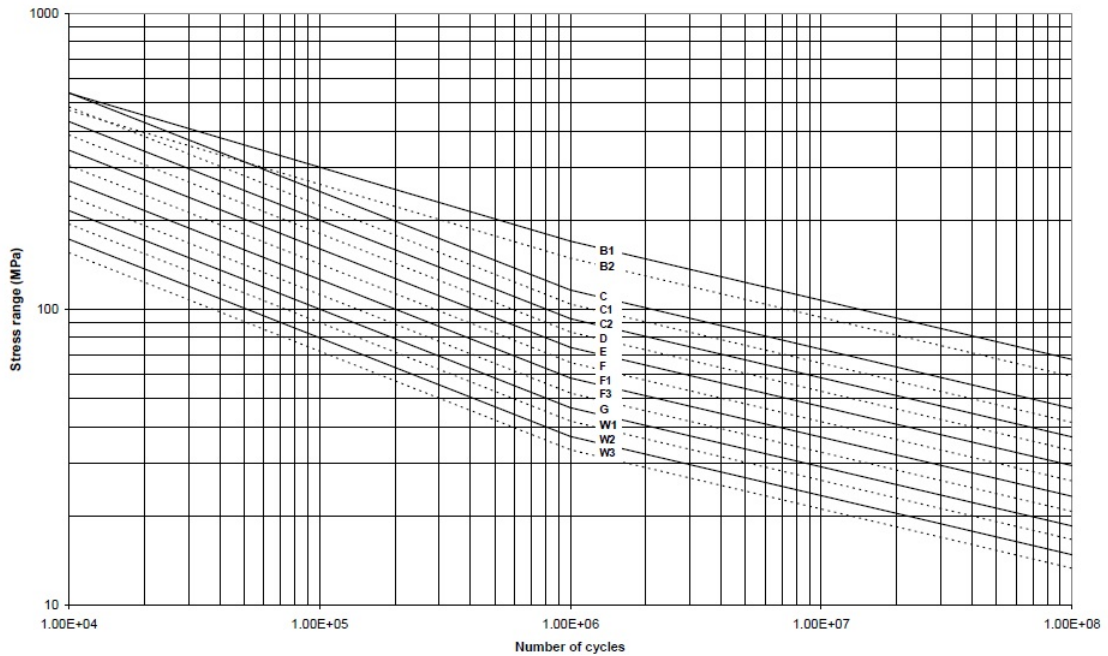
FIGURE 2.3: Characteristic S-N curves in DNV. High cycle design S-N curve for different joints with cathodic protection in seawater in the DNV. This curve does take into account environmental effects. The tests results have not been acquired for low cycle fatigue. According to the authors curve B2 should be used for low cycle fatigue. The authors do mention that this extrapolation may not be conservative [5]

$$logN = log\bar{a} - m \ log\Delta\sigma \tag{2.2}$$

The design curve in figure 2.3 works as following. Find the proper design curve for your type of connection. The hot spot stress range for a structure subjected to cyclical loading should then be calculated. This can be done with figure 2.4 in case the type of joint in question is a simple X-joint with tubular sections. The hot spot stress can be calculated by multiplication of the nominal stress with the stress concentration factor. The proper design curve should then be used in figure 2.3 and the number of cycles it can withstand for a given stress range can then be found. The assumed standard deviation of the given S-N curves is 0, 20 according to [5]. It should then be analyzed what the expected number of cycles for the given structure is by analyzing the load and lifetime, which can be derived from the wave data for offshore structures. It should sub sequentially be checked if the number of cycles that are expected to occur exceed the design fatigue life.

The fatigue life of welded joints is also dependent on plate thickness according

to [5]. The authors stated that this effect is due to local geometry of the weld toe in relationship to thickness of the adjoining plates. The thickness effect can be accounted for by a modification of the stress. Equation 2.3 accounts for the thickness effect. t_{ref} is the reference thickness, which is equal to 25 mm for welded connections other than tubular sections. For tubular sections the t_{ref} is 32 mm.

$$logN = log\bar{a} - mlog\left(\Delta\sigma\left(\frac{t}{t_{ref}}\right)^k\right) \qquad (2.3)$$

Table B-2 Stress Concentration Factors for Simple X Tubular Joints		
Load type and fixity conditions	*SCF equation*	*Eqn. no.*
Axial load (balanced)	Chord saddle: $3.87\,\gamma\,\tau\,\beta\left(1.10-\beta^{1.8}\right)(\sin\theta)^{1.7}$	(12)
	Chord crown: $\gamma^{0.2}\tau\left(2.65+5(\beta-0.65)^2\right)-3\,\tau\,\beta\sin\theta$	(13)
	Brace saddle: $1+1.9\,\gamma\,\tau^{0.5}\beta^{0.9}\left(1.09-\beta^{1.7}\right)(\sin\theta)^{2.5}$	(14)
	Brace crown: $3+\gamma^{1.2}\left(0.12\exp(-4\beta)+0.011\beta^2-0.045\right)$ In joints with short cords ($\alpha<12$) the saddle SCF can be reduced by the factor F1 (fixed chord ends) or F2 (pinned chord ends) where $F1 = 1-\left(0.83\,\beta-0.56\,\beta^2-0.02\right)\gamma^{0.23}\exp\left(-0.21\,\gamma^{-1.16}\alpha^{2.5}\right)$ $F2 = 1-\left(1.43\,\beta-0.97\,\beta^2-0.03\right)\gamma^{0.04}\exp\left(-0.71\,\gamma^{-1.38}\alpha^{2.5}\right)$	(15)

FIGURE 2.4: SCF for simple tubular X-joints [5]

The authors of [5] designed curves primarily for joints because these are the likely locations where failure will occur; however, they limited their research field to mostly high cycle corrosion fatigue. The authors stated that the fatigue strength assessment of offshore structures is normally understood to be strength for high cycle loading. High cycle loading is normally understood to be more than 10.000 cycles. According to the authors the stress response from wave action typically shows more than 5 million cycles a year. The authors of [5] mainly made the Recommended Practice c203-2010-04 with the purpose of assessing high cycle fatigue for offshore structures because this is the most common loading condition. Most of the data for the S-N curves were gathered from tests typically between 10.000 and 1.000.000 cycles region. In the low cycle region (less than 10.000 cycles) the maximum stress range is that of the B1 curve as shown in figure 2.3. However,

this is not considered conservative and in cases of high utilization NORSOK N-006 [6] may be used. The method in [6] will be explained more thoroughly in the upcoming sections.

When assessing low cycle fatigue one can choose to regress the number of cycles against stress or strain, however, strain can account for non-linear behavior of materials when an element is stressed beyond the elastic limit. According to [5] offshore structures are typically designed for limit states such as the ultimate limit state in which case a load and material coefficient are used in the design phase to secure sufficient safety. Despite neglect of stresses due to local notches in the ULS design, the assessment of ULS implies that the strain ranges in ULS are limited and further analysis of low cycle fatigue for offshore structures is not required. Thus for design of offshore structures in the North Sea, it has not been a practice to analyze the structures specifically for low cycle fatigue. However, when non-linear methods are used for the documentation of the ULS, for example a storm loading on a structural element such as a loading platform, it has been recommended to analyze low cycle fatigue for that specific storm. In other words, low cycle corrosion fatigue may be an issue when storm conditions occur which cause extremely high excitation of structural members. These members are then pushed beyond the elastic limit.

According to [5] offshore structures may be subjected to high cycle fatigue and low cycle fatigue. The damage caused by both modes has an accumulative effect and a rather interesting method to express the extent of damage that is caused can be found in [5] and is called the Palmgren-Miner rule. There is no restriction on the rule except that the number of stress blocks should not be less than 20 and the damage should accumulate linearly. The rule is expressed in equation 2.4

$$\sum_{i=1}^{k} \frac{\eta_i}{N_i} = \frac{1}{a} \sum_{i=1}^{k} \eta_i (\Delta \sigma_i)^m \leq \eta \qquad (2.4)$$

According to [6] joints that are loaded by cyclic loads beyond their limit for linear behavior should be checked for the danger of a crack growing in the storm to a size that will impact the load carrying capacity of the joint. An interesting method has been presented in [6]. The method enables the analysis of low cycle fatigue in a severe storm. The method does require that the storm profile is well established.

According to [6] the stress strain curve for monotonous loading differs from the curve of cyclical loading. This can be seen in figure 2.5

The hot spot stress ranges are assumed be derived from linear elastic methods. The hot spot stress ranges during a storm may imply local yielding at a certain location. A correction factor is needed in order to derive a stress range that is representative for the actual strain range that takes into account the non-linearity in material behavior. To account for this non-linearity in this situation one can use a finite element model of the considered detail and perform cyclic non-linear elastic analysis based on a cyclic stress strain curve which is capable of providing the actual strain at the hotspot, however, an easier but possibly cruder method is the Neuber's rule. This procedure is established figure 2.6
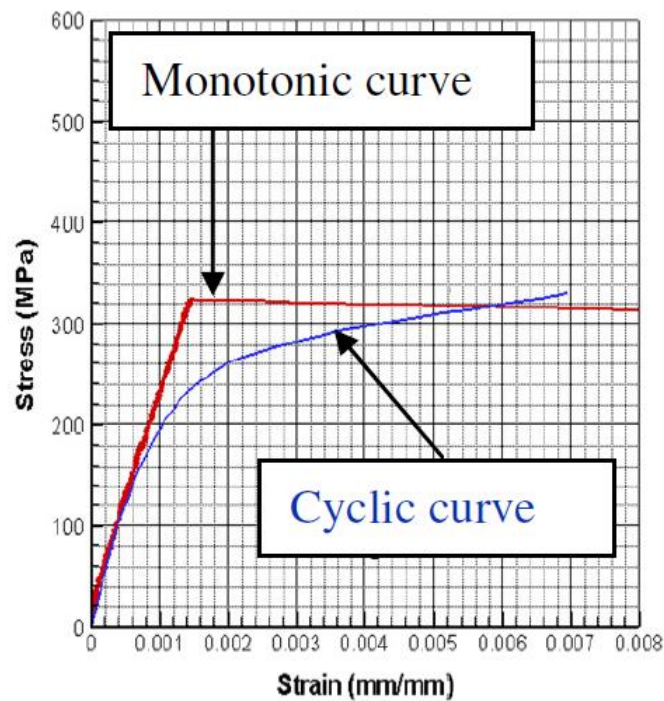
FIGURE 2.5: Cyclic stress strain curve. The cyclic strain curve when cyclic softening occurs. A low stress may correspond to a very high strain. This is a key concept in the understanding of low cycle fatigue. This is the reason why a strain based parameter is usually prefered. A stress based parameter may be confusing [6]

The equation for actual stress based on Neuber's formula can be solved by iteration. Then the strain is calculated from the Ramberg-Osgood relation. Then a pseudo elastic stress can be calculated with equations (2.5 , 2.6 and 2.7)
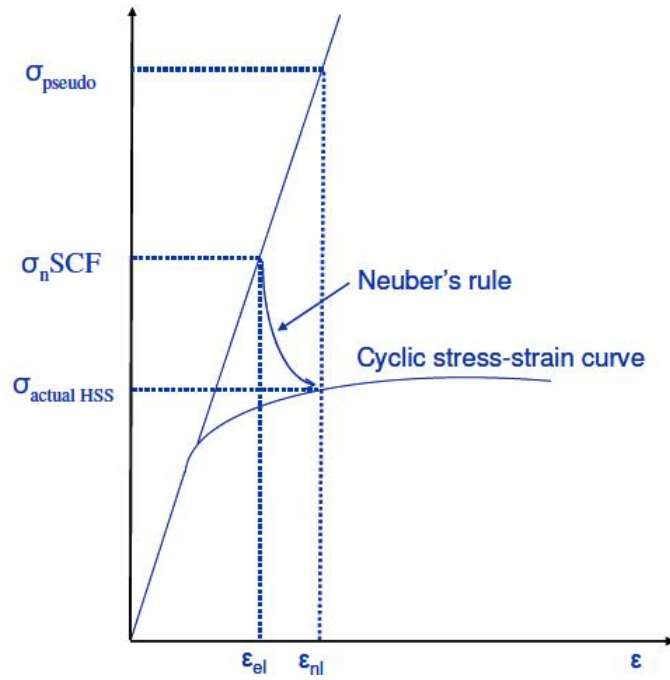
FIGURE 2.6: The pseudo elastic stress strain diagram versus the Cyclic stress strain diagram. A stress on the cyclic stress strain diagram corresponds to a much larger strain than on the elastic stress strain diagram [6]

$$\frac{\sigma_n{}^2 SCF^2}{E} = \sigma_{actualHSS} \left[\frac{\sigma_{actualHSS}}{E} + \left(\frac{\sigma_{actualHSS}}{K} \right)^{\frac{1}{n}} \right] \tag{2.5}$$

$$\varepsilon_{nl} = \frac{\sigma_{actualHSS}}{E} + \left(\frac{\sigma_{actualHSS}}{K} \right)^{\frac{1}{n}} \tag{2.6}$$

$$\sigma_{pseudo} = E\varepsilon_{nl} \tag{2.7}$$

In [6] a low cycle corrosion fatigue S-N curve has been presented for tubular sections. The curve is just like for high cycle fatigue, a log-linear relationship between fatigue life N and stress range $\Delta\sigma$. This S-N curve is one of the few S-N curves in the low cycle region in seawater for tubular sections with cathodic protection available. This S-N curve allows for the analysis of low cycle corrosion fatigue problems for tubular sections. This curve can be observed in figure 2.7. The curve may be used for the low cycle region but the stress in the curve may not exist because this stress should be calculated with linear elastic theory. It was previously

FIGURE 2.7: S-N curve for low cycle fatigue for tubular joints in seawater with cathodic protection. The curve is valid up to 100.000 cycles where it coincides with the high cycle fatigue curve.[6]
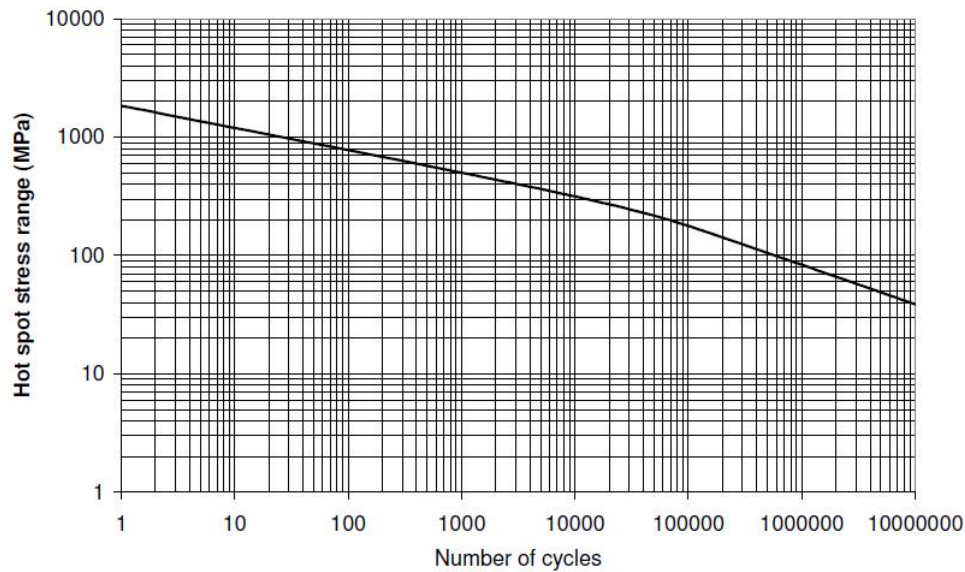
shown that the material starts to behave non-linear when subjected to cyclic plastic loading. Furthermore, in [6] there is no mention of low cycle corrosion fatigue in the natural environment without any cathodic protection. Contrary to high cycle corrosion fatigue, the authors did not look into low cycle corrosion fatigue without any cathodic protection.

Post-calculation of the number of cycles a structure can withstand and calculation of the Miner Sum. A probabilistic assessment for a structure can be made. A procedure for fatigue failure analysis is presented in [6]. The curves related to the probabilistic design method of [6] can be seen in figure 2.8. The different curves are for different assumptions on uncertainty. All curves include uncertainty in S-N data. The distribution of the logarithm of $\hat{N}$ is assumed to be a normal distribution with a standard deviation equal to 0,20. Four of the curves in figure 2.8 include uncertainty with respect to the Palmgren-Miner sum as failure criterion. The Palmgren-Miner is assumed to be log normally distributed with a median 1, 0 and a CoV 0,3. Further uncertainty is due to the environment, structural modeling and calculation of the nominal load effect in the structure; these uncertainties are described by Covnom. Finally some uncertainty in the stress calculation is included. This uncertainty is described by CoVhs. The probability of failure vs. the damage accumulated according to Palgrem-Miner rule are presented in figure

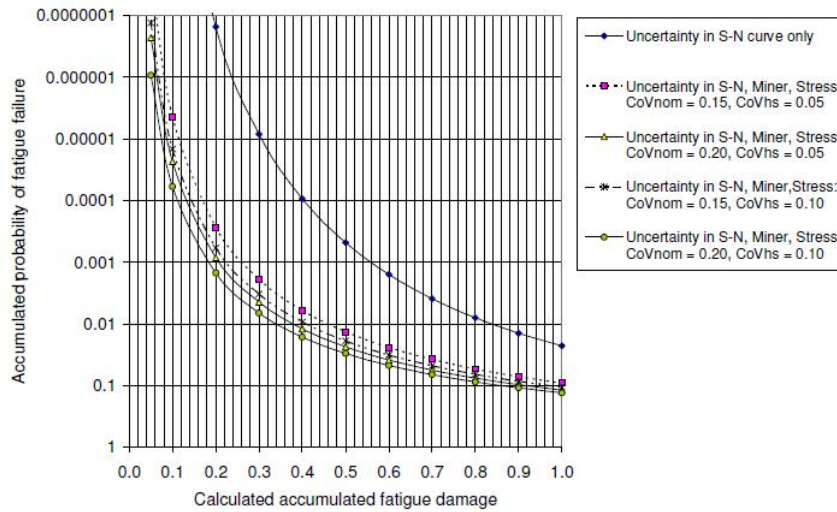2.8. This method can be applied for a wide variety of structural elements according to [6].

FIGURE 2.8: Probability of Failure vs the damage parameter according to Palgrem-Miner. Obviously the probability of failure increases with increasing damage [6]

It is interesting that [5] limits itself to mostly high cycle fatigue of offshore structures but it is definitely not unique. In [7] the authors also limited themselves to the high cycle region which is typically more than 10.000 load cycles. The ABS S-N curves can be seen in figure 2.9. Apparently the cyclic wave loading on offshore structures is primarily limited to the elastic limit of the material. The low cycle fatigue where failure typically occurs in less than 10.000 cycles is quite uncommon.

The S-N method of fatigue life assessment is generally stress-based and only fully applicable if the elastic limit has not been exceeded. However, in offshore construction the concentration of stresses in nodes and other connections can sometimes exceed the yield stress at so-called hot spots. The HSE guidance Notes placed restrictions on the applicability of the S-N curves in the low cycle region due to lack of experimental data [8] . The damage that may occur when these limits are exceeded was not addressed. For offshore installation the presence of stress peaks at joints can, under the right conditions, lead to cyclic stresses that exceed the yield stress at so called hot spots. However, the strain will remain limited with this post yield-behavior due to elastic global response of the structure. Currently
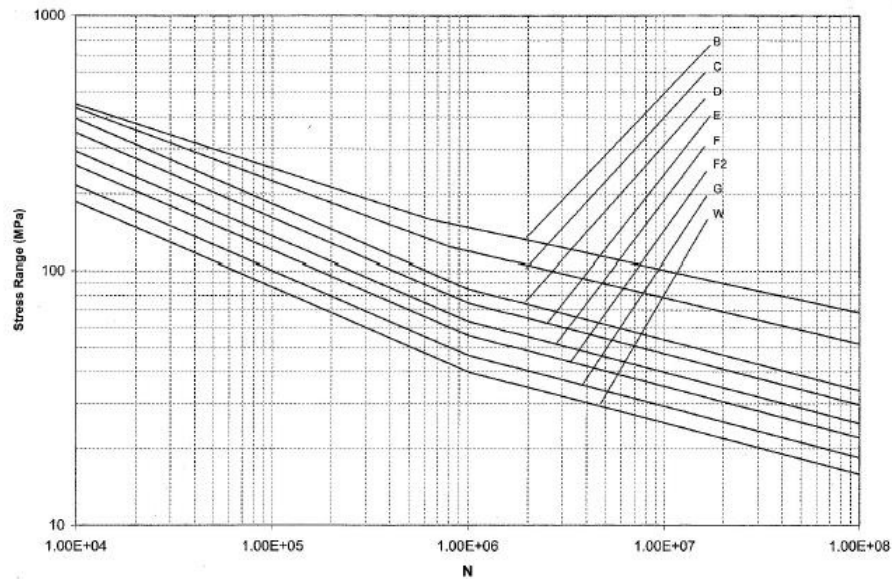
FIGURE 2.9: Offshore S-N Curves for non-tubular details in seawater Notice
that the ABS also limited themselves to cycles more than 10.000. The discontinuities in the [6] were on 10.000 cycles and 1.000.000 cycles. The same is true
for the DNV and API

there is no clarity on how this behavior should be accounted for when assessing
the fatigue limit state.

Neither the DNV RP C203 Recommended Practice nor the API RP2A Recommended Practice require separate considerations of the high stress low cycle fatigue
region. In both documents the S-N curves are continued to the low cycle-high stress
range without modification (though in graphs the S-N curves are not drawn for
the low cycle region).

In [9] API RP2A the basic design S-N curve is given by equation 2.8

$$logN = log_{10}k_1 - m\ log\Delta\sigma \tag{2.8}$$

The basic design S-N curves in the API are applicable for joints in air and submerged coated joints. For welded joints in seawater with adequate cathodic protection, the m = 3 branch of the S-N curve the fatigue life should be reduced by
a factor of 2.0, with the m = 5 branch remaining unchanged and the position of

the slope adjusted accordingly [9] . Just like the DNV the API also considers a thickness effect. The S-N curve for tubular joints can be seen in figure 2.10
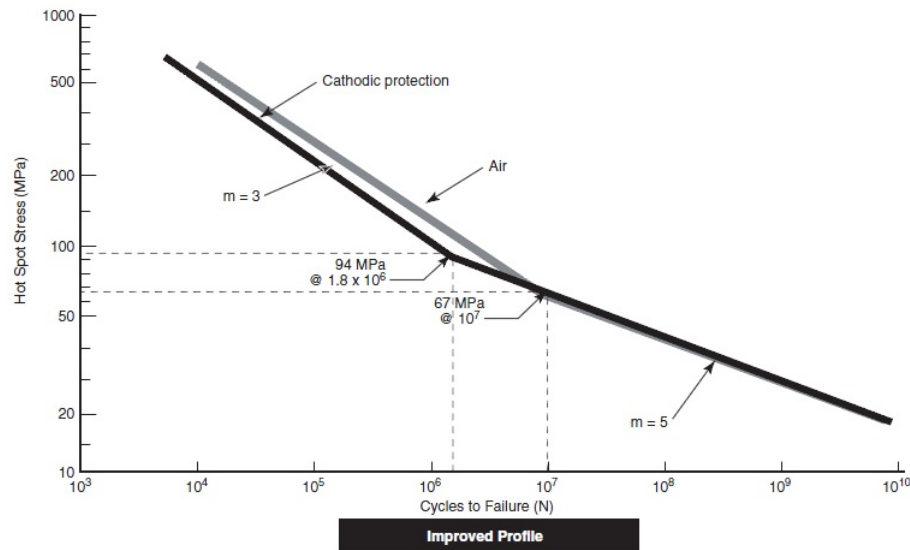

FIGURE 2.10: The S-N curve of the API for a tubular joints. The curve is also stopped at 10.000 cycles and not drawn into the lower fatigue life region. This is common for design codes. [9]

Curve	$\log_{10}k_1$	m
Welded Joints (WJ)	12,48	3 for N $< 10^7$ cycles
	16,13	5 for N $> 10^7$ cycles
Cast Joints (CJ)	15,17	4 for N $< 10^7$ cycles
	17,21	5 for N $> 10^7$ cycles

TABLE 2.1: Coefficients for the API S-N curve tubular sections [9]

For welded joints, improvement factors on fatigue performance can be obtained by a number of methods, including controlled burr grinding of the weld toe, hammer peening, or as-welded profile control to produce a smooth concave profile which blends smoothly with the base metal [9]. The grinding improvement factor is not applicable for joints in seawater without adequate cathodic protection.

Unfortunately no clear distinction is made between the low cycle and high cycle region in the API. The curve for tubular joints subjected to low cycle corrosion fatigue presented in the NORSOK clearly predicts a lower fatigue life than a high cycle corrosion fatigue curve extrapolated into the low cycle region. Questions may be raised on the reliability of the API guidelines in the low cycle region; however, if the general sentiment of the API is completely followed, it is unlikely that low

cycle fatigue will occur because the global design philosophy makes sure structural elements stay within the global elastic range.

2.2 Material Science

The following section contains scientific research papers of the material science world and are not design codes. However, the literature is useful in its own right.

In [10] the authors investigated the effect of strain and the environment on fatigue life in deleterious environments. The authors discovered that fatigue life not only depended heavily on the strain but on the environment as well. The authors tested 5 structural elements. One structural element was tested in open air as a baseline condition. 3 specimen were tested in a solution of 3.5 % NaCl with varying levels of acidity. The acidity chosen were a pH of 0, 3 and 6. A final element was tested in a solution of doubly deionized water with a pH of 3.

The authors found a negative relationship between acidity and the fatigue life. The relationship in a single solution could be well described by the Coffin Manson Relationship [11, 12] . (An interesting observation is that for cyclical elastic loading the coefficients of the Coffin Manson and Basquin relationship are linearly related but this does not hold true for cyclical plastic loading). The effect of the pH did not appear to be linear and was also not modeled. The Coffin - Manson coefficients were separately estimated for each environment. The Coffin Manson relationship is a commonly used method to model low cycle corrosion fatigue in non-deleterious environments ([11, 12]. The Coffin Manson relationship can be seen in equation 2.9 where ε'_f is the fatigue ductility coefficient, c is the fatigue ductility exponent $\frac{\Delta\varepsilon_p}{2}$ is the plastic strain amplitude and $2N$ the number of reversals to failure. The results of the experiments can be viewed in figure 2.11. An interesting finding seems to be that the S-N curves appear to diffract at the lower strain region which means that the environmental effect appears to be stronger in the high cycle region

$$\frac{\Delta\varepsilon_p}{2} = \varepsilon'_f \left(2N\right)^c \tag{2.9}$$
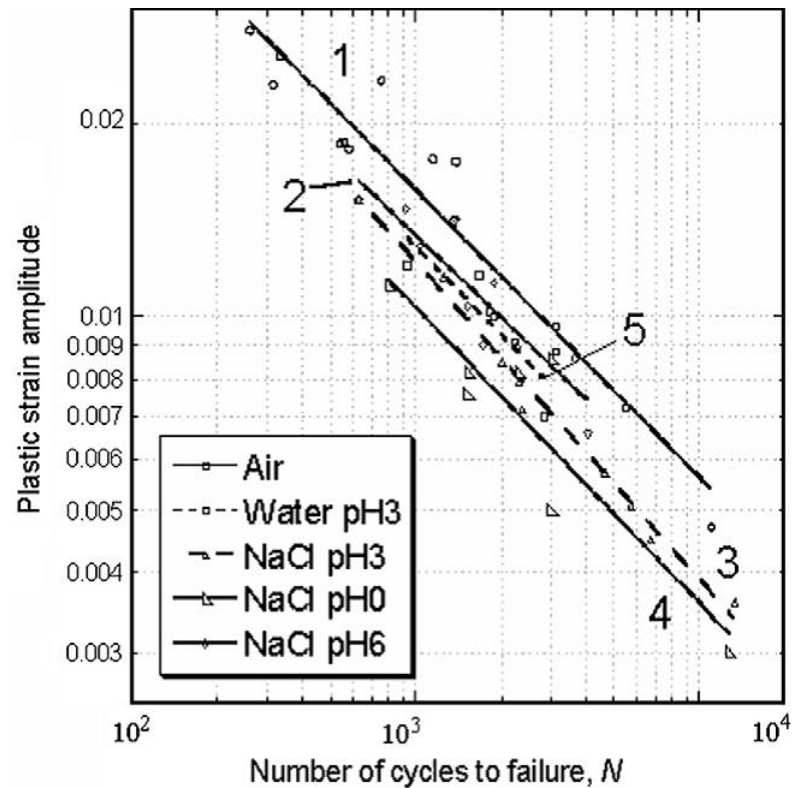
FIGURE 2.11: The strain versus the fatigue life on a logarithmic scale in several
environments. [10]

This research paper [10] is especially useful because it contains data of the fatigue
life versus the strain in a specific environment. The authors of [10] used a 1, 9 mm-
thick specimen of 316L-type cold-rolled sheet steel which can be seen in figure 2.12.
The problem with [10] is that the results are not useful for engineering purposes
because only virgin material has been tested. The weakest parts of structures are
generally the joints. Joints have not been tested.

[13] Showed that the shape and production method (cold rolled, hot rolled) have
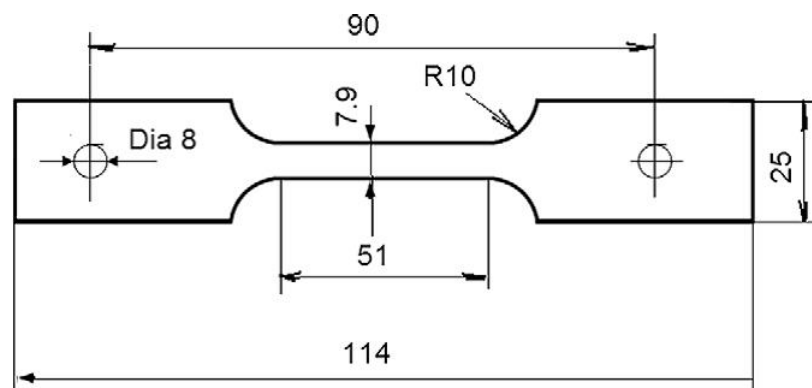an influence on the fatigue behavior of the material as well.

FIGURE 2.12: Dimensions of 1.9 mm-thick specimen of 316L-type cold-rolled sheet steel. [10]

In [14] the effect of strain rate, chemical composition of the specimen and strain was researched. The researchers found results consistent with [10], which is that a negative relationship between strain and fatigue life exists. The authors also found a positive relationship between strain rate and fatigue life. See figure 2.13, 2.14, 2.15. The specimen tested in 3.0 % NaCl also had a shorter fatigue life than specimen tested in air which is consistent with findings in [10]. The relationship between strain and fatigue life could also be modeled exceptionally well with the Coffin-Manson Relationship. The authors of [14] discovered that a lower strain rate leads to a lower fatigue life. The authors of [14] discovered that the effect of strain rate is less pronounced at very low cycle and high strain range region. They discovered that the effect of the environment is more pronounced at lower strain ranges. The authors of [14] also tested a weld and discovered that the fatigue life of welded joints is less than the corresponding base metal which can easily be explained when one considers residual tension and impurities in the welds. Figure 2.15 confirms the suspicion of the author of this thesis that the joints are the weakest parts of a structure subjected to low cycle corrosion fatigue. This research question is considered to be formally answered.
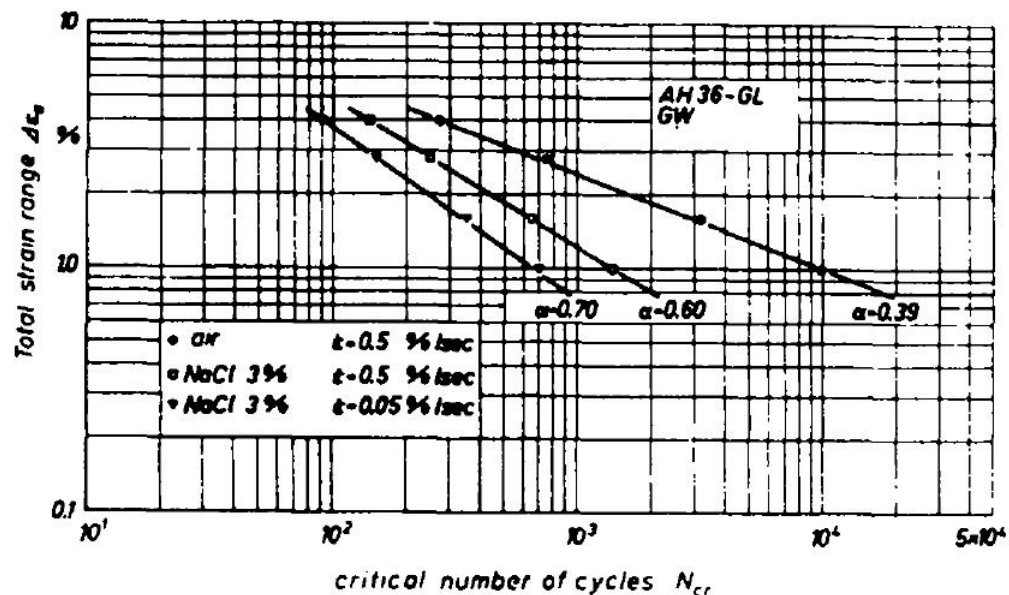

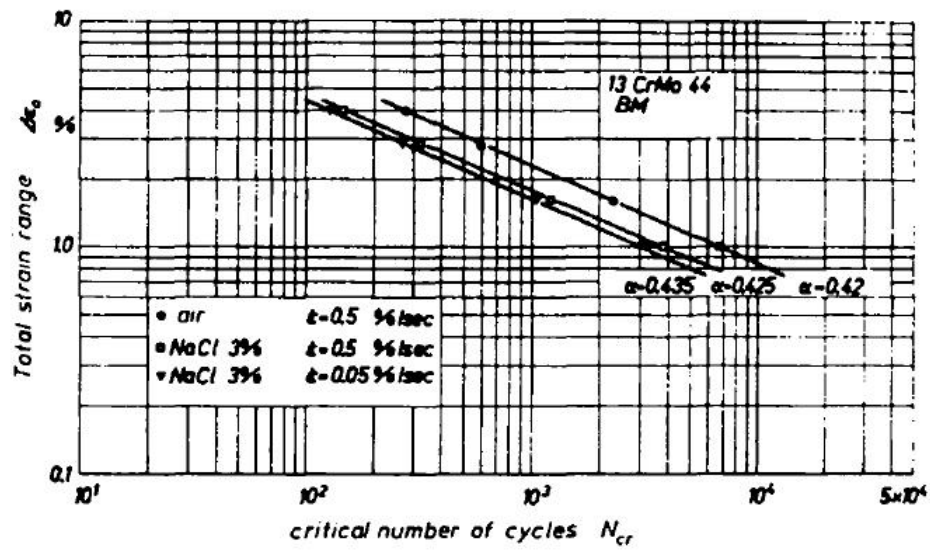FIGURE 2.13: The influence of environment and strain-rate on fatigue life N of base metal AH36-GL steel [14]

FIGURE 2.14: The influence of environment and strain-rate on fatigue life N on the base metal 13 CrMo 44. It appears that the type of base metal affects the fatigue resistence [14]
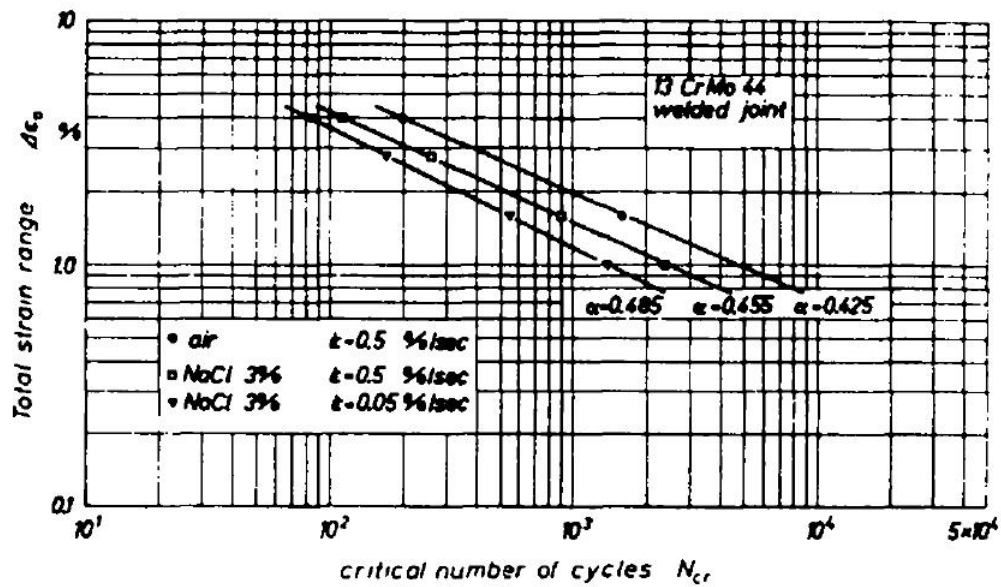

FIGURE 2.15: The influence of environment and strain-rate on fatigue life N of welded joints (13 CrMo 44). [14]

2.3 Boilers and Naval Architecture

Low cycle Fatigue has been a major problem for boiler systems and a plethora of literature for this field has been published. In [15] this has been covered extensively for boilers, however, the problem with these publications for civil engineering is that the tests are generally done for very high temperatures and high pressure environments and these environments are not representative of the North Sea or any typical civil engineering environment. Moreover, the environmental variables are for example, the amount of dissolved oxygen. This is generally not a parameter of interest for civil engineering. However, the paper contains some interesting data.

In naval architecture, low cycle corrosion fatigue has been a problem for a while, however, according to [16] Typical Class Society rules do not directly address low cycle fatigue problems. In [16] the authors attempt to give a credible tool to assess low cycle fatigue in a corrosive environment. The authors formally analyzed the stress strain curve under cyclical plastic loading. This can be seen in figure 2.16. It can be seen that for common ship building materials the cyclic stress strain curve is no longer linear but assumes a logarithmic profile when subjected to cyclical loading. The authors also analyzed the difference between the linear elastic stress and the pseudo elastic stress. This can be seen in figure 2.17. Figure 2.18 shows the test results of [17] and [18] based on a Neuber correction. The specimen used in [18] is shown in figure 2.19 with a longitudinal non-load carrying fillet welds. The design curve in figure 2.18 is plotted for reference. The medium of the pooled TWI and DSME is calculated according to ordinary least squares [16]. The design curve is usually defined as the medium minus two standard deviations. The design curve yields more conservative results. In [17] test data is based on a fatigue experiment of a non-load carrying partially penetrated cruciform fillet joint. This can be seen in figure 2.20. The test was performed under strain control conditions and the strain ratio was set to be zero. This translates into a strain value that fluctuates between zero and a specific maximum value.

[17] also found material coefficients K' and n for ship building materials which are to be used in the Ramberg-Osgood relationship combined with Neuber's rule. The material coefficients are given in 2.2. These coefficients allow for calculation of the hot spot stress under cylical plastic loading as mentioned before.
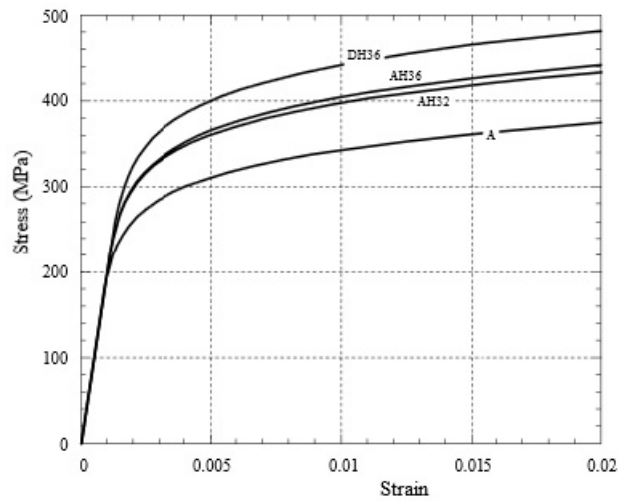
FIGURE 2.16: Cyclic stress strain curves for several ship building materials [16]
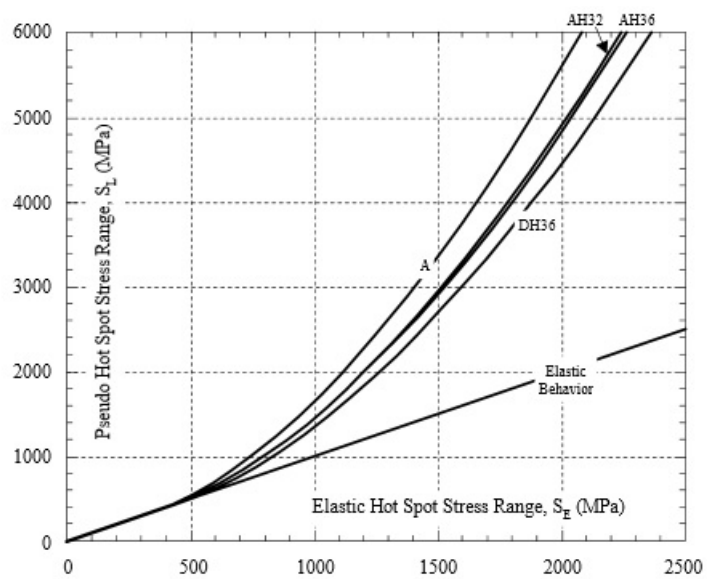

FIGURE 2.17: Psuedo elastic stress vs linear elastic stress ship building materials [16]
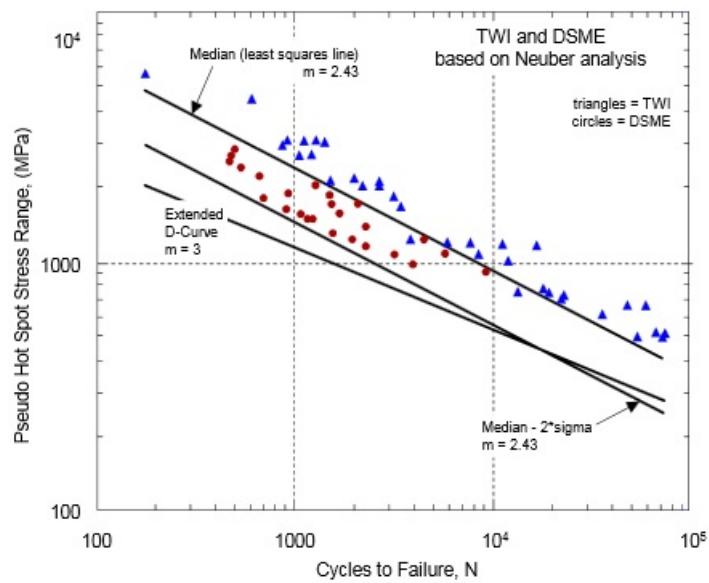
FIGURE 2.18: Low cycle fatigue S-N curves and real tests results [17] and [18]
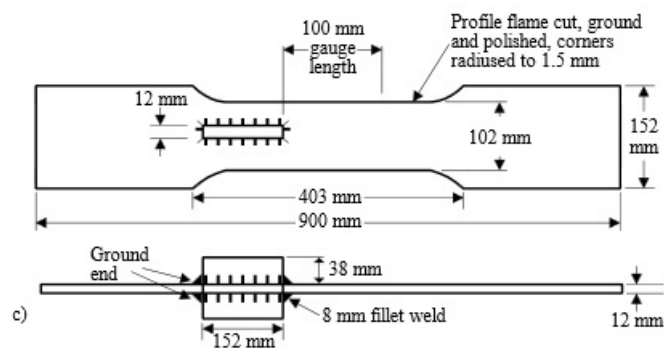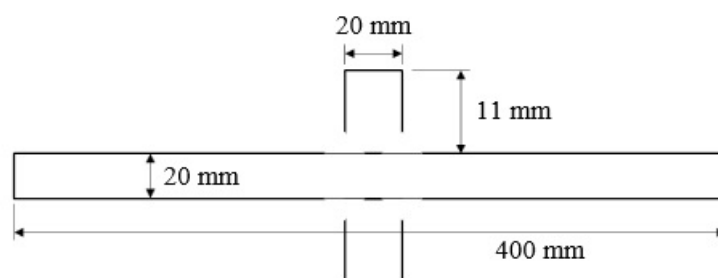

FIGURE 2.19: Low cycle fatigue specimen [18]

FIGURE 2.20: Low cycle fatigue specimen [17]

Material	A	AH32	AH36	DH36
K' (MPa)	592	669	694	739
n	0.114	0.108	0.112	0.106

TABLE 2.2: Material coefficients n and K' [17]

2.4 Crack progagation

The previous sections only focused on fatigue life N. However, there is another interesting aspect of low cycle corrosion fatigue, which is low cycle corrosion fatigue crack propagation. The most popular fatigue crack model used in material science and fracture mechanics is the Paris-Erdogan law [19]. This can be seen in equation 2.10, where ΔK (MPa m$^{\frac{1}{2}}$) is the range of the stress intensity factor and C and m are material constants (regression coefficients). $\frac{\partial a}{\partial N}$ is the crack growth rate. The number of publications that can be found on crack propagation for steels that are frequently used in civil engineering and are also subjected to low cycle corrosion fatigue is very meager. There is a very old publication [20] which showed that Monel 400 and Monel k-500 alloys subjected to low cycle corrosion fatigue displayed a much larger crack propagation rate than they would have shown if subjected to high cycle corrosion fatigue. More importantly it was shown that the crack propagation rate could be modeled quite well with the Paris-Erdogan law. The literature available for crack growth rate in steels subjected to high cycle fatigue is numerous. For high cycle fatigue it appears in both [21] and [22] that crack propagation is affected by the environment. This can be seen in figure 2.21. The crack growth is higher in a corrosive environment than in air. Unfortunately there is not much literature for low cycle corrosion fatigue crack propagation

$$\frac{\partial a}{\partial N} = C\Delta K^m \tag{2.10}$$

2.5 Conclusions

The first message of the literature review is that low cycle corrosion fatigue for offshore structures has been mostly neglected because the structures are designed with a global elastic philosophy. However, low cycle corrosion fatigue may become an issue when an offshore structure is loaded by a storm. A second message is
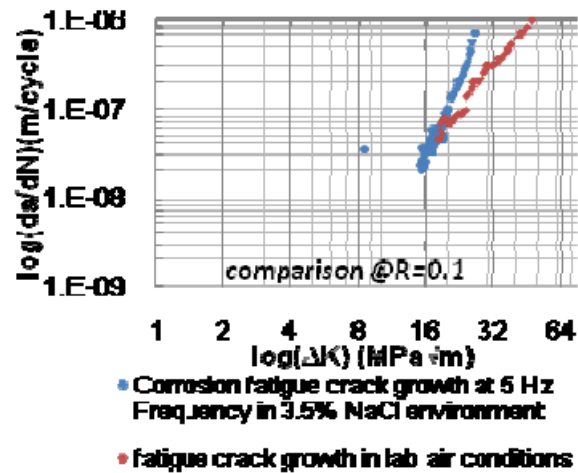
FIGURE 2.21: Crack growth of steel in a deleterious electrochemical environment compared with an environment in air. Notice that the crack growth rate is larger in the deleterious environment. [22]

that tubular joints are the most commonly used joints in offshore structures. A third message is that the effect of the environment becomes more pronounced at the high cycle range and deteriorates in the low cycle range. Fourthly, it appeared that low cycle corrosion fatigue life depends on the type of deleterious solution, strain rate, structure type and material type. Finally, it appeared that welds are the weakest parts of the structure to low cycle corrosion fatigue.

Chapter 3

Low Cycle Corrosion Fatigue Defined

In this chapter the author will discuss general aspects related to low cycle corrosion fatigue. The boundary between LCF and HCF is rather ambiguous. There is no solid consensus on where this boundary actually is. The author will also discuss some findings about HCCF, such as fatigue life improvement techniques, found in [21] and how they may be also applicable to LCCF. The author will then delve deeper into environmental aspects such as pH and oxygen concentration and it will be discussed how these issues affect the fatigue life. Finally there will be part about the static and dynamic analysis of structures that experience cyclic plastic loading and how ignoring changes in material properties of elements subject to LCF can the affect static and dynamic equilibrium assessment of structures.

3.1   Low Cycle Region

The fatigue life N that forms the boundary between low cycle fatigue and high cycle fatigue is arbitrarily defined. The boundary is set at 100.000 in the NORSOK [6]. This same boundary is set at 40.000 cycles by [2]. The boundary of 10.000 cycles is also frequently used. In [10] the authors informally set the boundary at 10.000 cycles. Furthermore, many design codes limit the images of their S-N curves to the 10.000 cycle boundary.

It is the hypothesis of the author that the boundary between high cycle and low cycle fatigue is actually the fatigue life of a structure when it experiences significant local yielding. Quantifying what significant local yielding in the micro structure of the cross section is has never been performed.
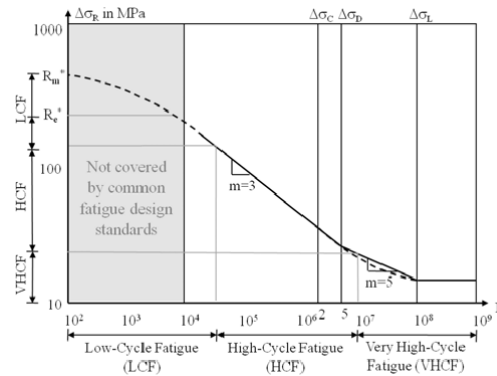

FIGURE 3.1: The different type of fatigue regions with the most common slopes m [2]

To illustrate what is meant by significant local yielding, have a look at figure 3.2. The plate can be cyclically loaded in tension by two sides and globally not yield, however, as soon as local yielding of the weld occurs in significant quantities to promote micro-crack coalescence due to cyclical loading, the structure will experience low cycle fatigue. The author expects this boundary to be at approximately 10.000 cycles. The point at which significant local yielding will occur depends on the specifications (quality) of the welded connection. Virgin material tends to have this 10.000 cycle boundary near global yielding of the material. This is illustrated in figure 3.3. Contrary to connections, which experience their significant local yielding point much sooner, which has been illustrated in figure 3.4. To enhance the problem even further, cyclical loading of yielding structures gives a much higher strain than cyclical loading of structures in the linear elastic region. This was previously illustrated and can be seen in figure 3.5. This higher strain can eventually lead to micro fractures and rapid failure (in less than 10.000 cycles).
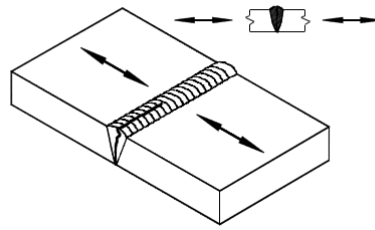
FIGURE 3.2: Single side Butt Weld made from one side without back strip [5]
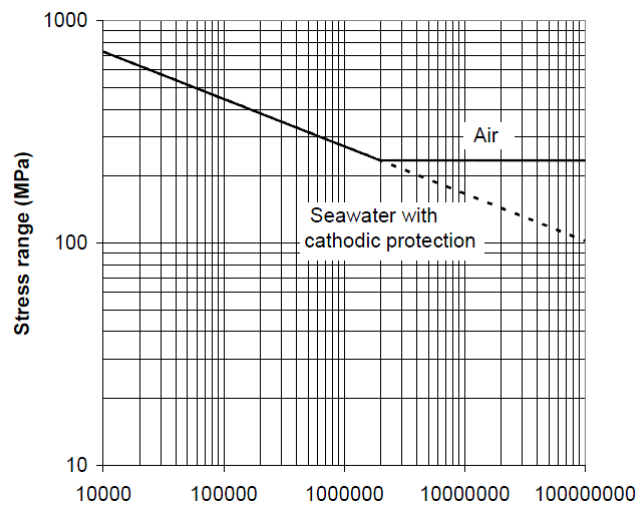

FIGURE 3.3: High cycle S-N curve base material high strength steel [5]
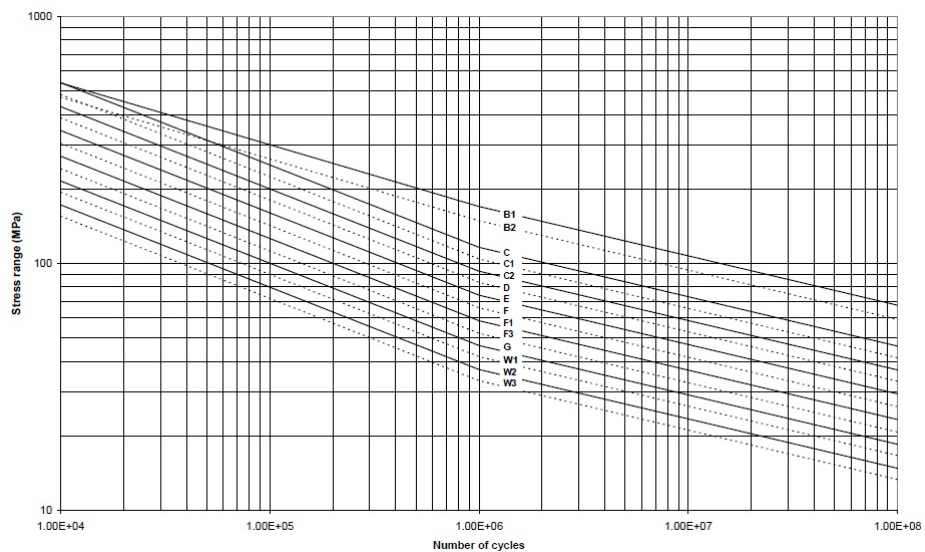
FIGURE 3.4: High cycle design S-N curve for different joints with cathodic protection in seawater in the DNV. Notice that the point at which the 10.000 cycles boundary is crossed varries heavily with the connection type. [5]
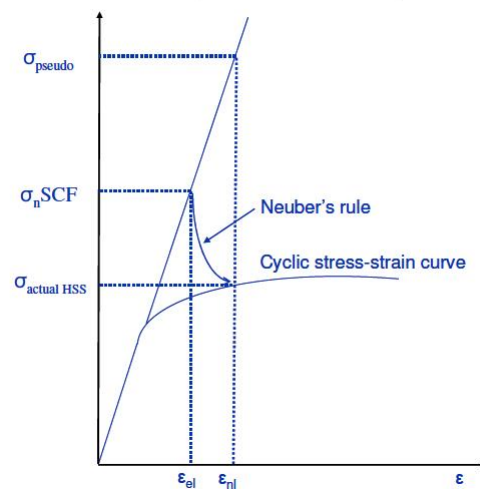
FIGURE 3.5: The pseudo elastic stress strain diagram versus the Cyclic stress strain diagram. A stress on the cyclic stress strain diagram corresponds to a much larger strain than on the elastic stress strain diagram [6]

3.2   Fatigue Parameters

Fatigue Improvement effects There are several ways to improve the fatigue life. One method is grinding. According to [21] grinding appeared to have a very strong favorable effect on fatigue life in the high cycle region in seawater. Specimen that were subjected to grinding had a fatigue life in the high cycle region that is approximately 2 times more than normal specimen. Another aspect that seems to improve fatigue life is TIG dressing. However, the effect of TIG dressing seems to be favorable only in short lives [21]. Another strong improvement is plasma dressing. The plasma dressing in high cycle corrosion fatigue in [21] appeared to increase the fatigue life in seawater by a factor 2. Changing the weld angle from 70 degrees to 45 degrees didn't seem to have a significant favorable effect for high cycle fatigue. These changes were only studied for high cycle fatigue but there is reason to believe that they are also applicable to low cycle fatigue but it's not known to which extent.

Post-Weld Heat Treatment & Stress Ratio In the elaborate study done in [21] it was found that stress ratio and heat treatment seem to be related. The authors found that stress relieving due to heat treatment has a very strong favorable effect on high cycle fatigue life in air. This effect is also dependent on the stress ratio R. The authors found that an R of -1 leads to a higher high cycle fatigue life than an R of 0.1. The authors also made the interesting discovery that in seawater heat treatment seems to be quite marginal or perhaps even negligible. The authors attribute this to a more detrimental effect of seawater on the fatigue life of a stress relieved specimen. These findings may also be applicable to low cycle fatigue. However, it's the hypothesis of the author that stress relieving may have a more favorable effect at high strain low cycle region. There is no data to verify this. In [21] it was also found that a stress ratio of 0.1 leads to a lower fatigue life than an R of -1. This is probably also true for low cycle fatigue.

Weld Metal Composition According to [21] the type of metal used for welding doesn't matter. Two makes of 2.5 % Ni-alloyed electrodes of different makes were used. There appeared to be no clear difference in fatigue life for tests done in both seawater and air. There is reason to believe that this may also not matter in low cycle fatigue but there is no data for it.

3.3   Corrosion

In the context of this thesis corrosion a reaction between iron and oxygen. In nature most metals, including iron, will be in an oxide form. It actually takes energy to remove the base element from its oxide form. Steel contains the base element iron Fe. The potential with respect to Cu.CuSO$_4$ is between -500 mVolts and -800 mVolts. An element that will accept electrons is called a cathode and the element that loses electrons is called an anode. During corrosion iron (anode) loses electrons to a cathode (e.g. copper). This cathode can be anything with a lower potential, even iron itself (the potential in the steel grid can also vary), however, it may also be an adjacent element like copper which has a very low potential -200 mVolt. This makes copper a very strong cathode. In order to get corrosion you need a conductor between the two elements in which electrons can pass, an electrolyte (also called a salt bridge) , an anode and a cathode. The reactions that take place are the following. Iron loses electrons Fe$\rightarrow$ Fe^{2+} + 2 e$^-$. At the cathode the free electrons can react with oxygen and water O$_2$ + 4 e$^-$ + 2H$_2$O$\rightarrow$ 4OH$^-$. From this reaction it can be seen that oxygen is a key indicator in the corrosion process. The positively charged iron will then react with oxygen through 4 Fe^{2+} + O$_2\rightarrow$ 4Fe^{3+} + 2 O^{2-}. There are now two types of iron in the solution Fe^{2+} and Fe^{3+}. These will react with water to form ferrous-hydroxide. This occurs though Fe^{2+} + 2 H$_2$O$\rightleftharpoons$ Fe(OH)$_2$ + 2 H$^+$ and Fe^{3+} + 3 H$_2$O$\rightleftharpoons$ Fe(OH)$_3$ + 3 H$^+$. Finally the hydration equilibrium takes place through Fe(OH)$_2\rightleftharpoons$ FeO + H$_2$O , Fe(OH)$_3\rightleftharpoons$ FeO(OH) + H$_2$O and 2 FeO(OH)$\rightleftharpoons$ Fe$_2$O$_3$ + H$_2$O. The red brownish color substances are hydrated iron(iii)oxides Fe$_2$O$_3\cdot$nH$_2$O and iron(iii) oxide-hydroxide FeO(OH)$\cdot$Fe(OH)$_3$. In essence what these reactions do is cause the structural element to slowly lose mass because the products of these reactions are soft and are easily scratched off. This process can go rather quickly in the presence of sufficient oxygen.

3.4   Cathodic Protection

The principal idea behind cathodic protection is to make the structural element serve as a cathode and not an anode. This can be achieved by firing many electrons at the structural steel element so its potential stays high and electrons cannot leave. If electrons cannot leave the element there can be no reaction of Fe^{2+}

because it simply isn't formed. There are a variety of systems that can achieve this, such as galvanic sources. This system involves simply coating the material in an element that can serve as a anode for structural steel. Theoretically this is not cathodic protection because the reactions will only take place after the coating is damaged at an area. Remember you need an electrolyte between the anode and the cathode. This is not the case if the zinc coating is over the steel because the cathode is completely covered. However, if the area is damaged cathodic protection can activate because the zinc coating will serve as the anode for the damaged area of exposed steel. Therefore the steel will not corrode if the area of damage isn't too large. Another system of cathodic protection is an immersed system, which involves application of a power source to the conductor between the anode and the cathode. This system has many advantages and is endorsed by the author because it has a very high reliability. Contrary to galvanic systems, immersed systems can be checked if still operational.

In the literature review the phrase "adequate cathodic protection" was used. There are many ways this can be interpreted but the design value according to the DNV is -0.80 Volt. This can be found in Recommended Practice DNV-RP-B401 [23]. In case the reader is unfamiliar with cathodic protection and its fundamentals it's advised to read [24]. Cathodic protection of around -900 mVolt is enough to stop carbon steel from losing electrons for a significant amount. In [21] it was found that cathodic protection is most effective at lower stress ranges. Overprotection on the other hand revealed an unfavorable effect on the fatigue life compared to regularly protected specimen. However, overprotection still performs superiorly to no cathodic protection at all. Overprotection occurs at approximately 1100 mVolt.

3.5 Effect pH on Corrosion

The Potential of hydrogen or pH is by definition the negative logarithm of the concentration of H^+. This can be calculated with $pH=-\log[H^+]$ in which the concentration $[H^+]$ is in mol/liter. The corrosion rate, which is defined as depth/time on a corroding surface is dependent on the pH. The corrosion rate of steel explodes when the pH level drops below 4.0. This can be seen in figure 3.6 The molecule FeO becomes soluble which means that post its formation on the corroding surface it is immediately dissolved in the solution. If it had stayed on the corroding surface

it would serve as some sort of a protective barrier against further corrosion deeper into the surface of the corroding metal [25]. In a solution with a pH less than 4 the corrosion rate also no longer depends on just depolarization of oxygen but also on hydrogen evolution. At pH values above 10 the corrosion rates starts dropping to virtually zero which is due to the reaction of oxygen $Fe(OH)_2$ in the oxide layer to form more protective Fe_2O_3. The pH of the North Sea tends to fluctuate between 7.5 and 8.4. This means that pH the North Sea is not a parameter that one should worry about when designing offshore structures with respect to low cycle corrosion fatigue life. Furthermore, you cannot influence the pH of the North Sea in any reasonable way.
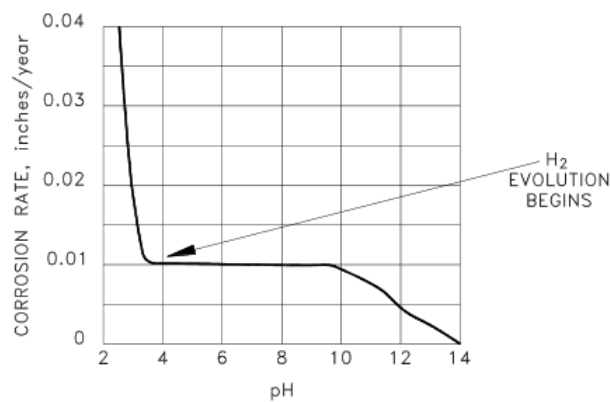

FIGURE 3.6: The corrosion rate of steel is dependent on the pH. The critical levels are at pH values below 4.0 [25]

3.6 Temperature, Oxygen & Chlorine

$[O_2]$ and temperature are negatively correlated. However, the $[O_2]$ and temperature are both positively correlated with corrosion rate. An example of the effect of dissolved oxygen (DO) and temperature can be seen in figure 3.7. Figure 3.7 doesn't give the complete story because temperature actually reduces oxygen solubility but it does allow for easier diffusion of O_2 into the $Fe(OH)_x$ layer, which effects the corrosion rate because oxygen can then reach the unaffected metal. At a certain temperature a tipping point will be reached and an increasing temperature will lead to a declining corrosion rate but this is irrelevant for a North Sea environment because this temperature is very high. The temperature of the North Sea spans between $6\,°C$ and $17\,°C$. In this range it can be seen in figure 3.7 that the temperature is positively correlated with corrosion rate. Another aspect which

might matter is the depth. An increase of the pressure will lead to an increase of the oxygen solubility which will lead to more corrosion. Furthermore, the oxygen solubility is also affected by the concentration of NaCl. For a concentration of 3,5 % NaCl the oxygen solubility is less than in fresh water.

Furthermore, there is the issue of pitting. This is localized corrosion on a small surface area where the formed ferrous-hydroxide passivation layer has been depassified (This may not even be visually noticable). This area becomes an anode and a cathode nearby will induce a current. In this area there will be large concentration of Cl^- ions and ferrous hydroxide products will form (corrosion products) and H^+ ions. The pH in this area may drop below 4. You can see that this is the danger zone in figure 3.6. Pits are particularly attractive to brittle micro-crack formation due to stress concentrations that may form around their irregular geometry. This phenomenon is referred to as stress corrosion cracking and is a topic in its own right and it will not be discussed further.
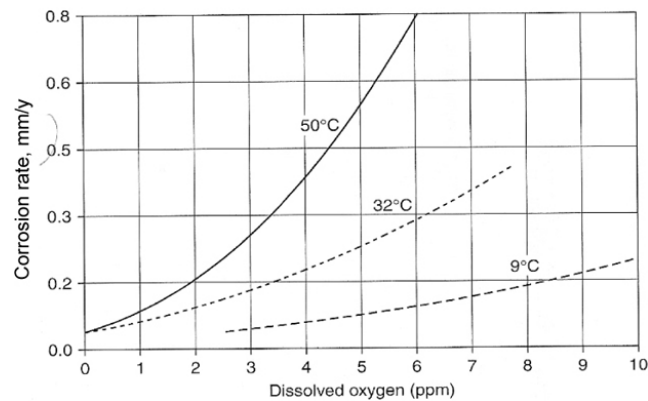

FIGURE 3.7: Corrosion rate depends heavily on the temperature and concentration of dissolved oxygen in the liquid [26]

3.7 Static and Dynamic Analysis

Structures are analyzed for both external and internal static equilibrium. The models used for the analysis of stresses in structures that are based on linear elastic mechanics are principally wrong if a structure experiences cylical plastic loading. The reason is that the behavior of a structural element that experiences low cycle fatigue no longer possesses a linear elastic stress-strain diagram and the yielding stress is reduced. The micro structure of a steel specimen fundamentally changes.

The regular linear elastic stress strain and cyclic stress strain diagram were given in figure 3.5. The cyclic elastic stress strain diagram is fundamentally different. This fundamentally different cyclic stress strain diagram is the result of a stabilized hysteresis loop. This process is illustrated in figure 3.8. It can be seen that the stress at which the behavior becomes non-linear is reduced. The material can behave in a variety of ways in case it is cyclically loaded beyond the elastic limit. This is illustrated in figure 3.9.
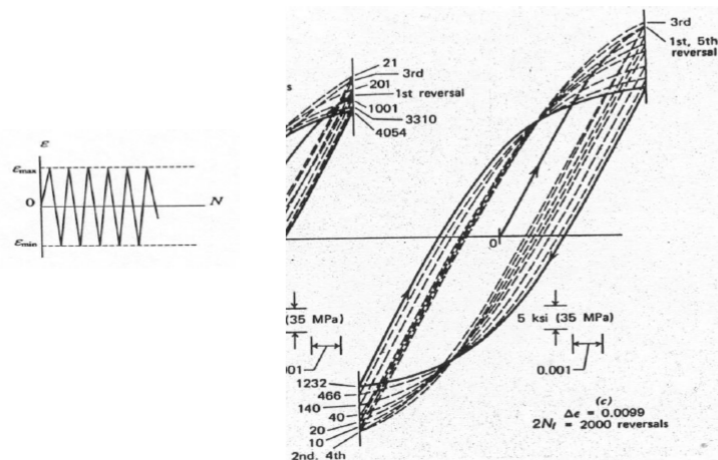

FIGURE 3.8: Hysteresis loop of partially annealed copper. It can be seen that the load bearing capacity goes down due to cyclic plastic loading. [27]

In case monotonic material properties are used for the calculation of dynamic stability or static equilibrium serious mistakes could be made for the plastic strain if the structure has been subjected to low cycle fatigue. The low cycle fatigue strain can be calculated with the well known Ramberg Osgood relationship [28] given in figure 3.10. The Ramberg Osgood relationship can be seen in equation 3.1. The σ can be calculated with equation 3.2. The value n is an indication of
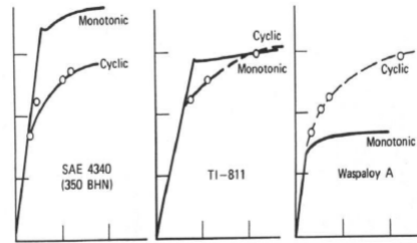
FIGURE 3.9: Stabilized stress strain curve under cyclic loading. [27]

the material's work hardening behavior. It is the slope of the regression in figure 3.11. The K and n for some engineering alloys are given in the Appendix. The E is the Young's modulus for linear elastic behavior.
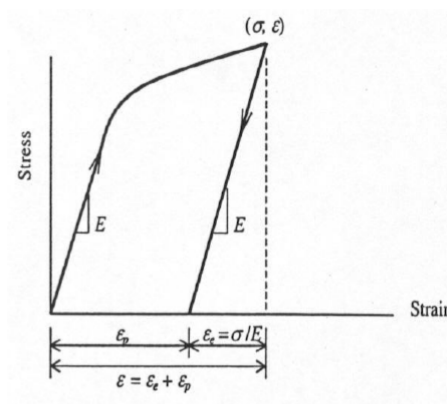

FIGURE 3.10: Stabilized stress strain curve under cyclic loading [27]

$$\varepsilon = \varepsilon_e + \varepsilon_p = \frac{\sigma}{E} + \left(\frac{\sigma}{K}\right)^{\frac{1}{n}} \tag{3.1}$$

$$\sigma = K(\varepsilon_p)^n \tag{3.2}$$

Notice: These facts should not be forgotten. Usually a structure is checked for static equilibrium and fatigue life separately. This can cause a serious underestimation of the strain in a structure ! The load bearing capacity could also be heavily overestimated. A structure may therefore have a much higher failure probability than is acceptable.
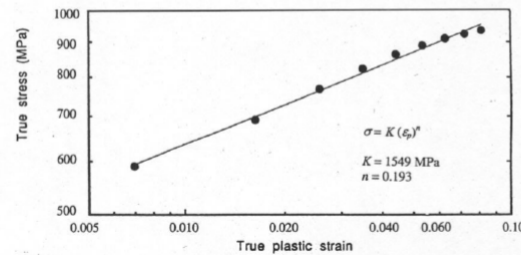
FIGURE 3.11: The true plastic strain is plotted versus the the true stress. This is a loglinear relationship according to Ramberg Osgood. The value n is the slope of the line and the strength coefficient K is the intercept at $\varepsilon = 1$ [27]

3.8 Conclusions

What can be learned from this chapter is that the low cycle region has no formal definition. The author has the hypothesis that this boundary is defined as fatigue life of a cross section that experiences significant local yielding. It is the hypothesis of the author that the fatigue life N will be at approximately 10.000 cycles when "significant local yielding" is experienced by a cross section. Quantification of "significant local yielding" in the micro structure of the cross section has never been performed. Low cycle corrosion fatigue is a complex interaction between two hazardous mechanisms, corrosion and crack formation in structural members. There have been several studies done for high cycle corrosion fatigue and in these studies it has been revealed that techniques such as grinding and post-weld heat treatment can prolong the fatigue life. There is no reason to believe that this is not also applicable to low cycle fatigue but its unknown to which extent. The pH is an influential parameter on corrosion rate but the corrosion rate appears to be constant between a pH of 4 and 10. The pH in the North Sea is approximately between 7,5 and 8,4 which means that the rate of corrosion in a regular North Sea environment will be independent of the pH. The temperature does appear to be quite an influential parameters on the corrosion rate in a North Sea environment. The S-N curves from experimental data should therefore be constructed in environments with a temperature of at least the maximum temperature of the North Sea. It should also be noted that low cycle fatigue is a complicated loading condition that changes the behavior of the material in a fundamental way. It will affect the load bearing capacity in even a static sense. This should not be forgotten when analyzing structures that are subject to wide ranges of cyclic plastic behavior due to cyclical loading.

Chapter 4

Environmental Effect Fatigue Life

An interesting observation in Chapter 2 was that the effect of the environment diminishes in the LCHS region. In this chapter the author will investigate this phenomenon. The goal is to discover if a low cycle corrosion fatigue problem becomes a general low cycle fatigue problem. In case it can be shown that a LCCF problem becomes a LCF problem, it is interesting to find out at which point (stress range or strain range) that this may occur. In the event that one can figure out a certain turning point it will allow an engineer to use general low cycle fatigue data such as S-N curves to solve LCCF problems. This objective will be achieved by analyzing LCCF curves and LCF curves and studying the difference. An observation in Chapter 3 was that the stress range in which a type of connection enters the low cycle (< 10.000 cycles) depends on the structure. Base material that meets the right criteria can enter the low cycle region at virtually the yielding stress. This phenomenon will also be elaborated upon in this chapter.

4.1   Environmental Impact Design Codes

In [6] the curves in equation 4.1 and 4.2 were reported for LCF in air and LCCF in seawater with cathodic protection. A plot of the curves is given in figure 4.1. It can be observed in figure 4.1 that tubular sections in air have superior fatigue lives under a given stress range than tubular sections with cathodic protection in seawater. The SN-curves for tubular sections in seawater with cathodic protection and tubular sections in air are plotted in figure 4.2 on a logarithmic scale. The differential between the fatigue life N of LCF and LCCF increases with decreasing

stress range. This means that the fatigue life difference between LCCF and LCF becomes larger as the stress range is lowered. This has been plotted in figure 4.3. In this figure you can see that difference in fatigue life between tubular sections with cathodic protection in seawater and tubular sections in air increases as the stress range decreases.

$$logN_{air} = log19.\bar{4}05 - 5.834log\Delta\sigma \tag{4.1}$$

$$logN_{seawater} = log16.\bar{0}84 - 4.927log\Delta\sigma \tag{4.2}$$
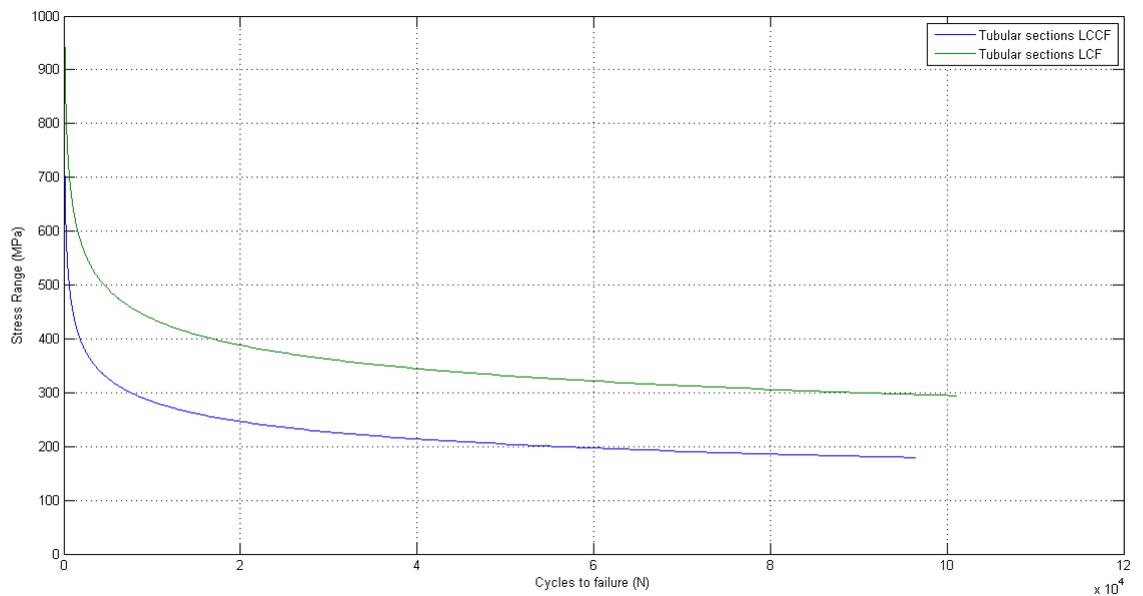
FIGURE 4.1: LCCF and LCF for tubular sections. Notice that the fatigue life converges as the stress range increases [6]

According to [6] low cycle fatigue is typically less than 100.000 cycles but this boundary is arbitrary. Low cycle fatigue can be defined as the point when a material is subjected to plasticity due to cyclical loading. It was established in chapter 3 that it is the hypothesis of the author that "significant local yielding" coincides with a fatigue life of 10.000 cycles.

A connection is well in the low cycle fatigue region far before reaching global plasticity. This means that in theory the connection should still be in the linear-elastic zone of the stress strain diagram when it crosses into the low cycle zone.
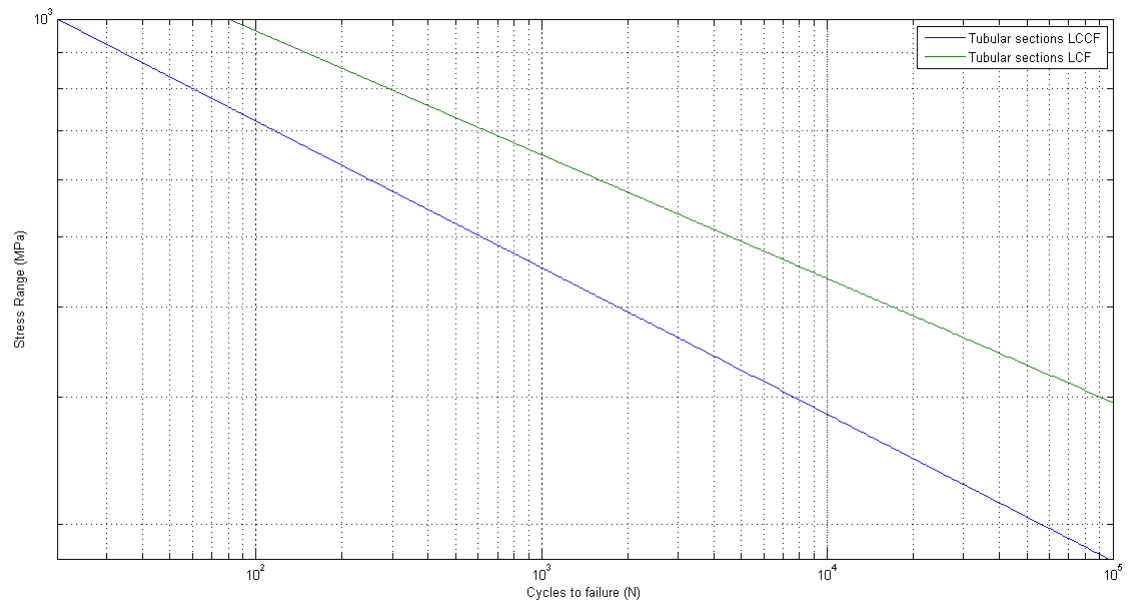
FIGURE 4.2: LCCF and LCF for tubular sections on a logarithmic scale. Notice that the fatigue life converges as the stress range increases
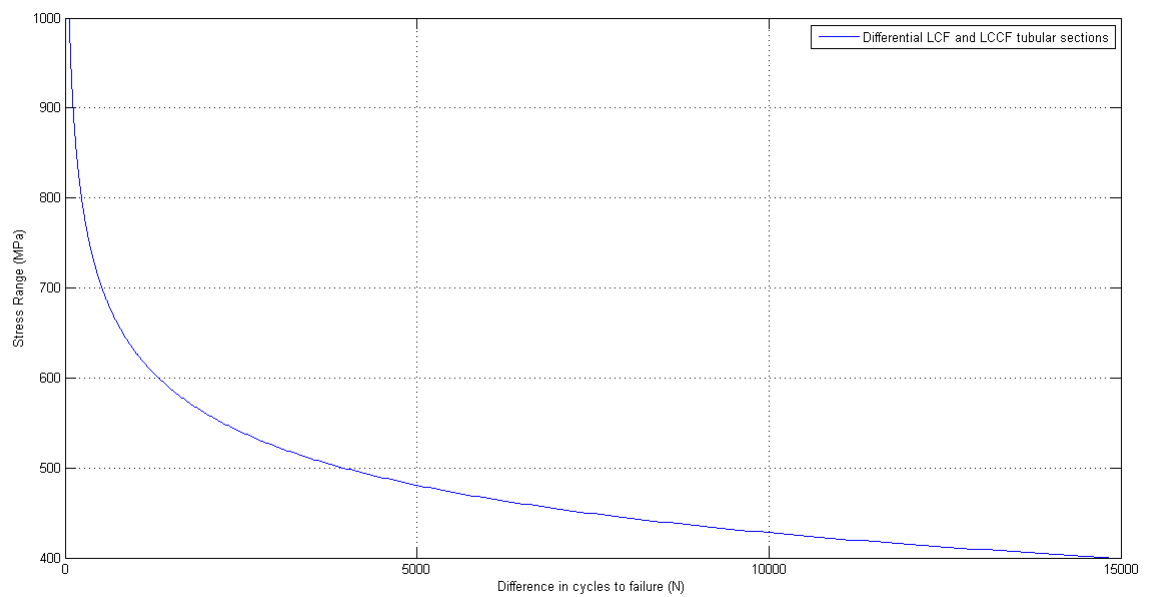

FIGURE 4.3: Differential LCCF and LCF tubular sections. Notice that with decreasing stress range the difference in fatigue life increases. The effect of the environment appears to be diminishing in the low cycle range

However, it's the hypothesis of the author that connections cross into the low cycle zone earlier due to residual tension in the connection. The amount of residual tension depends on the type of connection and the welding method. It appears that base material of high strength steel with a yield strength above 500 MPa and a surface roughness equal to R_a of 3,2 or superior crosses into the low cycle zone (10.000 cycles or less) at approximately the yield stress. This can be seen in figure 4.4. It can also be seen that the fatigue life of base material is superior to any type of connection. It can also be seen that the fatigue life for base material in air or base material with cathodic protection coincides for an N of less than $2 \cdot 10^6$ cycles. Furthermore, it does appear that base material appears to have an endurance limit in air but this limit is not present for base material with cathodic protection in seawater.
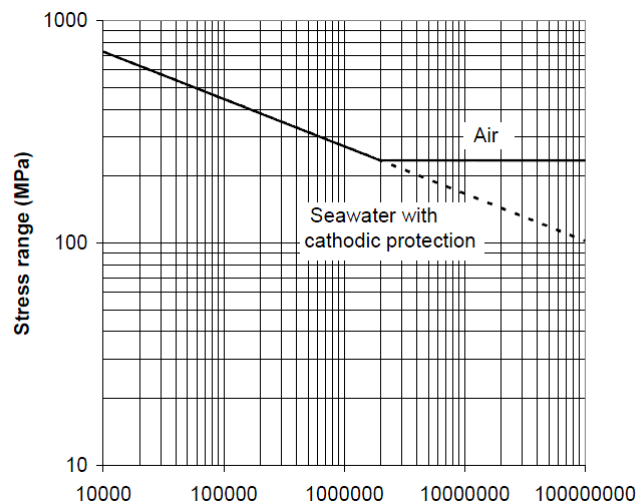

FIGURE 4.4: S-N curve for base material. The fatigue life for base material in air coincides with the fatigue life for base material with cathodic protection in seawater. It also appears that sections in air have an endurance limit but sections with cathodic protections in seawater have no such limit. [5]

In [6] it was claimed that the S-N curves reported in figure 4.1 coincide with the high cycle fatigue curve for tubular sections. The author checked this claim and it proved to be more or less true. The difference was only marginal. The author performed a check by calculating the stress an element can withstand at 100.000 cycles with both the low and high cycle equations. This stress was not completely equal but came very close. This validates the claim of [6].

It appears in figure 4.1 that the fatigue life of element with cathodic protection in seawater is always less for tubular sections than the fatigue life in air (in general

this appears to be true for all types of connections but not necessarily true for base material. Figure 4.4).

In figure 4.1 the design value ($\mu(\Delta\sigma) - 2\sigma$) of fatigue life is reported. When one examines the 2,5 % probability of non-exceedence it's better to use the expected value of the S-N curve reported in 4.5. Examination of the figure 4.5 revealed that at around 500 MPa the LCF in air and the LCCF is approximately similar. This is caused by the logarithmic relationship between the variables stress and fatigue life.
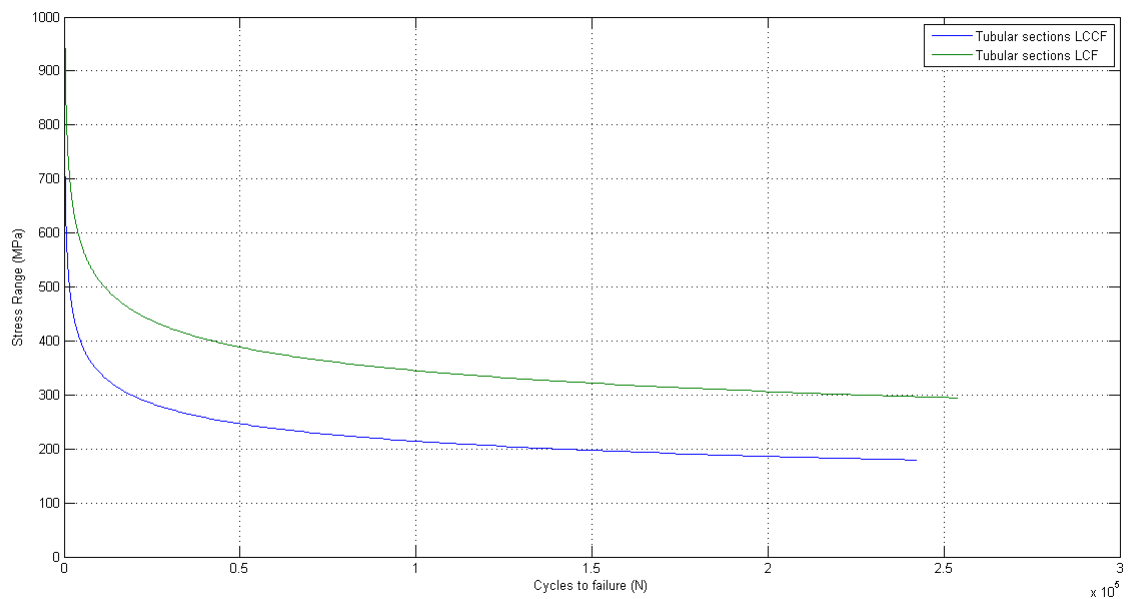
FIGURE 4.5: Expected value of fatigue life LCCF and LCF for tubular sections[6]

To illustrate this phenomenon the author will investigate the number of cycles and its confidence interval at a stress range of 500 MPa where visual inspection of figure 4.5 reveals little discrepancy between LCF and LCCF. The number of cycles that a specimen can withstand are calculated with equation 4.3 and 4.4.

$$X_1 = logN_{seawater} = 16.084 + 0.4 - 4.927 \ log500 = 3.586 \tag{4.3}$$

$$X_2 = logN_{air} = 19.405 + 0.4 - 5.834 \ log500 = 4.459 \tag{4.4}$$

Both variables are normally distributed which means that their difference is also normally distributed. The variance of the difference is the sum of both individual variances given independence. The covariance of independent variables is zero. $X_3 = X_2 - X_1 = 4.459 - 3.586 = 0.960$. $Var(X_3) = Var(X_1) + Var(X_2) = 0.2^2 + 0.2^2 = 0.08$. The probability that X3 is less than zero is the probability that low cycle fatigue in air will fail before low cycle fatigue in seawater with cathodic protection. The probability that X_3 is smaller than zero can be calculated with equation 4.5. The probability that X_3 is less than zero is 0.00033172355. This reveals that even in the LCHS region the probability that the environment plays no significant role is extremely low.

$$Pr(X_3 < 0) = \Phi \left(\frac{X_3{}^2}{Var(X_3)} \right) \tag{4.5}$$

In figure 4.3 the differential between the low cycle fatigue life in air and low cycle fatigue life in seawater with cathodic protection was plotted. It would be interesting to see if the environmental impact depends on the type of connection or not. In case the environmental impact (difference between corrosion fatigue life and fatigue life) is independent of the type of connection it would eliminate the need for special low cycle corrosion fatigue curves because the environmental impact can just be subtracted from low cycle fatigue curves. The differential has been plotted in figure 4.6 and figure 4.7. It can be seen that the environmental impact depends on the type of structure and stress range. This could also have been anticipated from a previous hypothesis of the author which states that time is an element in environmentally assisted fatigue. This disables any opportunity of simply subtracting environmental impact from low cycle S-N cuves based on the environmental impact from a single structure. This means that the environmental impact should be separately tested for each type of connection. Another interesting observation can be seen in figure 4.8 and figure 4.9. It appears that just like in LCCF the impact of the environment increases as the stress range decreases.
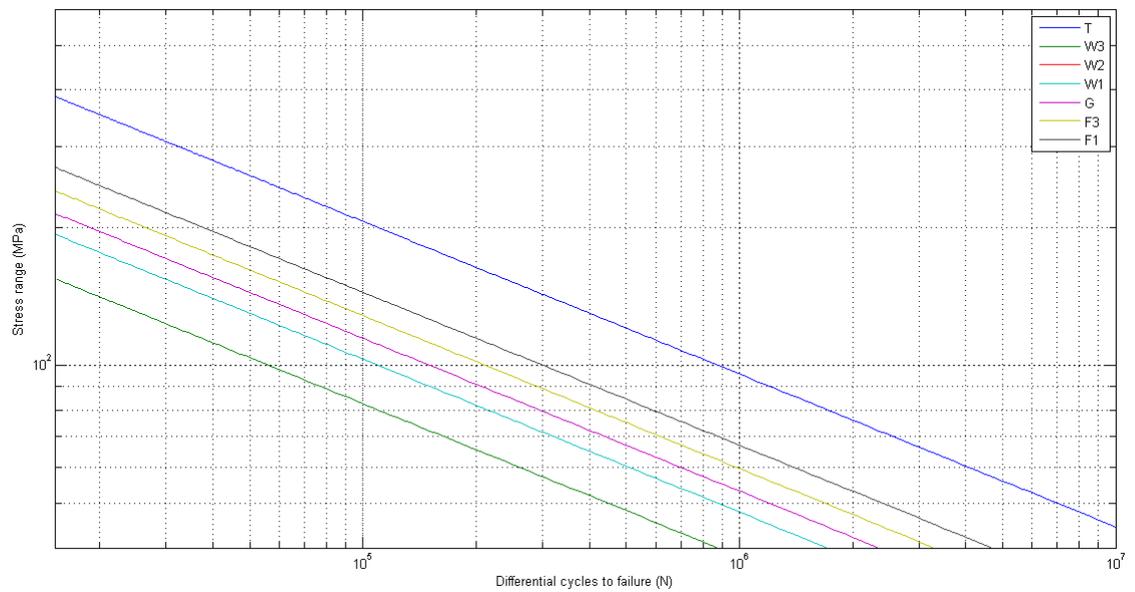
FIGURE 4.6: Logarithmic differential between the HCCF and the HCF for a given stress range for several types of connections. Notice that the environmental impact depends not only on stress range but also on connection type [6]
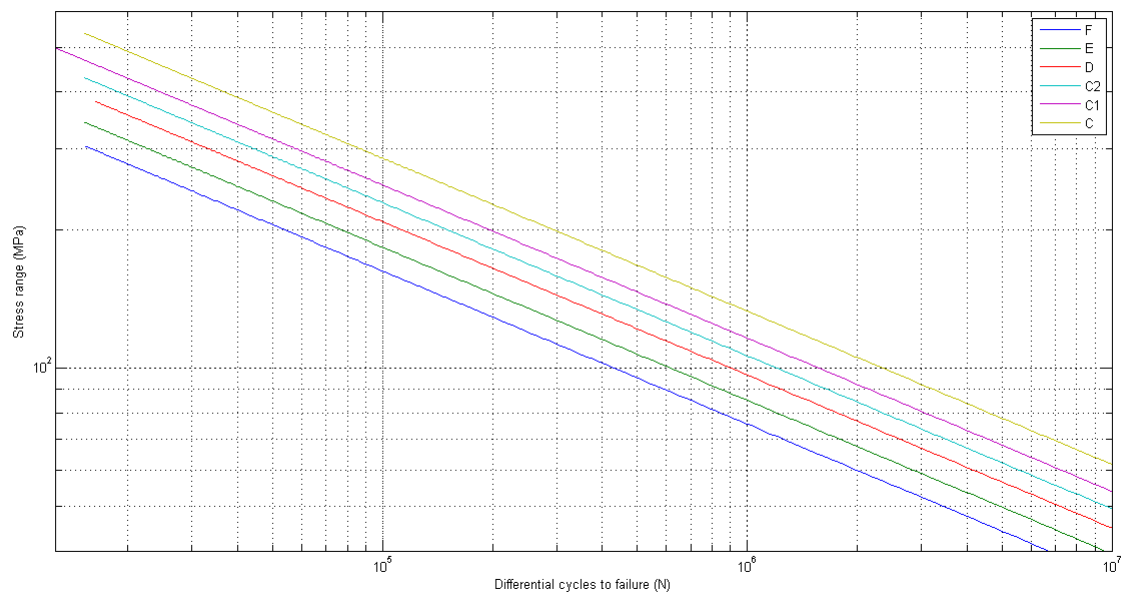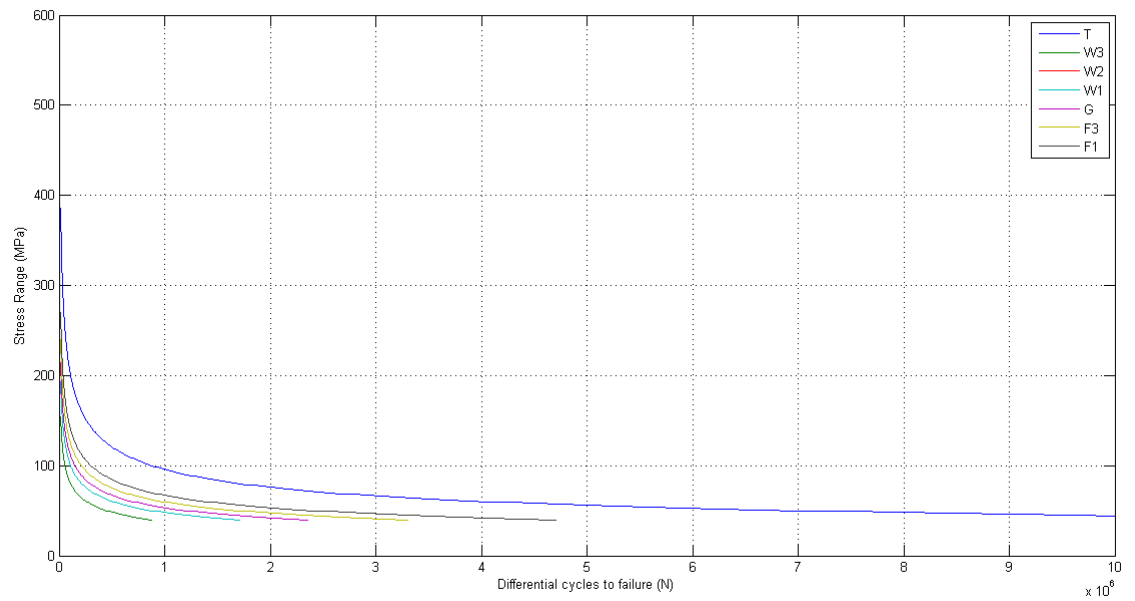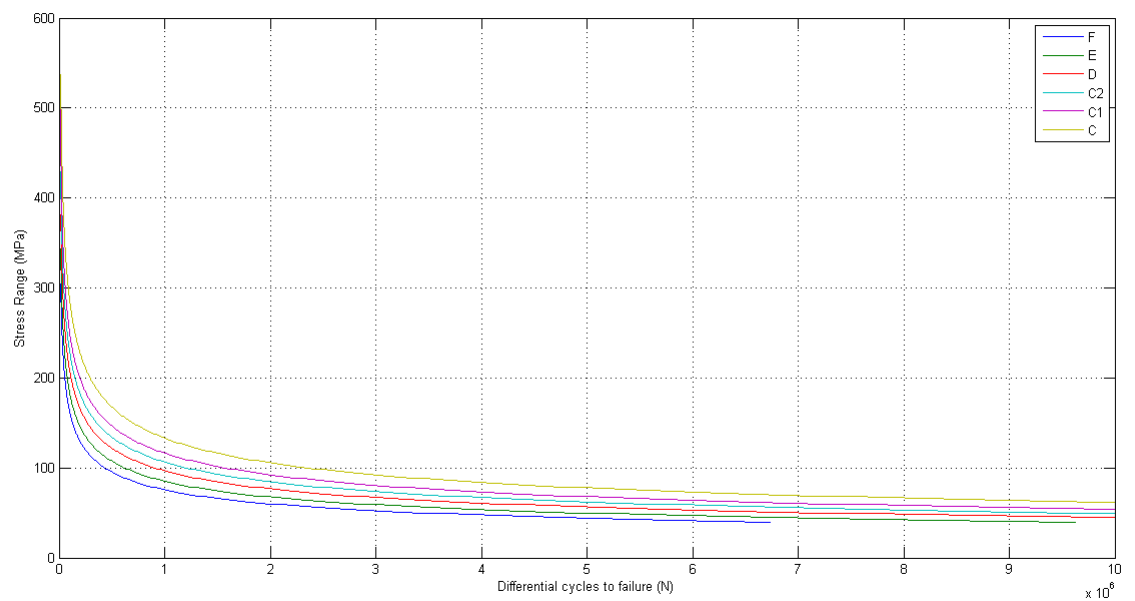

FIGURE 4.7: Logarithmic differential between the HCCF and the HCF for a given stress range for several types of connections. Notice that the environmental impact depends not only on stress range but also on connection type [6]

FIGURE 4.8: Differential between the HCCF and the HCF for a given stress range for several types of connections. Notice that the environmental impact depends not only on stress range but also on connection type [6]

FIGURE 4.9: Differential between the HCCF and the HCF for a given stress range for several types of connections. Notice that the environmental impact depends not only on stress range but also on connection type [6]

4.2 Environmental Impact Material Science

Material scientists have experimented with the phenomenon of low cycle corrosion fatigue as well. Contrary to the approach in design codes where a stress-cycle relationship is established, material scientists establish a relationship between strain ε and fatigue life N. The relationship that best describes the stress strain characteristic is the Coffin-Manson relationship [11, 12]. The relationship used in [10] is given in equation 4.6. The parameters are reported in table 4.1.

$$N = A(\Delta\varepsilon_p)^{-b} \tag{4.6}$$

Kind of Environment	A	b
Air	0.0461	2.3770
3.5 % NaCl, pH 6	0.0377	2.3546
3.5 % NaCl, pH 3	0.1458	2.0044
3.5 % NaCl, pH 0	0.0491	2.1450
Water, pH 3	0.0641	2.1964

TABLE 4.1: Parameters Coffin Manson relationship [10]

The plot which contains the S-N curves for several environments reported in table 4.1 have been reported in figure 4.10. The same plot can be seen on the logarithmic scale in figure 4.11. The observation in the design codes that the environmental impact diminishes in the lower cycle region is also valid for the data in [10]. It appears that for strains beyond 0.014 in figure 4.10 the fatigue life is heavily converged. This means that the fatigue life of elements subjected to very high strains in electrochemically hazardous environments does not differ that much from the fatigue life of elements subjected to very high strains in air. However, the authors of [10] failed to clearly report standard deviations or measures of uncertainty for their findings which makes further probabilistic analysis impossible.

The author has quantitatively analyzed the decrease in discrepancy of the LCCF curves by finding the expected value for the fatigue curves in figure 4.10 under a given strain range. The number of cycles can be calculated with equation 4.7 in which i is an indicator variable for the environment type in table 4.1. The conditional expectation of the the fatigue life of a specimen is $E(N_i|\varepsilon)$. The conditional expectation $E(N_i|\varepsilon)$ can be estimated with $E(N_i|\varepsilon) \approx \sum_{i=1}^{i=5} N_i|\varepsilon$. The conditional variance $Var(N_i|\varepsilon) \approx E(N_i|\varepsilon - E(N_i|\varepsilon))(N_i|\varepsilon - E(N_i|\varepsilon))$. The conditional variance as a function of ε has been plotted in figure 4.12

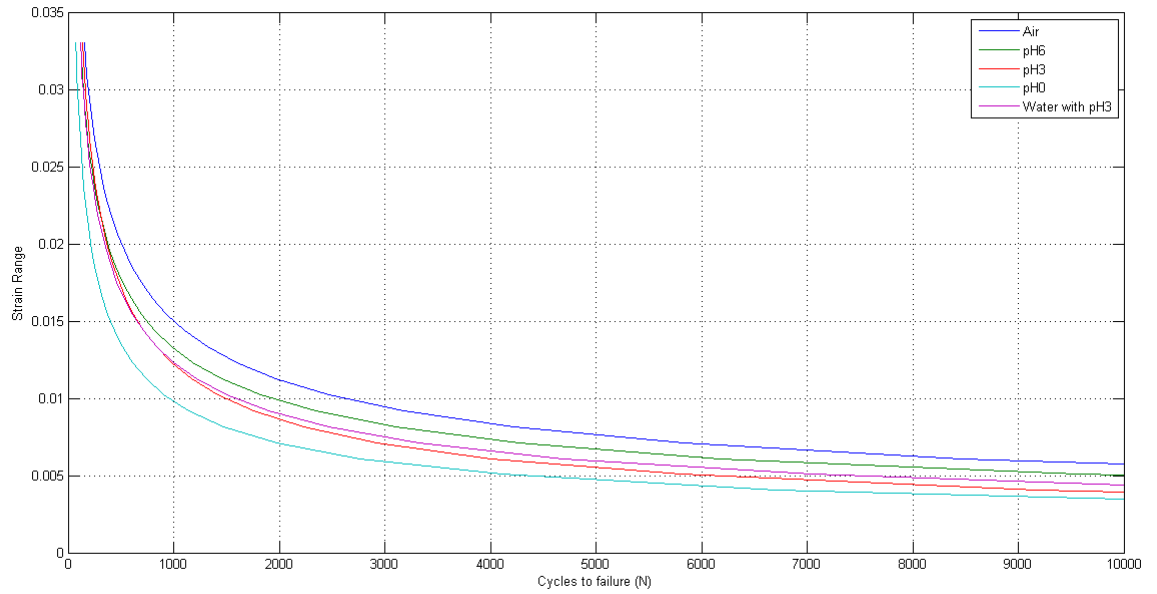$$E(N_i|\varepsilon) = E(A(\Delta\varepsilon_p)^{-b_i}|\varepsilon) \tag{4.7}$$

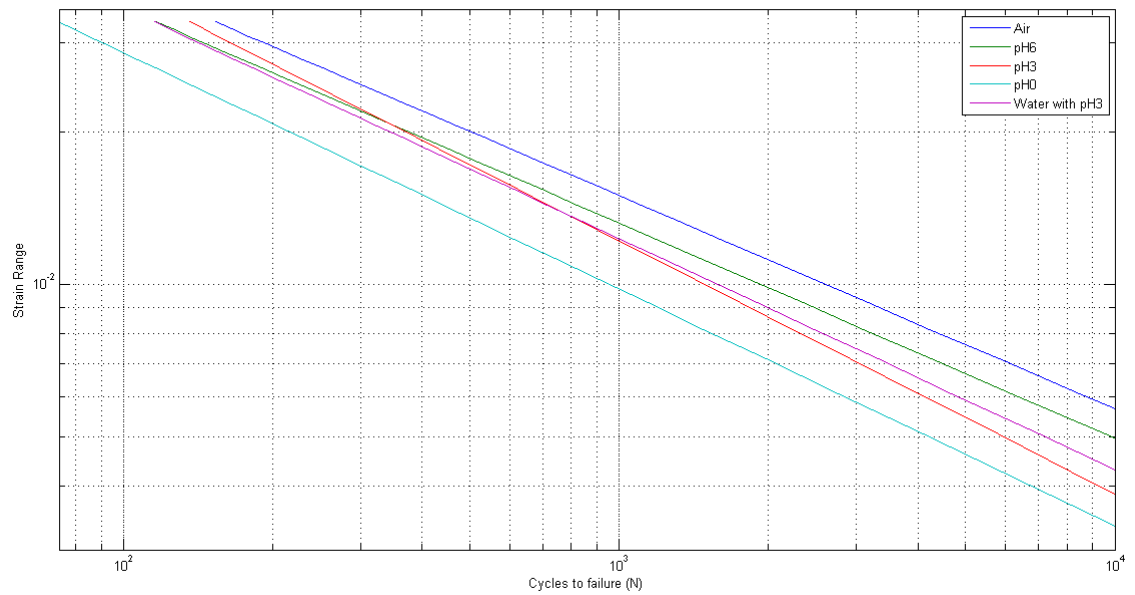FIGURE 4.10: LCCF of a steel specimen subjected to various levels of acidity
[10]

FIGURE 4.11: LCCF of a steel specimen subjected to various levels of acidity
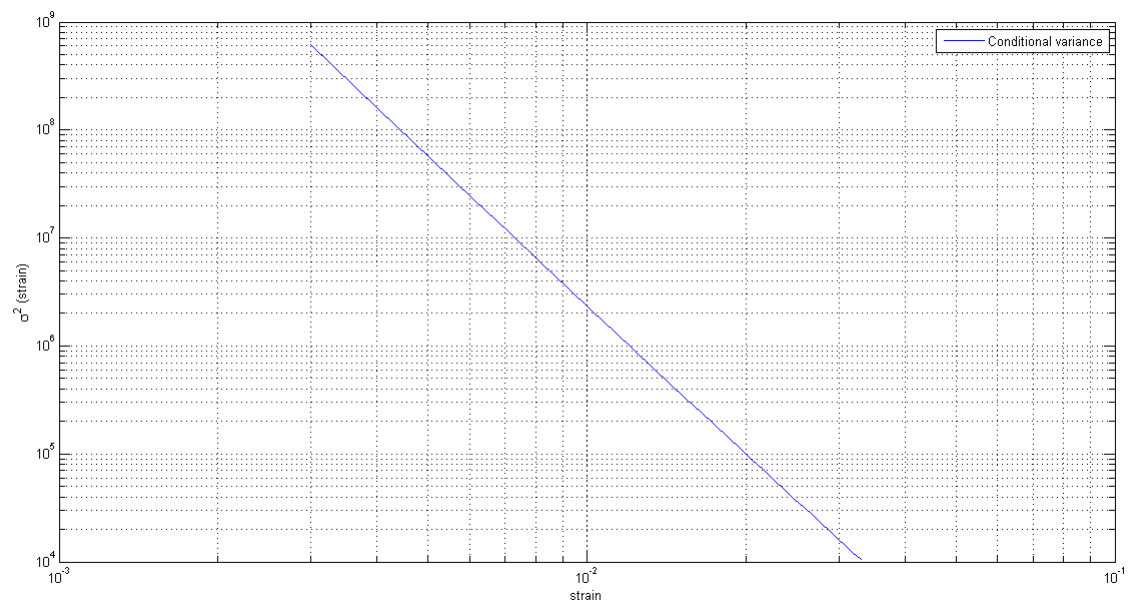on a logarithmic scale [10]

FIGURE 4.12: Conditional variance of the number of cycles N_i as function of
the strain. Notice that the conditional variance decreases with increasing strain
. This is an indication that the effect of the environment disappears slowly as
the strain rate increases

It appears to be a returning phenomenon that the effect of the environment diminishes in the lower cycle region. The hypothesis of the author for this phenomenon is that the corrosion element in low cycle corrosion fatigue takes some time to affect the specimen but very low cycle fatigue may occur in a very short time span. Corrosion requires chemical reactions which in turn also require time. In case the stress is very high, the specimen will fail due to plasticity and therefore rapidly form micro fractures before much of the material can corrode. The opposite is true for high cycle fatigue. The stress range cannot cause significant micro fractures in the material but the corrosion phenomenon continues which will do more lasting damage over time than the stress itself. Another interesting observation is that the the type of connection is also an indicator of the effect of the environment. The least susceptible to fatigue is high strength base material. The stress required for base material to enter the low cycle fatigue zone is virtually equal to the yield stress. It is the hypothesis of the author that the residual tension due to welding is the main indicator of this phenomenon. Connections which are susceptible to a lot of residual tension enter the low cycle zone at a relatively low stress (less than the theoretical yield stress) because before any loading, the connection has residual tension due to welding and a slight $\Delta\varepsilon$ can cause the material to yield locally yet not globally. This local yielding causes more rapid micro-fractures and leads to eventual failure of the connection.

Understanding the above phenomenon is interesting in its own right but it has no lasting practical value for offshore structures. The stress depends on the loads and this depends on the wave and wind loading on the structure. The structure will be loaded by a wide range of different loads which will be met by different stress states in a structural element. This means that simply ignoring the environmental aspect is not possible for complex loading situations except if the situation only requires consideration of high stresses. Furthermore, it was shown that even for very high stresses a LCCF problem corresponds to a lower fatigue life than a LCF problem.

4.3 Conclusions

The conclusions of this chapter are that the environmental effect decreases in the low cycle region. This effect is both observed in curves from design codes where the authors use a stress versus fatigue life relationship and in articles from material

scientists where the authors use a fatigue life versus strain curve known as the Coffin Manson relationship. However, it was not possible to completely ignore the environmental effect, even at extremely high stresses, because the probability that an element in air could withstand more cycles than an element with cathodic protection in seawater was extremely low. The general message of this chapter is that despite reduction of the environmental effect at low cycles the effect is still quite significant. Moreover, a structural element is generally loaded by loads of different magnitudes during its lifetime. This means that it will be affected by stress ranges where the effect of the environment is significant and stress ranges (high stresses) where the effect of the environment is less significant. The previous makes ignoring the environmentally assisted fracturing impossible to ignore except in cases where a structural element in a deleterious environment is only subjected to very high loads (corresponding to very low cycles). This is a situation that does not appear to occur in engineering practices for offshore structures.

Chapter 5

Mathematical Modeling Low Cycle Fatigue

In this chapter two models will be presented for the prediction of LCCF life. One model is based on a principle of constant slopes m in every distinguishable fatigue region. One region is the ultra high cycle region, which is typically above 1.000.000 cycles. The second region is the high cycle region, which is typically between 10.000 cycles and 1.000.000 cycles. The third region and for the author of the thesis the most interesting region is the low cycle region, which is typically below 10.000 cycles. A second model that will be presented is based on regression analysis. This model will be explained in more detail below.

5.1   Constant Slopes (Method 1)

An interesting observation from the literature review in Chapter 2 was that in every region, the slope m in equation 2.2, appears to be constant. This is the case for the DNV. API and EC3. This may give room for a hypothesis that in every region, LCHS region and HCLS region, the slope m can be considered constant. This means that if one knows the slope for one type of structure then the slope for all other structures are automatically known because they are similar. Under this assumption one may calculate $\log \bar{a}$ because the low cycle region must shift gradually into the high cycle region. The low cycle region is set at 10.000 cycles or less. The stress range that both the LCCF S-N curves and the HCCF S-N curves give at 10.000 cycles must coincide. This allows for calculation of the stress state at

10.000 cycles with the high cycle S-N curve. This stress state can sub sequentially be used for the calculation of the yet unknown parameter $\log \bar{a}$ for the low cycle fatigue SN curve. The known slope is 4.927 [6] for tubular sections. Figure 2.7. The previous allows for calculation of the stress range at 10.000 cycles based on the high cycle curve, then the level $\log \bar{a}$ can then be found. The parameters are reported in table 5.1. The procedure is illustrated in steps below for the W3 curve found in the [5]. The parameters used here are for the W3 curve.

- The stress range for 10.000 cycles based on the high cycle curve is calculated below. $log\Delta\sigma = \frac{logN - log\bar{a}}{m} = \frac{10.570 - log(10.000)}{3} = 2.19$

- We know that the HCCF curve and the LCCF curve must coincide at the 10.000 cycle boundary so the stresses are the same. $log\bar{a} = logN + mlog\Delta\sigma = log(10.000) + 4.927 * 2.19 = 14.7901$

Another method involves calculation of the angle that the LCCF curve makes with HCCF at the 10.000 cycle barrier. This method is illustrated in figure 5.1. The angle can be calculated with the directional vectors. The directional vector for the LCCF curve for tubular sections can be calculated by taking two points on the logarithmic LCCF curve for tubular sections (x_1, y_1) and (x_2, y_2). The directional vector for the HCCF curve for tubular sections can be calculated by taking two points on the logarithmic HCCF curve for tubular sections (x_3, y_3) and (x_4, y_4). The directional vectors V_1 can be calculated with $V_1 = \begin{vmatrix} x_1 \\ y_1 \end{vmatrix} - \begin{vmatrix} x_2 \\ y_2 \end{vmatrix}$. The directional vector V_2 can be calculated with $V_2 = \begin{vmatrix} x_3 \\ y_3 \end{vmatrix} - \begin{vmatrix} x_4 \\ y_4 \end{vmatrix}$. The angle can be calculated with equation 5.1. This angle is equal to 6.9619 degrees.

$$\cos \theta = \frac{V_1 * V_2}{||V_1|| * ||V_2||} \tag{5.1}$$

The results for all $\log \bar{a}$ have been reported in table 5.1. This is the most important result of this section. The assumption of constant slopes generates lower values for the number of reversals to failure compared to extrapolation of the high cycle fatigue curve to the low cycle region.The SN-curves can be seen in figure 5.2 and figure 5.3.
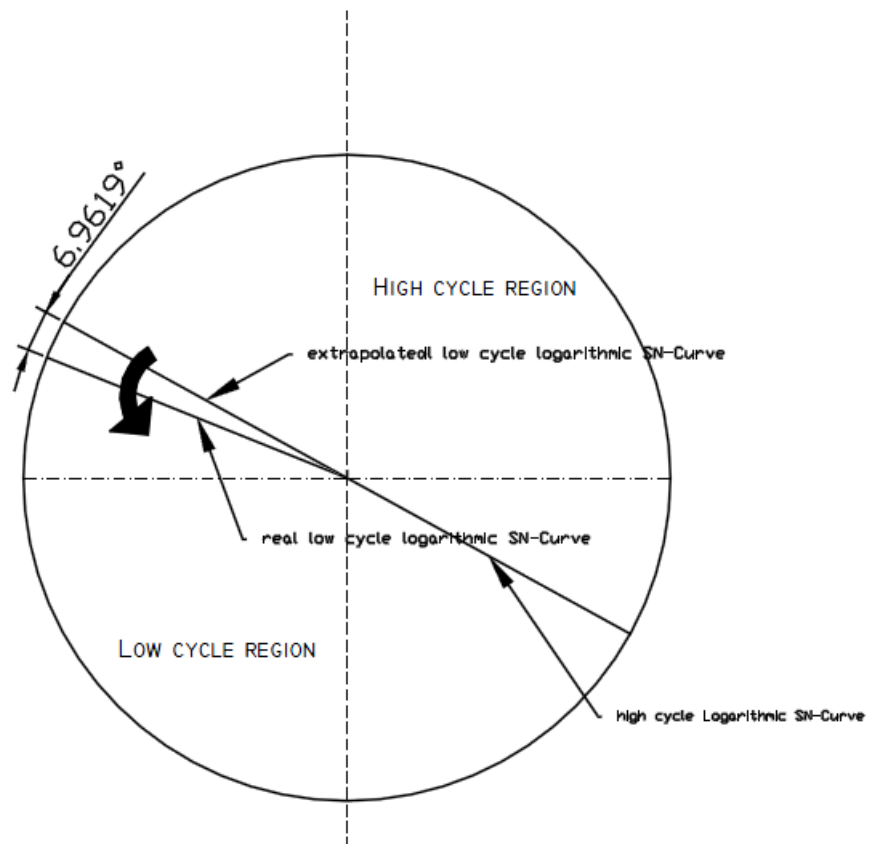
FIGURE 5.1: The S-N curves rotate a specific angle when crossing into the low cycle zone from the high cycle zone. The high cycle curves are taken from the DNV

log$\Delta\sigma$	$\Delta\sigma$ MPa	Connection	log $\bar{a}$ HCCF	calculation log $\bar{a}$ LCCF
2.5880	387.2576	T	11.7640	16.7511
2.1900	154.8817	W3	10.5700	14.7901
2.2357	172.0547	W2	10.7070	15.0151
2.2870	193.6422	W1	10.8610	15.2680
2.3327	215.1130	G	10.9980	15.4930
2.3820	240.9905	F3	11.1460	15.7361
2.4330	271.0192	F1	11.2990	15.9874
2.4850	305.4921	F	11.4550	16.2436
2.5367	344.0857	E	11.6100	16.4982
2.5820	381.9443	D	11.7460	16.7215
2.6337	430.1963	C2	11.9010	16.9761
2.6980	498.8845	C1	12.0940	17.2930
2.7307	537.8568	C	12.1920	17.4540

TABLE 5.1: Parameters low cycle fatigue. $\Delta\sigma$ is the stress where the 10.000 cycle boundary is crossed
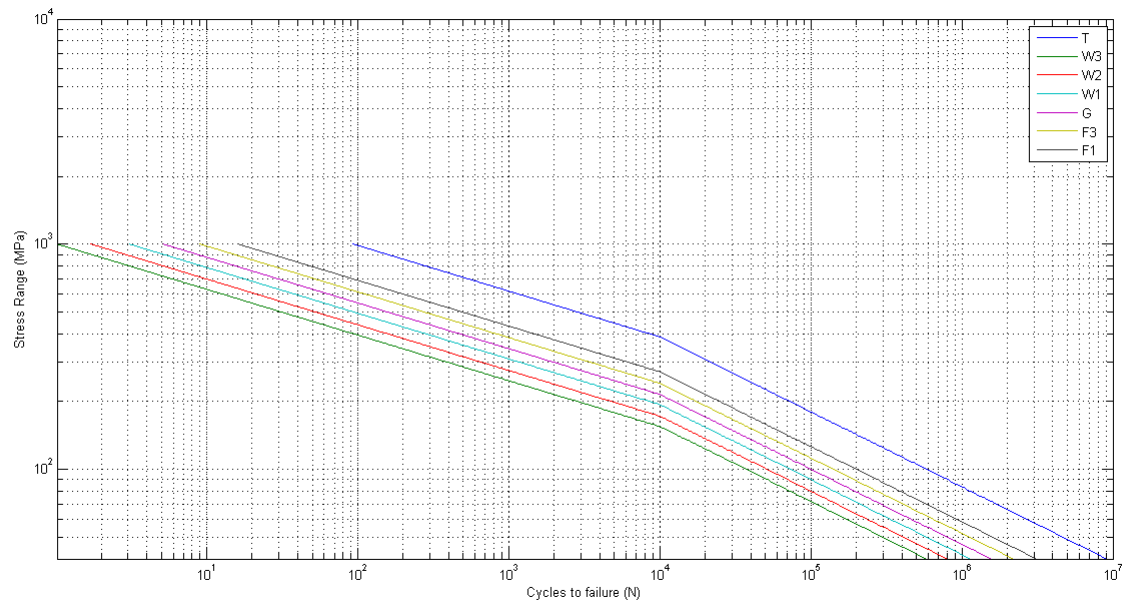
FIGURE 5.2: The S-N curves for LCCF for various types of connections. The slope decreases at 10.000 cycles based on the constant slope method
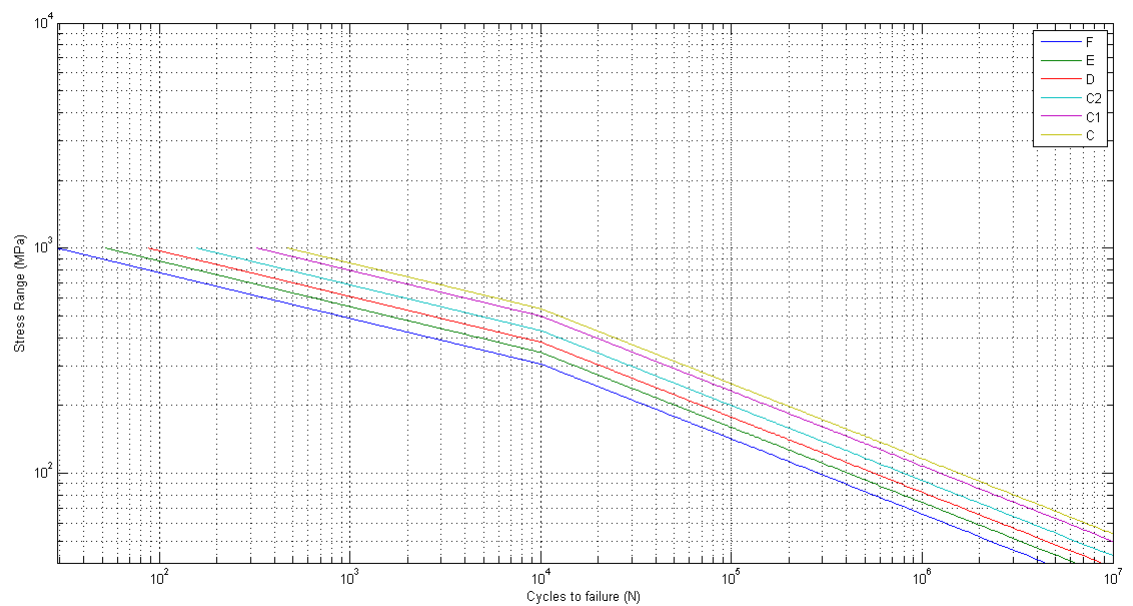
FIGURE 5.3: The S-N curves for LCCF for various types of connections. The slope decreases at 10.000 cycles based on the constant slope method

The notion that the synthesized S-N curves based on rotation give a lower fatigue life than extrapolated high cycle curves is to be expected and corresponds well with the assumption of consistency of slopes. The slope for the high cycle fatigue region m is generally equal to 3 but there are exceptions. The curve B1 and B2 [5] have an m of 4 in the high cycle fatigue region, therefore these cannot be modelled based on the assumption of constant slopes across connection types. Another shortcoming is that the base material (equation 5.2) has a slope m of 4.70 in the high cycle region which means that it also cannot be modeled based on the hypothesis of the author that slopes must be constant. This is quite a shortcoming because it does not allow modeling base material in the low cycle corrosion fatigue zone.

$$logN_\gamma = 17.447 - 4.70 * log\Delta\sigma + \varepsilon \qquad (5.2)$$

A comparison between extrapolation of the high cycle curve and the design curve, using the parameters in table 5.1 has been presented in figure 5.4. The remainder of the curves can be seen in Appendix A.
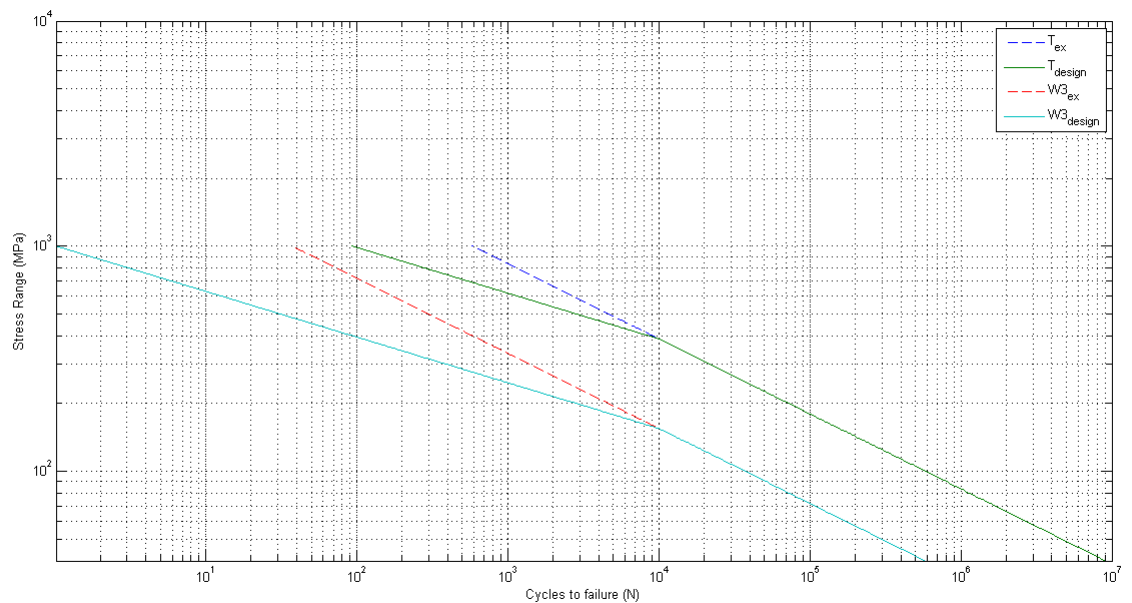
FIGURE 5.4: Comparison between the extrapolated curve for the high cycle region into the low cycle region for T and W3 curves and the curves created with the assumption of consistent slopes. It can be seen that extrapolation of the high cycle curves into the low cycle region would lead to an overestimation of the fatigue life

5.2 Regression (Method 2)

A second method to predict fatigue life in the low cycle region is using regression analysis. The low cycle fatigue curve for tubular sections in seawater is available. The hypothesis of the author is that the fatigue life that extrapolation of the high cycle fatigue curve into the low cycle zone predicts contains predictive power for the number of cycles that a specimen can really withstand in the low cycle region. The regression model that the author proposes is given in equation 5.3

$$logN_\gamma = \alpha + \beta * logN_\alpha + \varepsilon \qquad (5.3)$$

$logN_\gamma$ is a vector that contains the number of cycles that a specimen can withstand in the low cycle region according to the low cycle curves reported in [6]. $logN_\alpha$ is a vector that contains the number of cycles that a specimen can withstand in the low cycle region according to extrapolation of the high cycle curves reported in [5]. β is the regression coefficient and ε is a vector that represents the uncertainty. In order to perform a regression analysis the author will require data. This data will be simulated using low cycle and high cycle models for tubular sections represented in equation 5.4 and equation 5.5. The ε is a variable with $N(0, \sigma^2)$ distribution. The σ is 0.2.[5] The parameters for equation 5.5 are given in table 5.1.

$$logN_\gamma = 16.084 + 0.4 - 4.927 * log\Delta\sigma + \varepsilon \qquad (5.4)$$

$$logN_\alpha = 11.764 - 3.0 * log\Delta\sigma \qquad (5.5)$$

In order for the data simulation to be possible the system must be subjected to a series of assumptions. The first assumption is stable regressors. This means that $logN_\alpha$ which will be referred form now on as the X matrix which has a probability limit $\frac{1}{n}X'X$ that is equal to Q. The vector $logN_\gamma$ will be referred to as the y vector. The second assumption is that the errors ε_i have zero mean. The third assumption is that there is no autocorrelation which means that the errors ε_i and ε_j are uncorrelated. The fourth assumption is homoskedasticity, which means that all errors come from a single distribution and have the same variance. The fifth assumption is that the parameters α and β are constant. The sixth assumption is that the linear model $logN_\gamma = \alpha + \beta * logN_\alpha + \varepsilon$ is correctly specified. The seventh assumption is that the errors ε_i have a $N(0, \sigma^2)$ distribution. The final

assumption is that the vector which contains the errors ε and the X matrix are uncorrelated.

The α and β can be found by applying the ordinary least squares regression in matrix format. The equation for the OLS coefficients is given in equation 5.6. The equation for the variance is given in 5.7. The equation for standard error of regression is given in 5.8. The vector e is the vector of residuals given by $y - X(X'X)^{-1}X'y$. n is the number of observations and k is the number of parameters in the model specification which is 2 in this case. The regression coefficients and standard errors are given in table 5.2. The result of the equations can be seen in 5.2. The R-squared is 0.87 which is an indication for a very high level of internal fit. The R-squared can be calculated with $R^2 = 1 - \frac{SS_{resid}}{SS_{total}}$. The s^2 is 0.04.

The simulated y-vector from [6] data against the X-matrix is illustrated in figure 5.5. The model is fitted with equation $\hat{y} = X(X'X)^{-1}X'y = Hy$ where H is $X(X'X)^{-1}X'y$ is also illustrated in 5.5. It appears in figure 5.5 that the regression coefficients using an OLS method reported in table 5.2 are capable of forecasting the real LCCF curve remarkably well. A major assumption that has to be made now, which is that the regression model may be applied to other curves, aside from the curve for tubular sections, reported in table 5.1.

$$\beta = (X'X)^{-1}X'y \tag{5.6}$$

$$Var(\beta) = \sigma^2(X'X)^{-1} \tag{5.7}$$

$$s^2 = \frac{e'e}{n-k} \tag{5.8}$$

	Coefficient	Std. error
α	-2.0384	0.261450
β	1.6466	0.070209

TABLE 5.2: Regression coefficients and standard errors
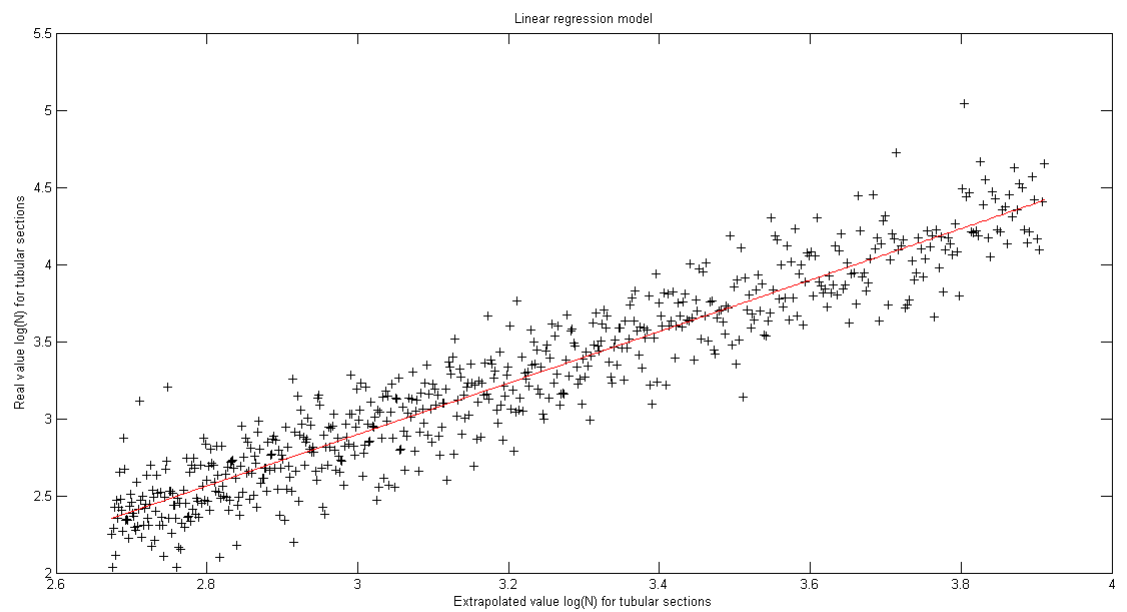
FIGURE 5.5

FIGURE 5.6: The red line is $\hat{y}$. The points are the simulated data points according to equation 5.4

The S-N curves that this method has generated for several types of connections
are reported in figure 5.7 and figure 5.8. The problem with these graphs is that
the low cycle fatigue curve for tubular sections appears to be fine, however, the
other curves appear to have problems.
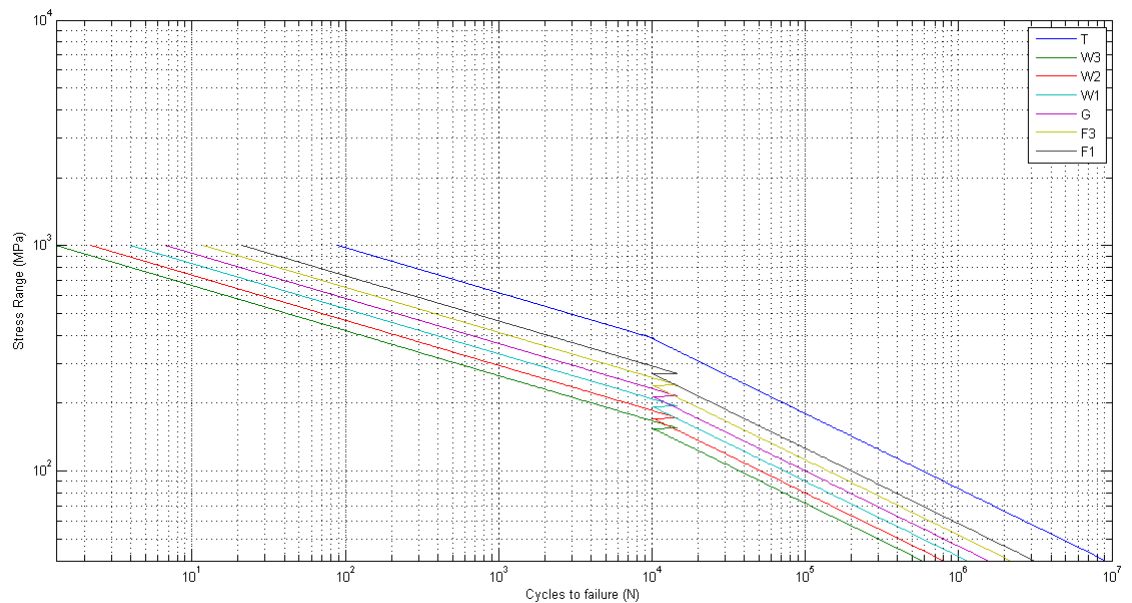
FIGURE 5.7: The S-N curves for LCCF for various types of connections. There
is a horizontal shift to the right which causes high cycle fatigue curves to be
more conservative in the low cycle region over a narrow interval. This is an
irreparable problem

This method of regression causes a horizontal shift to the right which causes this
method to predict a longer fatigue life in the low cycle region in a narrow inter-
val than simple extrapolation of the high cycle curve would have done. This is
illustrated in figure 5.9. It can be seen that the T-curve in the low cycle region
predicts less cycles than the extrapolated high cycle T-curve, however, the extrap-
olated W3 curve predicts less cycles in the low cycle region at around 10.000 cycles
than the W3 curve by method 2. This is a problem because it is the hypothesis
of the author that any good method to predict low cycle fatigue should predict
less cycles than an extrapolated high cycle curve. The same can also be seen for
other types of connections in 5.10. The remainder of the graphs that compare
extrapolated high cycle curves with synthesized low cycle curves by method 2 are
reported in Appendix C.
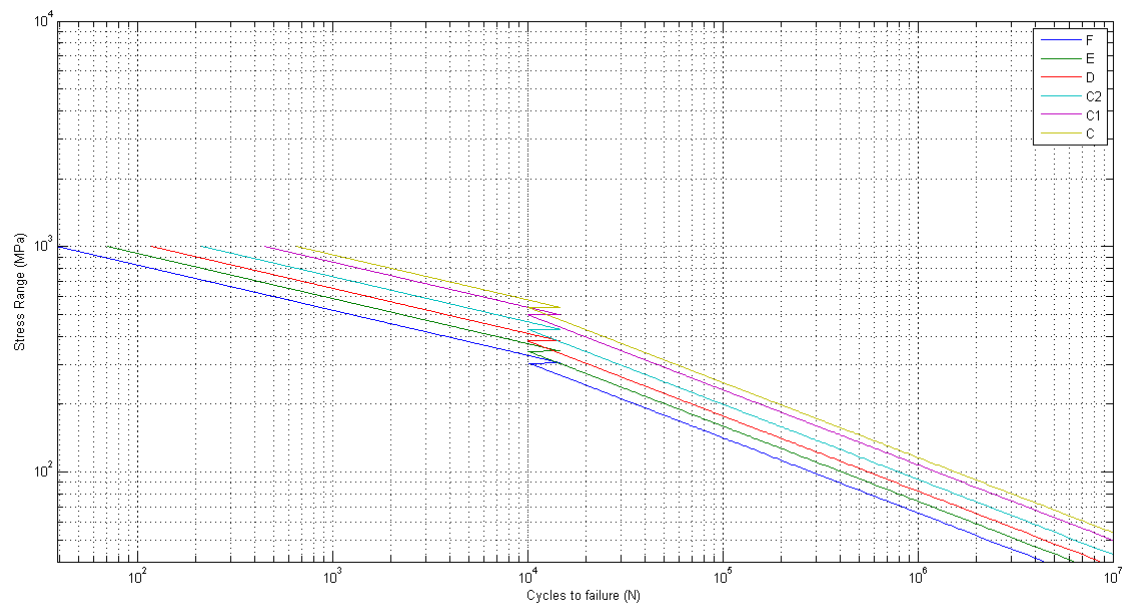
FIGURE 5.8: The S-N curves for LCCF for various types of connections. There is a horizontal shift to the right which causes high cycle fatigue curves to be more conservative in the low cycle region at a small interval. This is an irreparable problem
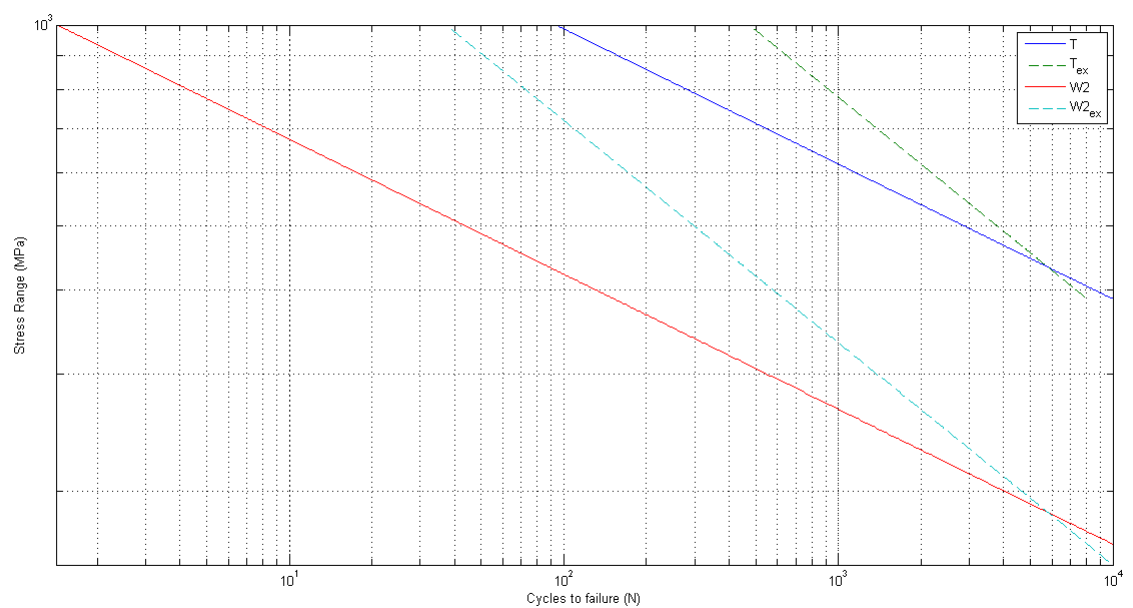
FIGURE 5.9: Comparison between extrapolated HCCF curves and LCCF curves by method 2. It appears that at some points the extrapolated HCCF is more conservative than LCCF curves by method 2. This is a problem
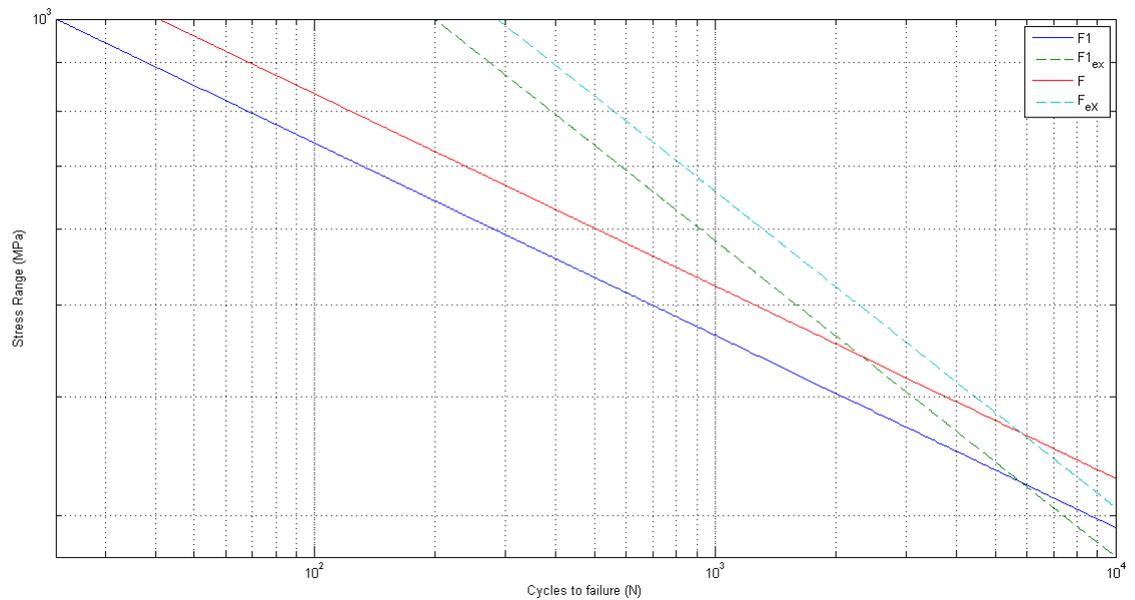
FIGURE 5.10: Comparison between extrapolated HCCF curves and LCCF curves by method 2. It appears that at some points the extrapolated HCCF is more conservative than LCCF curves by method 2. This is a problem

5.3 Conclusions

In this section two different models have been presented which lead to different outcomes for low cycle fatigue life in deleterious environment. There is no telling which model is superior. The model based on constant slopes does give more credible results because this model consistently predicts a lower fatigue life than extrapolated high cycle curves. The model of constant slopes does have a more solid theoretical background. The model based on regressions also fails to address one key concern and that concern is that it doesn't consistently predict less cycles than an extrapolated high cycle curve.

Notice: The low cycle S-N curves presented in this chapter are designed for certain types of joints. These joints can be found partly in the Appendix. A more comprehensive review of the joints can be found in [5]. Furthermore. The S-N curves are designed with a certain quality of joint in mind that involve heat treatment procedures. The minimum demands and procedures for welds can be found in [29] and [30] . There is also cathodic protection involved. The minimum cathodic protection and the procedures for application are found in [23].

Chapter 6

Calculation Example Low Cycle Fatigue

In this section the author will show a calculation example. The calculation will be performed for a tubular X-joint. The hot spot stress will be calculated using the method in [6] which uses the Ramberg Osgood relation [28] and Neuber's rule [31]. This should be used in case the engineer does not have possession over a FEM model for the structure. However, generally offshore structures do have a FEM model made to study the structural behavior. The second part of the calculation is an illustration on how to use model 1 based on constant slopes and model 2 based on regression analysis. The models were discussed in Chapter 5. Then it will be checked if the Miner's sum is less than 1.

6.1   Calculation Example

In the calculation example, we consider a structure that has been loaded beyond the elastic limit and faces 1000 load cycles with nominal stress of 400 MPa and 100 load cycles with a nominal stress of 500 MPa. Bear in mind that the stress strain curve is no longer linear but takes the shape of figure 3.5. Using equations (6.1, 6.2 and 6.3) the actual stress can be calculated.

$$\frac{\sigma_n{}^2 SCF^2}{E} = \sigma_{actualHSS} \left[\frac{\sigma_{actualHSS}}{E} + \left(\frac{\sigma_{actualHSS}}{K} \right)^{\frac{1}{n}} \right] \qquad (6.1)$$

$$\varepsilon_{nl} = \frac{\sigma_{actualHSS}}{E} + \left(\frac{\sigma_{actualHSS}}{K}\right)^{\frac{1}{n}} \tag{6.2}$$

$$\sigma_{pseudo} = E * \varepsilon_{nl} \tag{6.3}$$

σ_n is the nominal stress. SCF is the stress concentration factor from a linear elastic analysis. $\sigma_{actualHSS}$ is the actual stress at the considered hot spot from a non-linear finite element analysis using a cyclic stress strain curve. E is the Young's modulus and n and K' are the material coefficients. K' and n can be obtained experimentally for the actual material, weld and heat affected zone. However, for a first assessment [6] indicates that K' and n a value of 582 MPa and 0.111 can be used respectively. Some coefficients of n and K are given in [17] and [16]. For the heat affected zone, it is recommended to assume welded metal, if non-linear analysis is carried out to obtain a strain range according to [6]. The SCF will be assumed to be 1.40.

In the example used we have a tubular T section which requires curve T in the DNV Recommended Practice [5]. The number of cycles that a structure can withstand can then be calculated with model 1 based on constant slopes. This model was discussed in Chapter 5. The fatigue life is calculated below.

The 1000 load cycles of 400 MPa. $\frac{400^2(1.40)^2}{210000} = \sigma_{actualHSS}\left[\frac{\sigma_{actualHSS}}{210000} + \left(\frac{\sigma_{actualHSS}}{582}\right)^{\frac{1}{0.111}}\right]$. $\sigma_{actualHSS} = 309.25$ MPa. $\varepsilon_{nl} = \frac{298.15}{210000} + \left(\frac{298.15}{582}\right)^{\frac{1}{0.111}} = 0.004830575$. $\sigma_{pseudo} = 210000 * 0.00383586 = 1014.42$ MPa. This calculation shows you that the load bearing capacity of a structural element is less when cyclically loaded beyond the elastic limit. This should not be forgotten when a static analysis is performed. $logN_{\gamma} = 16.7511 - 4.927 * log560 = 3.210$. $10^{3.210} = 1624$ load cycles

The 100 loads cycles of 500 MPa. $\frac{500^2(1.40)^2}{210000} = \sigma_{actualHSS}\left[\frac{\sigma_{actualHSS}}{210000} + \left(\frac{\sigma_{actualHSS}}{582}\right)^{\frac{1}{0.111}}\right]$. $\sigma_{actualHSS} = 327.15$ MPa. $\varepsilon_{nl} = \frac{298.15}{210000} + \left(\frac{298.15}{582}\right)^{\frac{1}{0.111}} = 0.00713231$. $\sigma_{pseudo} = 210000 * 0.00383586 = 1497.78$ MPa. Again, this calculation shows you that the load bearing capacity of a structural element is less when cyclically loaded beyond the elastic limit. This should not be forgotten when a static analysis is performed. $logN_{\gamma} = 16.7511 - 4.927 * log700 = 2.733$. $10^{2.733} = 541$ load cycles

Finally it makes sense to perform a Miner Sum check in order to see if the structure will fail. This has been done in equation 6.4. It appears that for the given situation the structure does okay.

$$\sum_{i=1}^{2} \frac{\eta_i}{N_i} = \frac{1000}{1624} + \frac{100}{541} = 0.800 \tag{6.4}$$

In chapter 5 a second model was proposed. This model was based on regression and yielded credible results as well. The model parameters of Chapter 5 can again be seen in table 6.1 and the model itself is illustrated in equation 6.5. This model works in combination with the regular HCCF curve.

$$logN_\gamma = \alpha + \beta * logN_\alpha + \varepsilon \tag{6.5}$$

	Coefficient	Std. error
α	-2.0384	0.261450
β	1.6466	0.070209

TABLE 6.1: Regression coefficients and standard errors

1000 load cycles of 400 MPa. Firstly we must calculate the log of the number of cycles that the model can withstand according to high cycle fatigue. This value is the expected value. The design value should be the expected value minus two standard deviations. The standard error of regression for the model was found to be 0.2. $11.764 - 3.0 \cdot log560 = 3.51$. $-2.0384 + 1.6466 \cdot 3.51 = 3.74$. The σ is 0.2. The 2.5 % probability of non-exceedance is 3.3411. The number of cycles is $10^{logN_\gamma} = 10^{3.3411} = 2193,64$ load cycles

Secondly, we must repeat the procedure but now for a 500 MPa nominal load with 100 cycles. $logN_\gamma = 11.764 - 3.0 * log700 = 3.22$. $logN_\gamma = -2.0384 + 1.6466 * 3.22 = 3.26$. The σ is 0.2. The 2.5 % probability of non-exceedance is 2.86. The number of cycles is $10^{logN_\gamma} = 10^{2.86} = 724$ load cycles

Finally a Miner sum check must be applied to see if the structure is okay.

$$\sum_{i=1}^{2} \frac{\eta_i}{N_i} = \frac{1000}{2193.64} + \frac{100}{724} = 0.593 \tag{6.6}$$

The structure appears to be okay by the analysis of both models conjured in Chapter 5.

6.2 Conclusions

Two loads with two different amount of load cycles were examined using the models of Chapter 5. The nominal stress was converted to the actual hot spot stress using Neuber's rule combined with the Ramberg Osgood relationship. The actual stress is much less than the pseudo elastic stress due to the completely different shape of the stress strain relationship for cyclical plastic loading. Finally a Miner sum was applied in order to check if the structure was capable of withstanding the load regimes. The loads were assumed to be deterministic but in practice the load has a distribution which means that in practice simulation must be applied. The Regression method also seems to be less conservative. This is not surprising considering the findings in Chapter 5

Chapter 7

Recommendations

7.1   Experiments Required

To get a complete picture of low cycle corrosion fatigue a series of experiments must be performed. All joint types should be tested in the low cycle fatigue region in simulated seawater and preferably a fatigue life-strain curve should be fitted by method of the Coffin-Manson equation because it fits so well. Strain based parameters also accounts for non-linear behavior that occurs in low cycle fatigue. In [21] an elaborate study was done for high cycle corrosion fatigue in seawater. The same sentiment can be followed for the experimental setups of the low cycle fatigue except that much more specimen should be tested. This is time consuming and expensive however, it may be worth the investment. A cheaper way to gain insight into the problem would be to perform a research experiment which involves testing the low cycle corrosion fatigue life of a very common joint that has no data available in the low cycle region. Afterwards. It can be checked if the models of Chapter 5 perform well by analyzing the forecast errors. To get a complete picture of the low cycle corrosion fatigue phenomenon, the joints should be tested with cathodic protection and free corrosion in seawater. Tests for free corrosion in the low cycle region have never been performed. The results should be interesting as it may reveal the effect of cathodic protection in the low cycle range.

7.2 Heteroskedasticity

Moreover, the number of observations per specimen should preferably be more than 20. This will allow for more detailed insight into the variance of the uncertainty of the Coffin-Manson relationship. The author believes that the variance of the uncertainty is not homoskedastic which means that this variance may decrease or increase in the low cycle region. If the variance decreases it means that the confidence interval becomes smaller and fatigue life is in general underestimated. If the variance increases it means that the confidence interval becomes larger and the fatigue life is in general overestimated. A decreasing variance may be translated to significant savings in construction costs. However, it will require a lot of data points in order to get more insights into this phenomenon. The number of experiments is a lot which means that it will be an expensive experiment.

7.3 Significant Local Yielding

In chapter 3 the phrase "significant local yielding" was used. It would be an interesting research to find out the distribution of strains in the micro structure of a specimen with a non-destructive tests. This distributed could be used to find out if there is a relation between the probability of exceedance of the plastic strain and fatigue life. This probability of exceedance should be approximately similar for all connection types for a certain fatigue life. One point of interest would be the point at which a high cycle problems turns into a low cycle problem. A research project may answer this question.

7.4 Palgren Miner Sum

The Palmgren miner sum may be incorrect when analyzing low cycle and high cycle behavior for a single specimen. A research project could be done in which a specimen is subjected to both high cycle fatigue and low cycle fatigue. It should subsequently be checked if the specimen does indeed fail when the miner sum is approximately 1 on average for the tested specimen. In case this doesn't appear to be the case an option would be to try a continuous or discrete markov switching model where the state of the structure is classified. The states could range from

Perfect to Failure. In experiments the transition rate for continuous makrov chains or the transition probability for discrete chains from one state to the next can be found. This probability will likely be a function of known environmental parameters Λ, the stress range $\Delta\sigma$ and perhaps a classification of the current state Ξ. This transition probability can be expressed as $P(X_{t+1} = j | X_n = i) = f(\Lambda, \Xi, \Delta\sigma)$ A state must be identified that can be considered failure. The probability of entering this state can then be found. This probability is also the probability of failure. The idea of Markovian chains is illustrated in figure 7.1. Unfortunately the author has no idea on how to classify states as something observable. Perhaps an idea would be to use states such as "poor", "good" , "excellent" , however, a good quantification needs to be found for these states because in Markovian systems states must be <u>observable</u>. In case probabilities are known the system can be solved with the Chapman-Kolmogorov equations given as $p_{ij}^{n+m} = \sum\limits_{k=0}^{\infty} P_{ik}^n P_{kj}^m$ for $n, m \geq 0$.
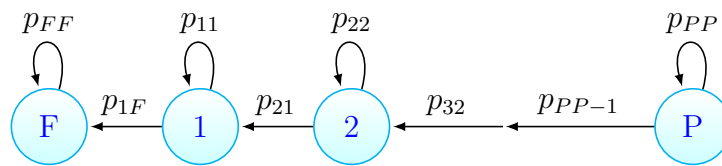
FIGURE 7.1: The specimen may start at any state, state P is defined as perfection and state F is defined as failure. In case the system enters state F it stays there because this is a recurrent state. The remainder of the states are transient

7.5 Strain Rate

It was also revealed in the literature review that the strain rate is an influential factor for determining the low cycle corrosion fatigue life. A lower strain rate leads to a lower fatigue life. It was the hypothesis of the author in chapter 4 that this is due to the element of time. In case corrosion has more time to attack the specimen the fatigue life will be less. This is the case for very low strain rates because the elapsed time between reversals is much more. This means that when low cycle or high cycle fatigue tests are done in a corrosive environment the strain rate must be representative of the strain rate of the loads in the environment in which the

specimen will be used. A series of experiments where very low strain rate is used will work well because corrosion gets sufficient time to attack the specimen, which will lead to conservative results.

Chapter 8

Conclusions

1. LCCF has not been an issue in offshore engineering and there is not a single design code that gives comprehensive guidance for dealing with LCCF or even LCF. The reason is that the design codes have a global elastic design philosophy and the need for comprehensive design codes for low cycle corrosion fatigue never existed

2. The weakest part of a structure to LCCF are the (welded) joints. The joints appear to fail well before the adjoining material.

3. The environment plays a significant role in the fatigue life of a structural element. The impact of the environment diminishes in the LCHS region. It is the hypothesis of the author that fatigue life is less affected by the environment because the duration between initiation of the load and ultimate failure is shorter which allots less time to the environment to penetrate the specimen. This hypothesis is further enforced by the fact that test results have revealed that the strain rate is positively correlated with the fatigue life of a specimen in a deleterious environment.

4. Two models were proposed to predict the low cycle fatigue life based on two very distinct assumptions. The first model is based on constant slopes in the relationship between the logarithm of the fatigue life and the logarithm of the stress level in a fatigue region. The regions which can be distinguished are the ultra high cycle region, the high cycle region and the low cycle region. This model has a decent theoretical background and predicted credible results for low cycle corrosion fatigue life. The second model to predict fatigue

life in the low corrosion cycle region is based on regression. This model uses the assumption that the fatigue life that a high cycle corrosion fatigue curve predicts in the low cycle region through extrapolation possesses predictive power for the actual corrosion fatigue life in the low cycle region. The regression performed yielded credible results and the internal fit of the regression was quite high. There are no better ways to predict low cycle fatigue life for various connections other than the methods that can be found in this thesis. There is no experimental data available which makes the method proposed in this thesis the only way. There is no independent dataset to validate the models proposed in this thesis. The models performed well and delivered credible results, however, experimental data is needed in order to judge their accuracy.

Appendix A

Method Based on Constant Slopes

In this Appendix the comparison between an extrapolated high cycle curve into the low cycle region and the low cycle curves created with the method based on constant slopes presented in Chapter 5.
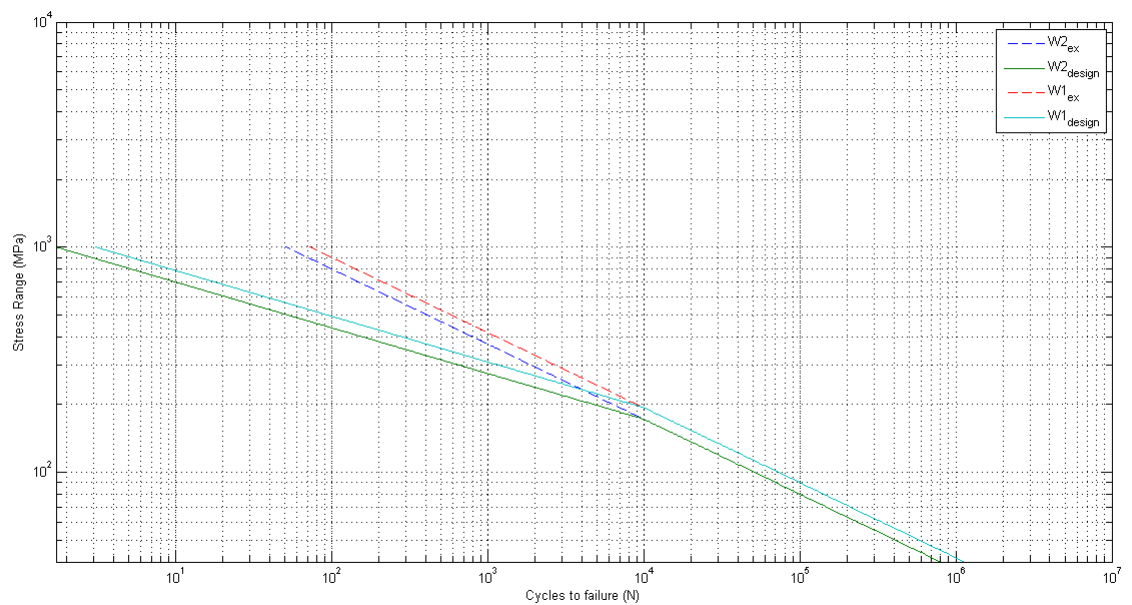
Comparison between the extrapolated curve for the high cycle region into the low cycle region for W2 and W1 curves and the curves created with the assumption of consistent slopes
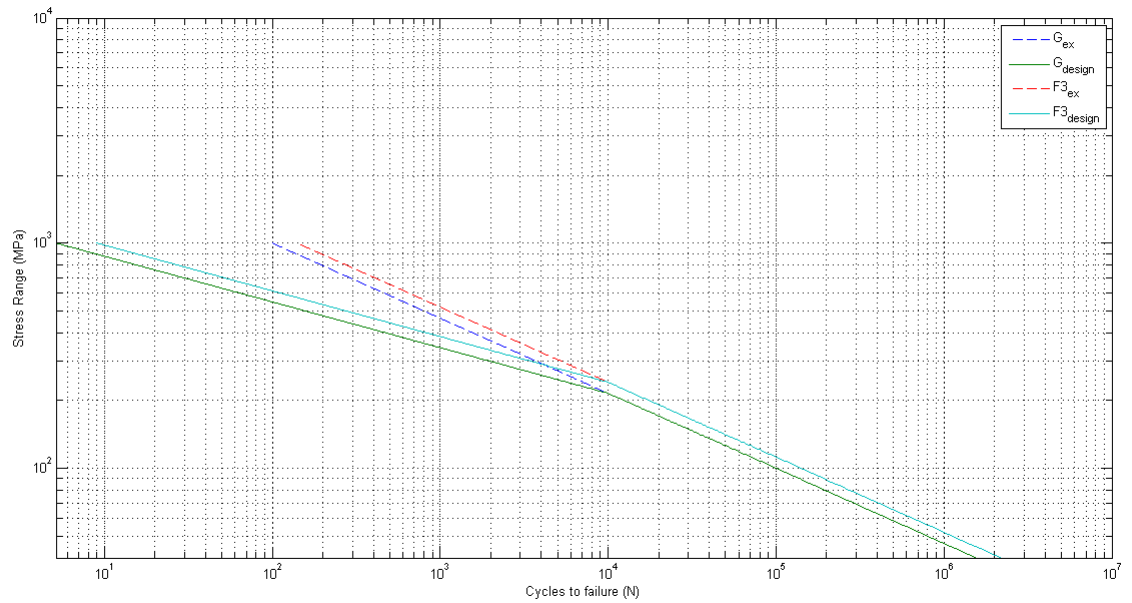
Comparison between the extrapolated curve for the high cycle region into the low cycle region for G and F3 curves and the curves created with the assumption of consistent slopes
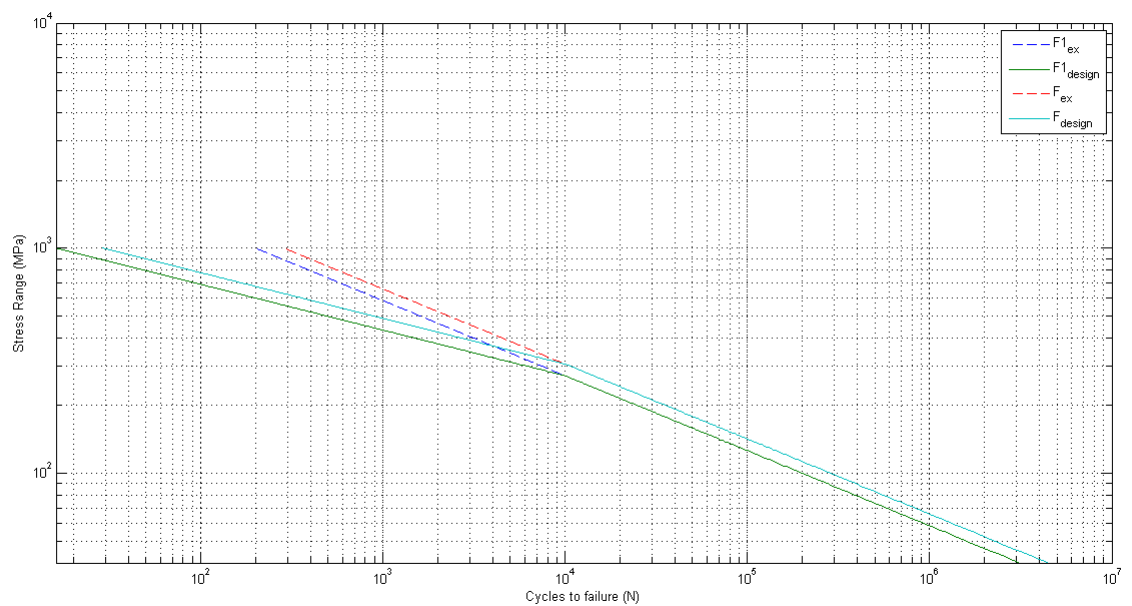
Comparison between the extrapolated curve for the high cycle region into the low cycle region for F1 and F curves and the curves created with the assumption of consistent slopes
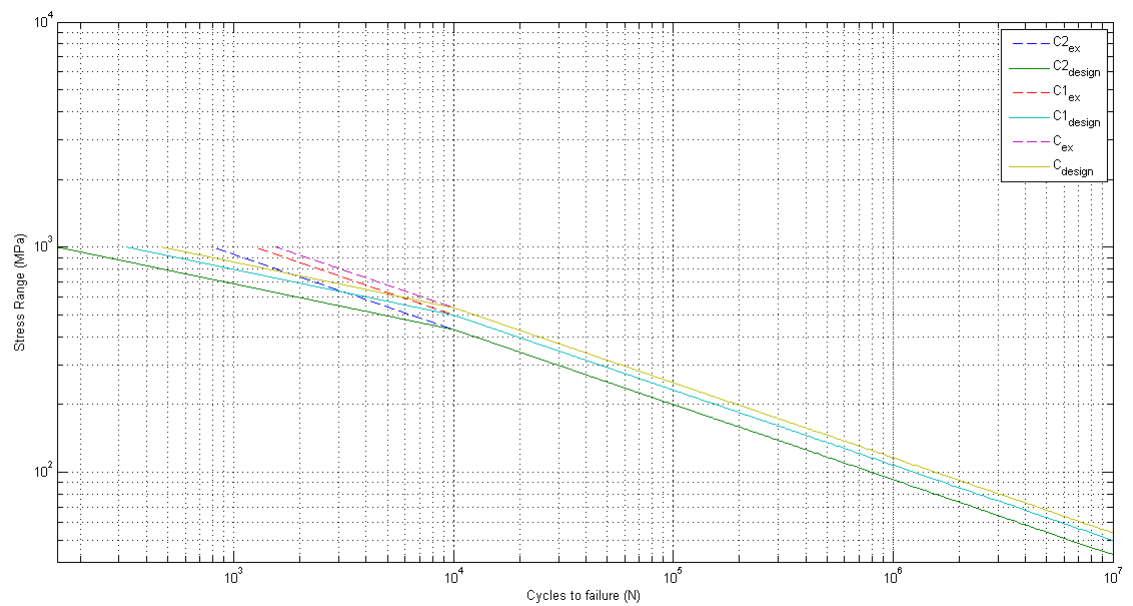
Comparison between the extrapolated curve for the high cycle region into the low cycle region for C2, C1 and C curves and the curves created with the assumption of consistent slopes

Appendix B

Connections According to DNV

In this Appendix the reader will find connections and base material which can analyzed for low cycle fatigue with the methods reported in Chapter 5. The data is taken from Recommended Practice C203 2010 04. The connections are briefly explained here. For more details the reader is refered to [5].

B.1   Non-Welded Details
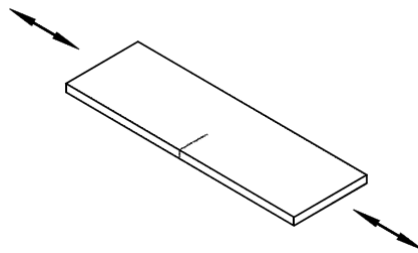
SN curve C. Manually gas cut material or material with machine gas cut edges with shallow and regular draglines [5].

B.2   Bolted Connections
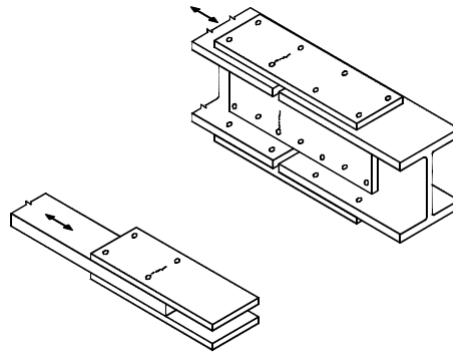
S-N curve C1. Beam splices or bolted cover plates. [5]
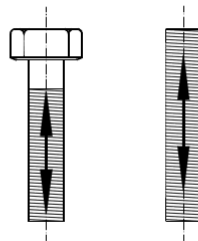
S-N curve F1. Bolts and threaded rods in tension. Cold rolled threads with no following heat treatment like hot galvanising. S-N curve W3. Cut threads. [5]
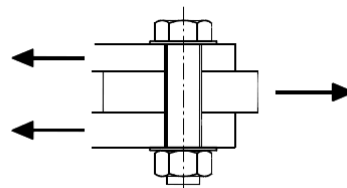
Bolts in single or double shear. [5]

B.3 Continuous Welds
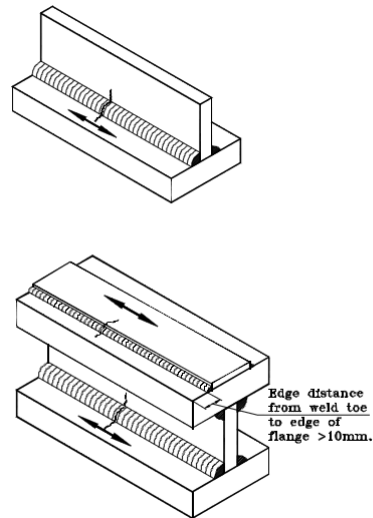
S-N curve C. Automatic welds carried from both sides. S-N curve C. S-N curve C2. Automatic fillet welds. [5]
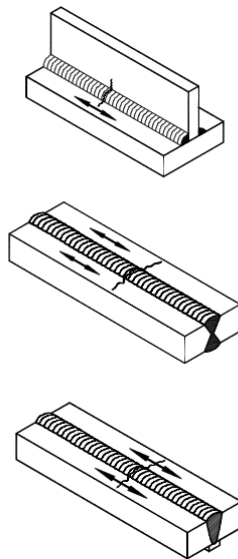
S-N curve C1. Automatic fillet or butt weld carried out from both sides with stop-start positions.S-N curve C1. Automatic butt welds made from one side only, with backing bar but without start-stop position. [5]
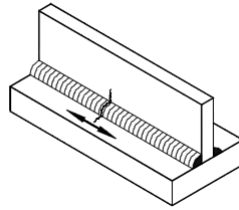
S-N curve C2. Manual fillet or butt welds. S-N curve C2. Manual or automatic butt welds carried out from one side only. [5]
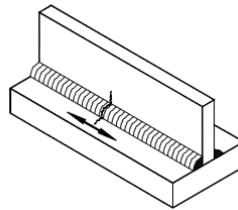
S-N curve C2. Repaired or automatic manual fillet or butt welds [5]

B.4   Intermittent Welds
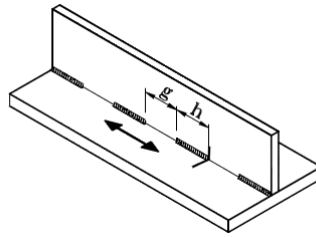
S-N curve E. Stitch or tack welds not subsequently covered by a continuous weld [5]
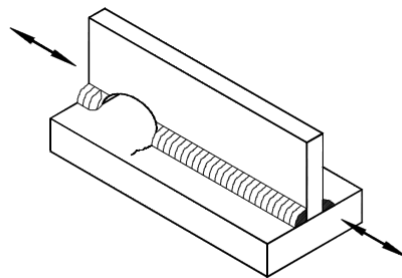
S-N curve F. Ends of continuous welds at cope holes. [5]
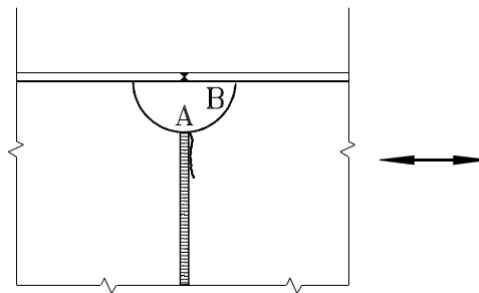
Cope hold with transverse butt weld [5]

B.5 Transverse Butt Welds

For more details on the requirements on the quality of the weld, the reader is referred to [5]
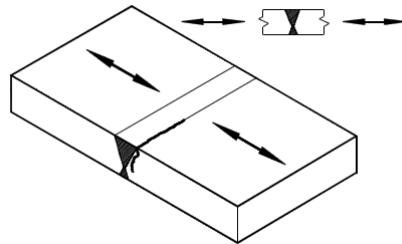
S-N curve C1. Transverse splices in plates flats and rolled sections [5]
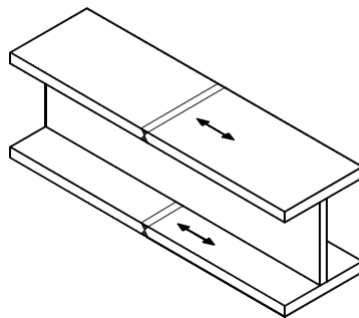
S-N curve C1. Flange splics in plate girders [5]
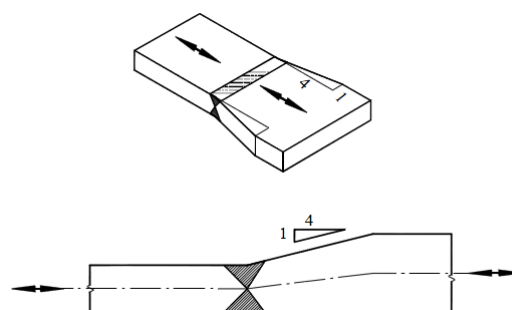
S-N curve C1. Transverse splices in plates or flats tapered in width or in thickness where the slope is less than 1:4 [5]
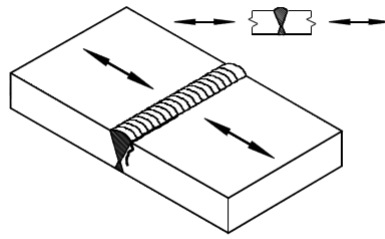
S-N curve D. Transverse splices in plates and flats [5]
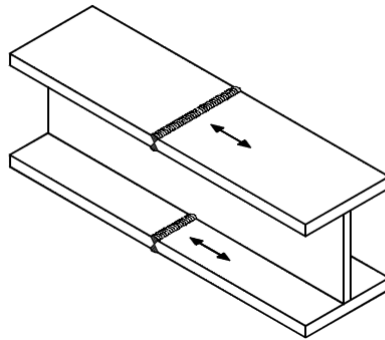
S-N curve D. Transverse splices in rolled sections or welded plate girders [5]
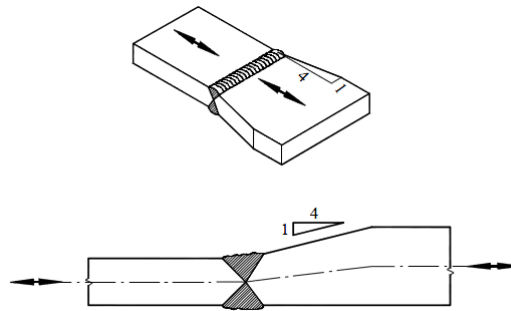
S-N curve D. Transverse splices in plates or flats tapered in width or in thickness where the slope is less than 1:4 [5]
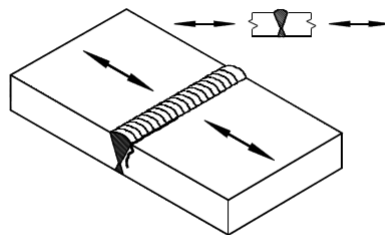
S-N curve E. Transverse splices in plates and flats [5]
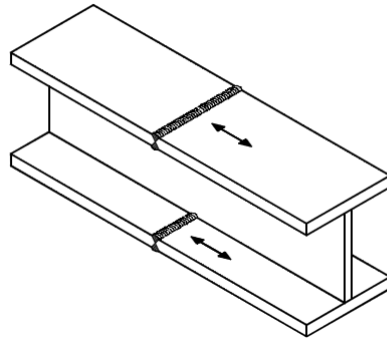
S-N curve E. Transverse splices in rolled sections or welded plate girders [5]
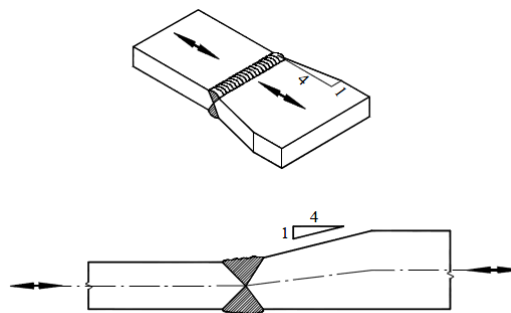
S-N curve E. Transverse splices in plates or flats tapered in width or in thickness
where the slope is less than 1:4 [5]
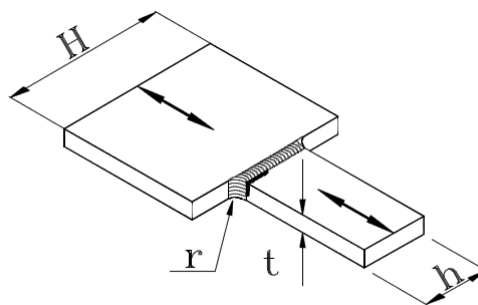
Transverse splice between plates of unequal width, width the weld ends ground
to a radius.S-N curve F1 for a ratio $\frac{r}{h} \geq 0,16$. S-N curve F3 ratio $\frac{r}{h} \geq 0,11$ [5]
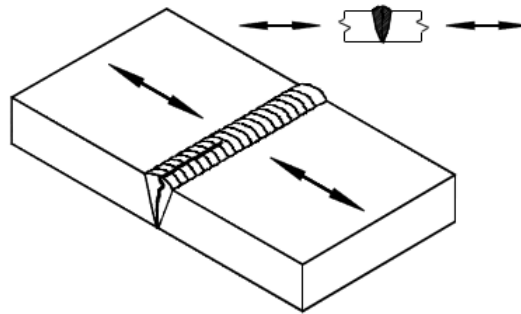
S-N curve W3. Butt weld amde from one side only without backstrip [5]
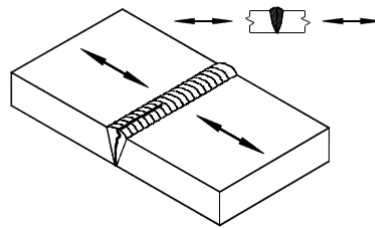
S-N curve W3. Butt weld amde from one side only without backstrip [5]
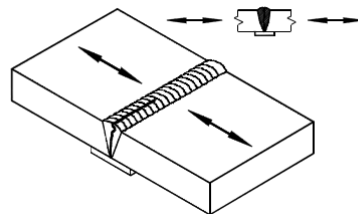
S-N curve F. Transverse butt weld on a temporary or a permanent backing strip without fillet weld [5]
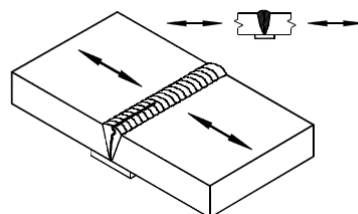
S-N curve G. Transverse butt weld on a backing strip fillet welded to the plate [5]

B.6   Welded Attachments

For more details on the requirements on the quality of the weld, the reader is referred to [5]
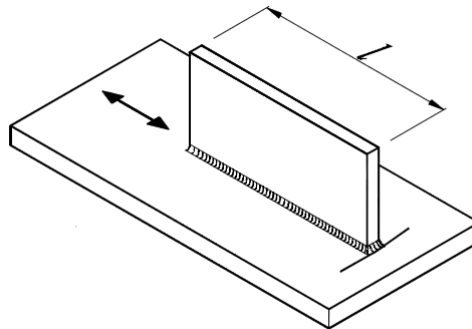
Welded longitudinal attachment. Doubling plate welded to a plate. S-N curve E for $l \leq 50$ mm . S-N curve F for $50 < l \leq 120$ mm. S-N curve F1 for $120 < l \leq 300$ mm. S-N curve F3 for $l > 300$ mm. [5]
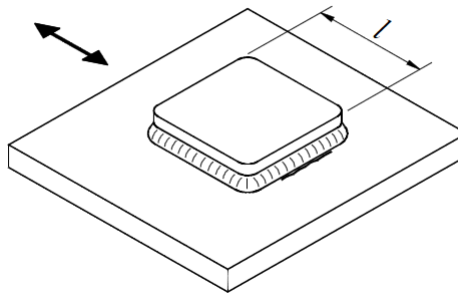
Doubling plate welded to a plate. S-N curve E for $l \leq 50$ mm . S-N curve F for $50 < l \leq 120$ mm. S-N curve F1 for $120 < l \leq 300$ mm. S-N curve F3 for $l > 300$ mm. [5]
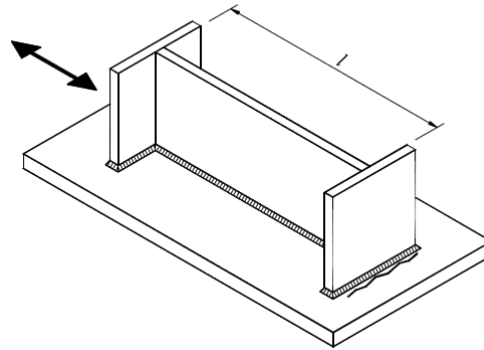
Longitudinal attachment weleded to transverse stiffener. S-N curve E for $l \leq 120$ mm . S-N curve F for $120 < l \leq 300$ mm. S-N curve F1 for $120 < l \leq 300$ mm. S-N curve F3 for $l > 300$ mm. [5]
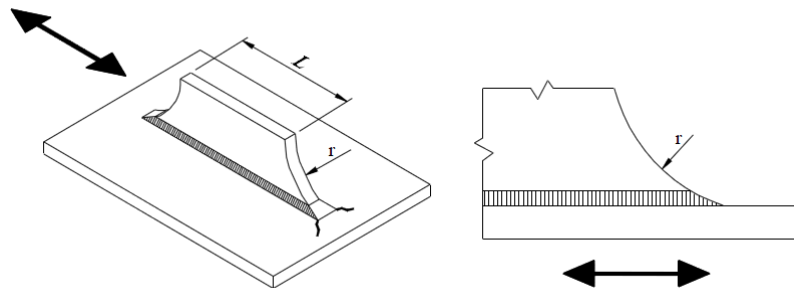
S-N curve E. Longitudinal fillet welded gusset with radius transition to plate or tube; end of fillet weld reinforcement (full penetration); length of reinforcement $> \mathrm{r}$. [5]
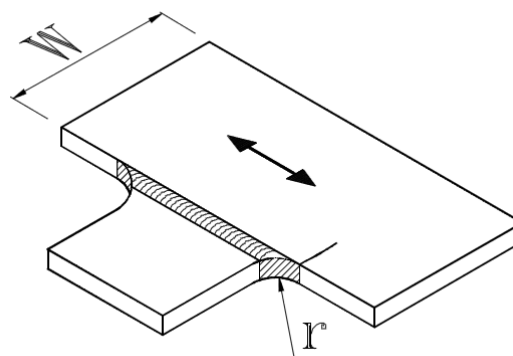

Gusset plate with radius welded to edge of a plate or beam flange. S-N curve E for $\frac{1}{3} \leq \frac{r}{W}, r \geq 150$ mm. S-N curve F $\frac{1}{6} \leq \frac{r}{W} < \frac{1}{3}$. S-N curve F1 $\frac{1}{10} \leq \frac{r}{W} < \frac{1}{6}$. S-N curve F3 $\frac{1}{16}/le\frac{r}{W} < \frac{1}{10}$. S-N curve G $\frac{1}{25} \leq \frac{r}{W} < \frac{1}{16}$. [5]
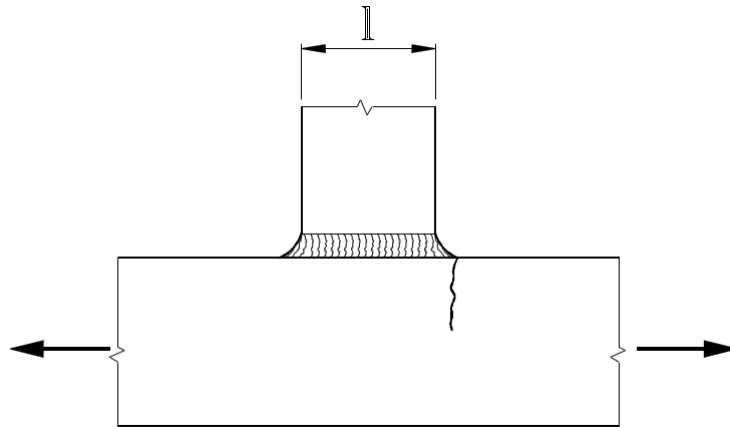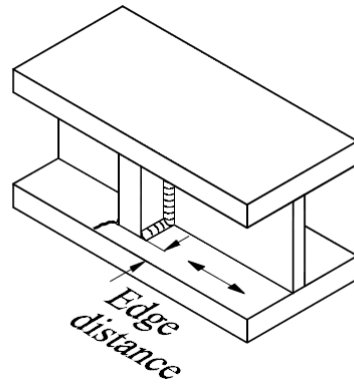
Gusset plate welded to the edge of a plate or beam flange. S-N curve G for $l \leq 150$ mm. S-N curve W1 for $150 < l \leq 300$ mm. S-N curve W2 for $l > 300$ mm [5]
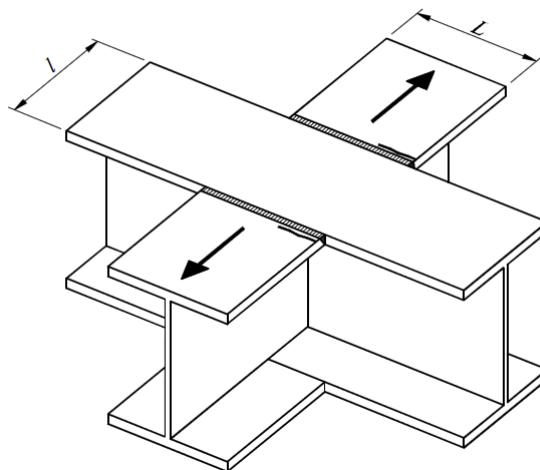
Flange welded to another flange at crossing joints. S-N curve G for $l \leq 150$ mm. S-N curve W1 for $150 < l \leq 300$ mm. S-N curve W2 for $l > 300$ mm [5]
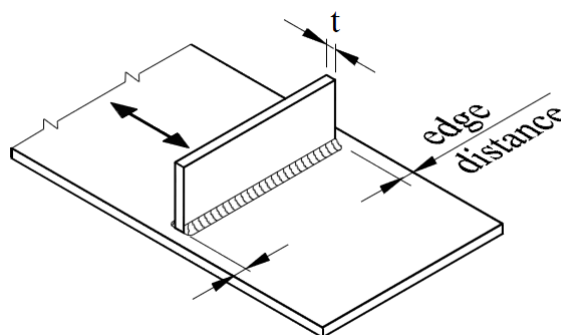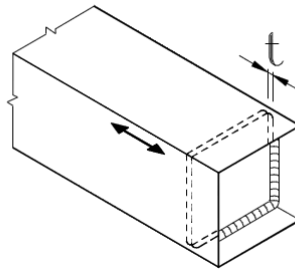

Transverse attachments with edge distance ≥ 10 mm. S-N curve E for $t \leq 25$ mm. S-N curve F for $t > 25$ mm [5]
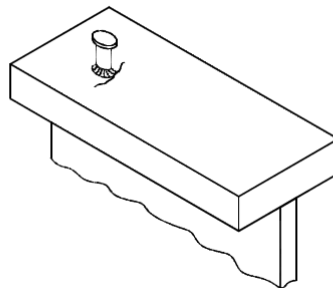
Vertical stiffener welded to a beam or a plate girder. S-N curve E for $t \leq 25$ mm. S-N curve F for $t > 25$ mm [5]

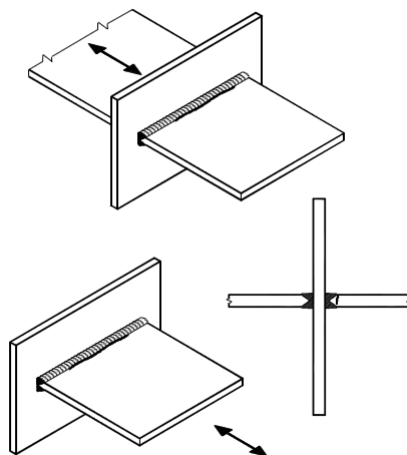Diaphragms of box girders welded to a flange or web. S-N curve E for $t \leq 25$ mm. S-N curve F for $t > 25$ mm [5]

Welded shear connector to base material. S-N curve E for Edge distance ≥ 10 mm. S-N curve G for Edge distance < 10 mm. [5]
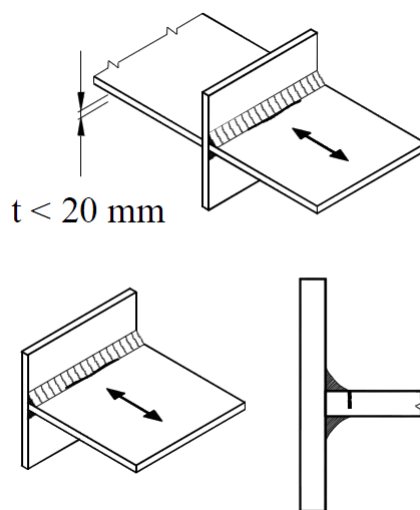
B.7 Welded Joints

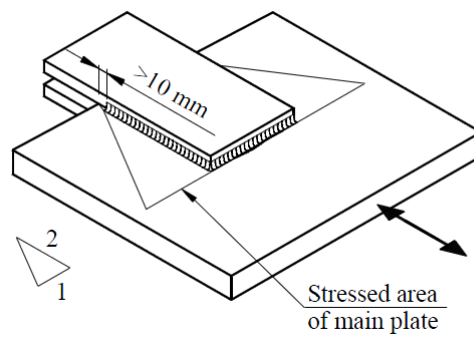For more details on the requirements on the quality of the weld, the reader is referred to [5]

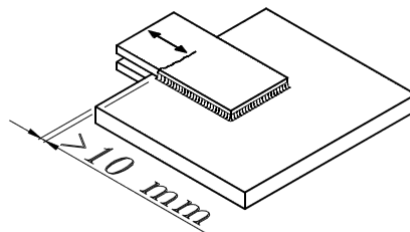S-N curve F. Full pentration butt welded cruciform joint [5]
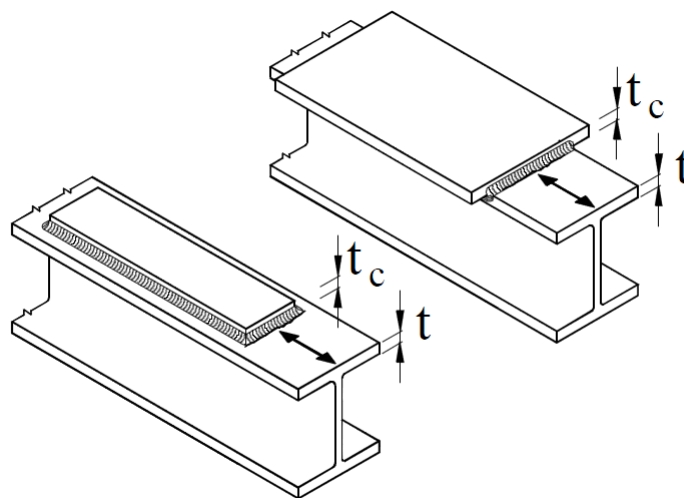

S-N curve W3. Partial penetration tee-butt joint or fillet welded joint and effective full penetration in tee-butt joint. [5]
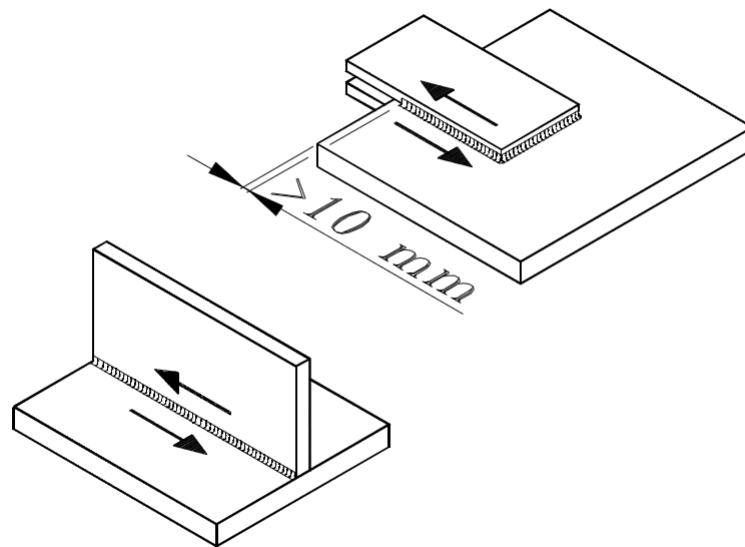
S-N curve F1. Fillet welded overlap joint crack in main plate [5]

S-N curve W1. Fillet welded overlap joint. Crack in overlapping plate [5]

End zones of single or multiple welded cover plates in beams and plate girders. Cover plates with or without frontal weld. S-N curve G for $tandt_c \leq 20$ mm. S-N curve W3 for $tandt_c > 20$ mm [5]

S-N curve E. Continuous fillet welds transmitting a shear flow, such as web to flange welds in plate girders. Filler welded lap joint [5]
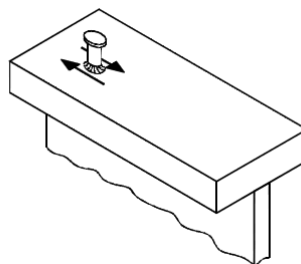
S-N curve E. Stud connectors (failure in the weld or heat effected zone [5]
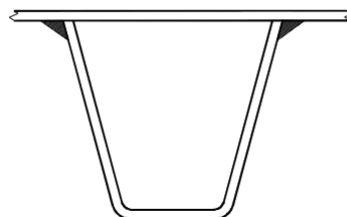
S-N curve E. Trapezoidal stiffener welded to deck plate with fillet weld or full or partial penetration butt weld [5]
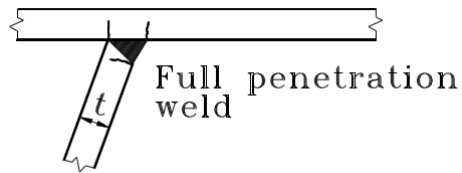
S-N curve F. Trapezoidal stiffener welded to deck plate with fillet weld or full or partial penetration butt weld [5]
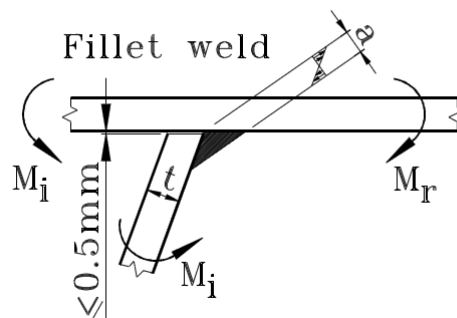
S-N curve G. Trapezoidal stiffener welded to deck plate with fillet weld or full or partial penetration butt weld [5]

B.8 Tubular Sections

An overview of examples with tubular sections is given in figure. The base material adjacent to the toes of full penetration welded tubular joints. An example of tubular formations is given in this section.
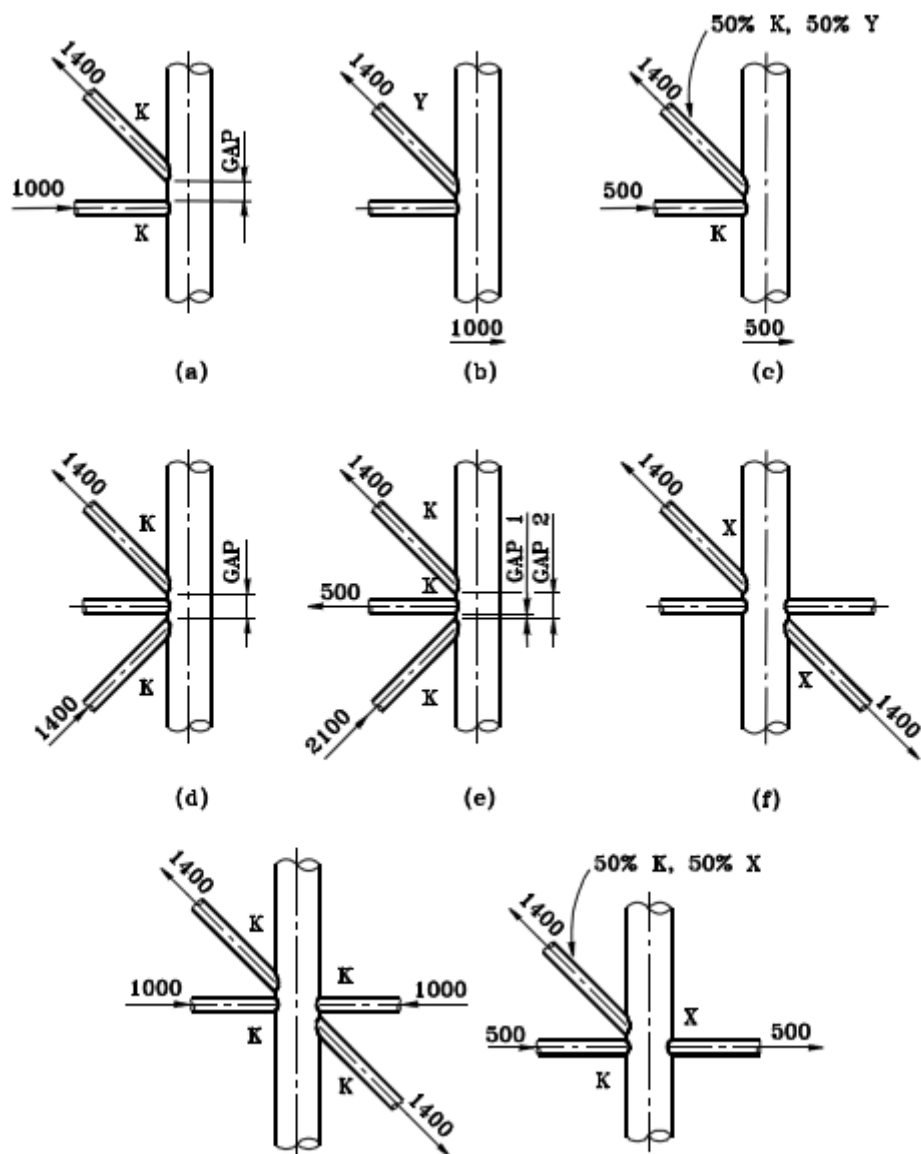
S-N curve T. Tubular sections [5]

For a complete overview of all the details that can be calculated with the S-N curves then reader is referred to Appendix A of [5] DNV Recommended Practice.

Appendix C

Method Based on Regression

In this chapter a comparison can be found between the extrapolated high cycle curves into the low cycle region and the low cycle S-N curves found by the method based on regression found in chapter 5.
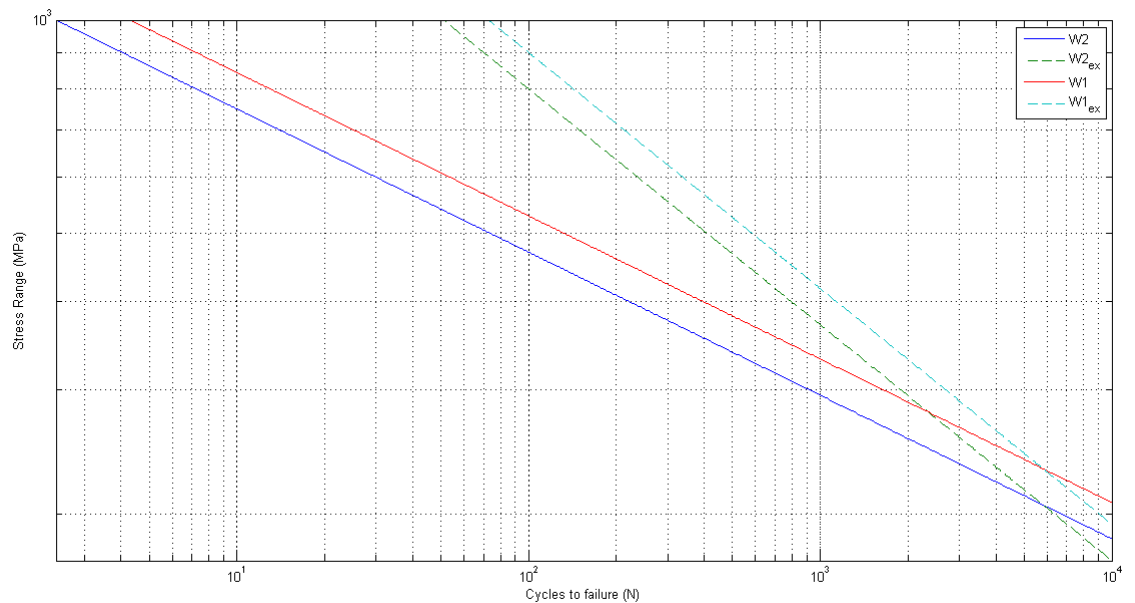
Comparison between the extrapolated curve for the high cycle region into the low cycle region for W2 and W1 curves and the curves created with the method based on regression
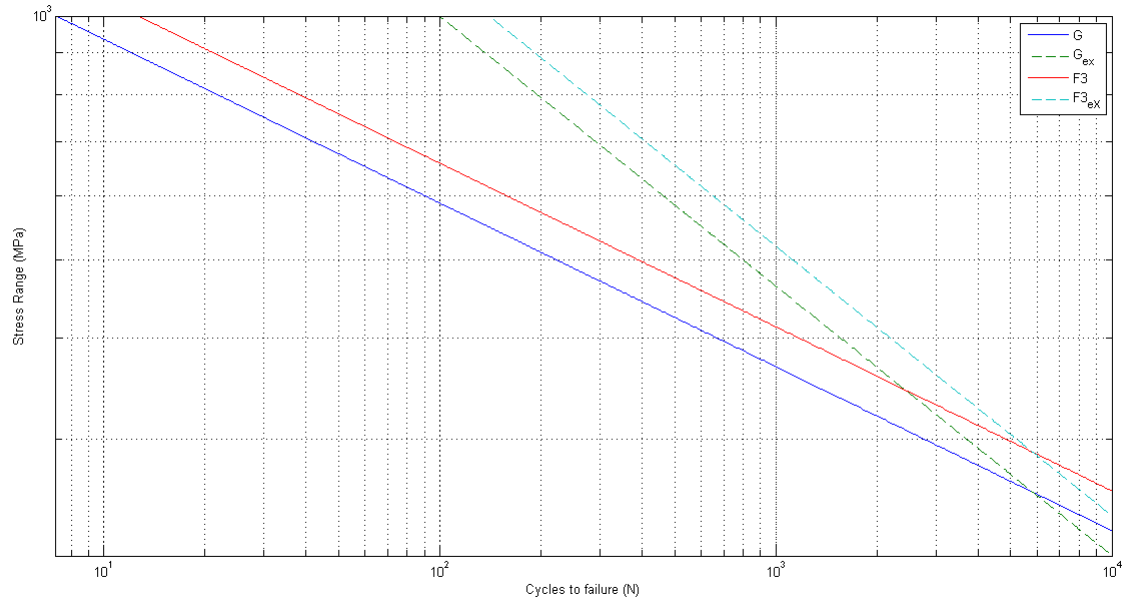
Comparison between the extrapolated curve for the high cycle region into the
low cycle region for G and F3 curves and the curves created with the method
based on regression

Comparison between the extrapolated curve for the high cycle region into the
low cycle region for E and D curves and the curves created with the method
based on regression

Comparison between the extrapolated curve for the high cycle region into the low cycle region for C2, C1 and W1 curves and the curves created with the method based on regression
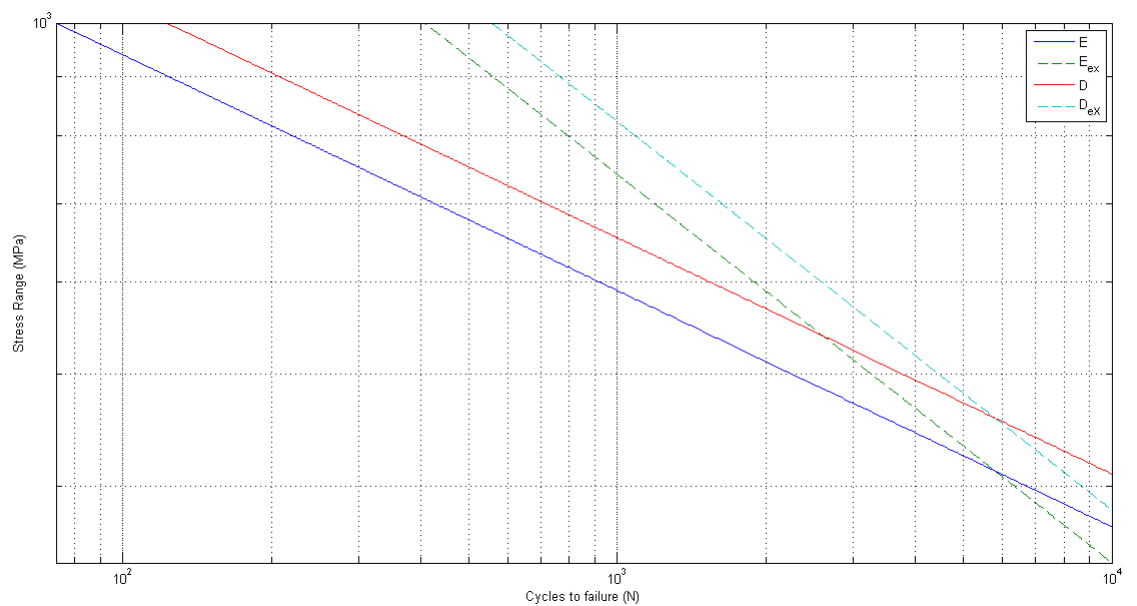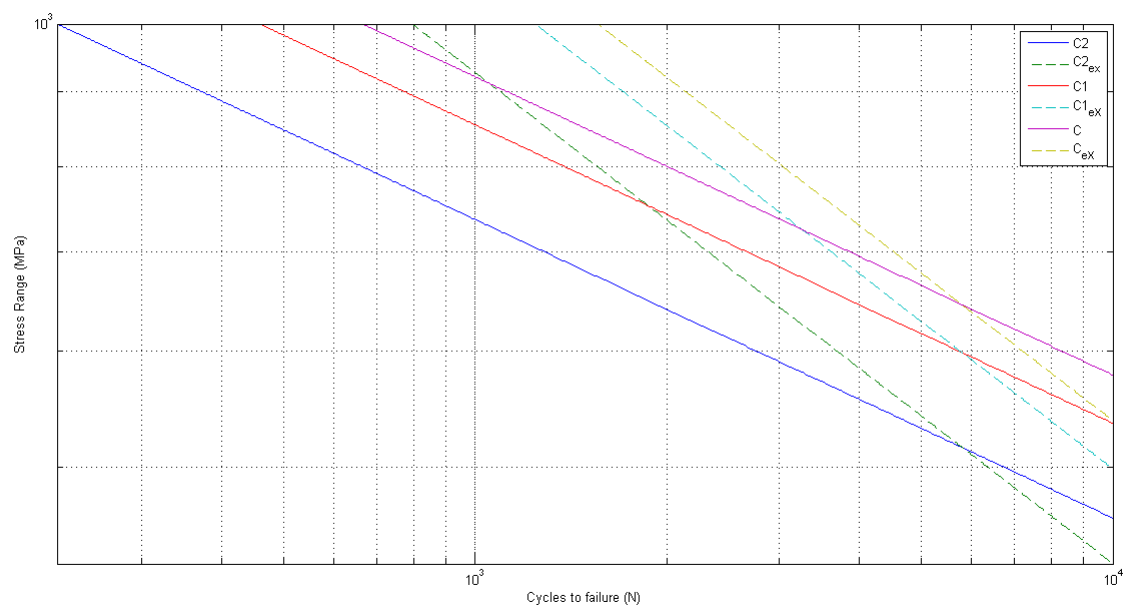
Appendix D

Material Coefficients Common Engineering Alloys

Material	Process Description	S_u MPa (ksi)	HB	E GPa (ksi-10¹)	%RA	S_y/S_y' MPa (ksi)	K/K' MPa (ksi)	n/n'	$\varepsilon_f/\varepsilon_f'$	σ_f/σ_f' MPa (ksi)	b	c
Steel												
1010	HR sheet	331 (48)	—	203 (29.5)	80	200/— (29)/—	534/867 (78)/(126)	0.185/0.244	1.63/0.104	—/499 —/(72)	-0.100	-0.408
1020	HR sheet	441 (64)	109	203 (29.5)	62	262/— (38)/—	738/1962 (107)/(284)	0.190/0.321	0.96/0.337	—/1384 —/(201)	-0.156	-0.485
1038ᶜ	Normalized	582 (84)	163	201 (29.5)	54	331/342 (48)/(50)	1106/1340 (160)/(195)	0.259/0.220	0.77/0.309	898/1043 (130)/(151)	-0.107	-0.481
1038ᶜ	Q & T	649 (94)	195	219 (31.5)	67	410/364 (60)/(53)	1183/1330 (172)/(193)	0.221/0.208	1.10/0.255	1197/1009 (174)/(146)	-0.097	-0.460
Man-Ten	HR sheet	510 (74)	—	207 (30)	64	393/372 (57)/(54)	—/786 —/(114)	0.20/0.11	1.02/0.86	814/807 (118)/(117)	-0.071	-0.65
RQC-100	HR sheet	931 (135)	290	207 (30)	64	883/600 (128)/(87)	1172/1434 (170)/(208)	0.06/0.14	1.02/0.66	1330/1240 (193)/(180)	-0.07	-0.69
1045	Annealed	752 (109)	225	— —	44	517/— (75)/—	—/1022 —/(148)	—/0.152	0.58/0.486	—/916 —/(133)	-0.079	-0.520
1045	Q & T	1827 (265)	500	207 (30)	51	1689/— (245)/—	—/3371 —/(489)	0.047/0.145	0.71/0.196	—/2661 —/(386)	-0.093	-0.643
1090ᶜ	Normalized	1090 (158)	259	203 (29.5)	14	735/545 (107)/(79)	1765/1611 (256)/(234)	0.158/0.174	0.15/0.250	—/1310 —/(190)	-0.091	-0.496
1090ᶜ	Q & T	1147 (166)	309	217 (31.5)	22	650/627 (94)/(91)	1895/1873 (275)/(272)	0.165/0.176	0.24/0.700	—/1878 —/(273)	-0.120	-0.600
1141ᶜ	Normalized	789 (115)	229	220 (32)	47	493/481 (72)/(70)	1379/1441 (200)/(209)	0.187/0.177	0.64/0.602	1117/1326 (162)/(192)	-0.103	-0.581
1141ᶜ	Q & T	925 (134)	277	227 (33)	59	814/591 (118)/(86)	1205/1277 (125)/(185)	0.074/0.124	0.88/0.309	1405/1127 (204)/(164)	-0.066	-0.514
4142	Q & T	1413 (205)	380	207 (30)	48	1378/— (200)/—	—/2266 —/(387)	0.051/0.124	0.65/0.637	—/2143 —/(311)	-0.094	-0.761
4142	Q & T	1929 (280)	475	207 (30)	35	1722/— (250)/—	—/2399 —/(348)	0.048/0.094	0.43/0.331	—/2161 —/(314)	-0.081	-0.854
4340	HR	827 (120)	243	193 (28)	43	634/— (92)/—	—/1337 —/(194)	—/0.168	0.57/0.522	—/1198 —/(174)	-0.095	-0.563

Common Material Coefficients [27]

Bibliography

[1] R.P. Gandloff. Environmental cracking corrosion fatigue. *Corrosion Tests and Standards: Application and Interpretation: 2nd Edition*, 2005. URL http://www.virginia.edu/ms/faculty/gangloffASTM_CH_26.pdf.

[2] Thomas. Ummenhofer Stefan. Herion, Jennifer. Hrabowski. Low-cycle fatigue behaviour of high-strength steel butt welds. *International Offshore and Polar Engineering Conference*, June 2011. URL http://www.isope.org/publications/proceedings/ISOPE/ISOPE%202011/data/papers/11TPC-929Herion.pdf.

[3] C. Ngan. Fatigue design basics in accordance with the canadian code and the eurocode. *Fatigue Design Basics in Accordance with the canadian code and the eurocode*, 2008. URL http://www.sigi.ca/engineering/documents/caroline_ngan_fatigue_comparison.pdf.

[4] Eurocode3. Eurocode 3 , part 1-9 , bs en 1993-1-9. *Fatigue Strength*, 1993. URL http://www.eurocodes.co.uk/PartDetail.aspx?EurocodePartID=24.

[5] Det Norske Veritas. Fatigue design of offshore steel structures. *Recommended Practice DNV-RP-C203*, April 2010. URL http://exchange.dnv.com/publishing/Codes/download.asp?url=2012-10/rp-c203.pdf.

[6] NORSOK STANDARD. Assessment of structural integrity for existing offshore load-bearing structures. *NORSOK Standard N-006*, March 2009. URL http://www.standard.no/PageFiles/9809/N-006u1.pdf.

[7] American Bureau of Shipping. Structures, guide for the assessment of offshore fatigue assessment of offshore structures. *American Bureau of Shipping*, 2010. URL http://www.eagle.org/eagleExternalPortalWEB/

`ShowProperty/BEA%20Repository/Rules&Guides/Current/115_`
`FatigueAssessmentofOffshoreStructures/Pub115_FAOS`.

[8] Health and Safety Executive. Offshore installations: Guidance on design, construction an d certification. *Fourth Edition (including Amendment 3, 1995), Department of Energy, publ. HSE Books*, 1995. URL `http://www.hse.gov.uk/offshore/guidance-technical.htm`.

[9] API RECOMMENDED PRACTICE 2A-WSD. Recommended practice for planning, designing and constructing fixed offshore platforms. *API RECOMMENDED PRACTICE 2A-WSD*, October 2005. URL `oc.its.ac.id/ambilfile.php?idp=1765`.

[10] et al Y.B. Unigovski. Low-cycle fatigue behavior of 316l-type stainless steel in chloride solutions. *Corrosion Science 3014-3020*, July 2009. URL `http://www.sciencedirect.com/science/article/pii/S0010938X09003977`.

[11] L.F. Coffin. A study of the effects of cyclic thermal stresses on a ductule metal. *AIME Trans 76, 1954. 931-950*, 1954.

[12] S.S. Manson. Behavior of materials under conditions of thermal stress. *NASA report 1170*, 1953.

[13] et al K.H. Nip. Extremely low cycle fatigue tests on structural carbon steel and stainless steel. *Journal of Constructional Steel Research Vol. 66. 96-110*, 2009. URL `http://www.sciencedirect.com/science/article/pii/S0143974X09001916`.

[14] et al E. Lachmann. The low cycle corrosion fatigue of ah36-gl and 13 crmo 44 steel in 3nacl solution. *Corrosion Science Volume 23, Issue 6*, 1983. URL `http://www.sciencedirect.com/science/article/pii/0010938X83901245`.

[15] W.J. O'Donnell. Code design and evaluation for cyclic loading sections. *Corrosion Science Volume 23, Issue 6*, 2008. URL `http://www.krrao.com/images/Chapter_39_pp643-674_Update_by_O_Donnell_7-1-08.pdf`.

[16] X. Wang. Low cycle fatigue analysis of marine structures. *American Society of Mechanical Engineers (ASME)*, September 2006. URL `http://www.eagle.org/eagleExternalPortalWEB/ShowProperty/BEA%20Repository/References/Technical%20Papers/2006/LowCycleFatigueAnalysis`.

[17] H.J. Heo et al. Design guidance for low cycle fatigue in ship structures. *PRADS2004*, September 2004. URL https://getinfo.de/app/A-Study-on-the-Design-Guidance-for-Low-Cycle-Fatigue/id/BLCP%3ACN054337231.

[18] TWI. Fatigue performance of welded highstrength steels. *A compendium of reports from a sponsored research programme*, 1974. URL http://www.amazon.com/dp/0853000727.

[19] F. Erdogan P. Paris. A critical analysis of crack propagation laws. *Journal of Basic Engineering — Volume 85 — Issue 4 — RESEARCH PAPERS*, January 2010. URL http://fluidsengineering.asmedigitalcollection.asme.org/article.aspx?articleid=1431537.

[20] Low cycle fatigue crack lpropagation characteristics of monel 400 and monel k-500 alloys. *U.S. NAVAL RESEARClt LABORATORY Washinglon, D.C.*, March 1965. URL http://www.dtic.mil/dtic/tr/fulltext/u2/613558.pdf.

[21] G Vaessen J. de Back, G.H. Fatigue and corrosion fatigue behavior of offshore steel structures. *Foundation for materials research in the sea*, April 1981. URL http://www.onepetro.org/mslib/servlet/onepetropreview?id=00008621.

[22] Raghu V. Prakash Chinnaiah. Madduri. International journal of mechanical and materials engineering. *National Technical Information Services, U.S*, January 2010. URL http://www.waset.org/journals/ijmme/v1/v1-1-5.pdf.

[23] Det Norske Veritas. Cathodic protection design. *RECOMMENDED PRACTICE DET NORSKE VERITAS DNV-RP-B401*, October 2010. URL http://exchange.dnv.com/publishing/Codes/download.asp?url=2011-04/rp-b401.pdf.

[24] J.B. Bushman. Corrosion and cathodic protection theory. *BUSHMAN & Associates, Inc.*, 2011. URL http://www.bushman.cc/pdf/corrosion_theory.pdf.

[25] U.S. Department of Energy. Doe fundamentals handbook chemistry volume 1 of 2. *National Technical Information Services, U.S*, January 1993. URL http://www.isibang.ac.in/~library/onlinerz/resources/chem-v1.pdf.

[26] Corrosion and materials selection in ccs systems. April 2010. URL http://cdn.globalccsinstitute.com/sites/default/files/publications/108126/corrosion-materials-selection-ccs-systems.pdf.

[27] Ali Fatemi. Cylic deformation and strain life. *University of Toledo*, 2011. URL https://www.efatigue.com/training/Chapter_5.pdf.

[28] W.R. Osgood W. Ramberg. Description of stress-strain curves by three parameters. *Technical Note No. 902, National Advisory Committee For Aeronautics, Washington DC*, April 1943. URL http://ntrs.nasa.gov/archive/nasa/casi.ntrs.nasa.gov/19930081614_1993081614.pdf.

[29] Det Norske Veritas. Fabrication and testing of offshore structures. *OFF-SHORE STANDARD DET NORSKE VERITAS DNV-OS-C401*, October 2010. URL http://exchange.dnv.com/publishing/Codes/download.asp?url=2013-04/os-c401.pdf.

[30] Det Norske Veritas. Design of offshore steel structures, general (lrfd method). *OFFSHORE STANDARD DET NORSKE VERITAS DNV-OS-C101*, April 2011. URL http://exchange.dnv.com/publishing/Codes/download.asp?url=2011-04/os-c101.pdf.

[31] H. Neuber. Theory of stress concentration for shear-strained prismatical bodies with arbitrary nonlinear stress-strain law. *J. Appl. Mech. 28(4), 544-550 (Dec 01, 1961)*, September 1961. URL http://appliedmechanics.asmedigitalcollection.asme.org/article.aspx?articleid=1394813.